Understanding the role of microglia in the pathogenesis of amyotrophic lateral sclerosis



Björn Friedhelm Vahsen

St John's College

Nuffield Department of Clinical Neurosciences

University of Oxford

Supervised by

Professor Kevin Talbot, Professor Martin Turner,
and Dr Elizabeth Gray

Submitted for the degree of *Doctor of Philosophy*

Michaelmas Term 2022

To

my parents and grandparents

Abstract

Amyotrophic lateral sclerosis (ALS), the third commonest neurodegenerative disorder, is primarily characterised by progressive motor neuron loss with additional involvement of non-neuronal cells. In particular, microglia, the resident macrophages of the central nervous system parenchyma, have been implicated in ALS pathophysiology. The commonest genetic variant associated with ALS is a hexanucleotide repeat expansion (HRE) in the chromosome 9 open reading frame 72 (*C9ORF72*) gene, resulting in C9ORF72 haploinsufficiency and RNA foci and dipeptide repeat formation. Mimicking C9ORF72 haploinsufficiency through *C9orf72* knock-out in mice led to a pro-inflammatory microglial state, but whether this phenotype is replicated in human C9ORF72-ALS microglia and if they contribute to motor neuron death in C9ORF72-ALS is currently unknown. In this thesis, first, a novel co-culture model of induced pluripotent stem cell (iPSC)-derived microglia and motor neurons was devised and demonstrated to be compatible with the identity and function of both cell types. Hereafter, iPSC-derived microglia were generated from three different C9ORF72-ALS patients, which showed C9ORF72 haploinsufficiency and expressed the dipeptide repeat proteins Poly(GA)/(GP), confirming the presence of hallmarks of the *C9ORF72* HRE in C9ORF72-ALS iPSC microglia. RNA sequencing demonstrated a dysregulated transcriptome in C9ORF72-ALS iPSC microglia, particularly after lipopolysaccharides (LPS) priming, with pathway enrichment associated with immune cell activation, cytokines, lysosomes, and the extracellular matrix. C9ORF72-ALS iPSC microglia showed phago-lysosomal impairment and a pro-inflammatory profile with increased expression of nuclear factor kappa B (NFκB) and pro-inflammatory

cyto-/chemokines, notably, IL1B and matrix metalloproteinase-9 (MMP9). In iPSC microglia-iPSC motor neuron co-culture experiments, LPS-primed, but not unstimulated, C9ORF72-ALS iPSC microglia induced apoptosis in co-cultured wild-type motor neurons, which was ameliorated by concomitant application of an MMP9 inhibitor, suggesting MMP9 directly contributes to microglial neurotoxicity. Finally, increased microglial release of dipeptidyl peptidase 4 (DPP4) was identified as a biomarker for MMP9-dependent microglial dysregulation in co-culture. In summary, these results demonstrate widespread dysregulation of C9ORF72-ALS iPSC microglia, suggesting a key role for microglia in C9ORF72-ALS pathophysiology.

Declaration

Except where acknowledgement is made, all the work presented in this thesis was performed by the author in the Nuffield Department of Clinical Neurosciences, University of Oxford. The work reported in this thesis has not been submitted for any other degrees at the University of Oxford or any other University or similar institution. The present thesis does not exceed the prescribed word limit as indicated by the relevant Degree Committee.

Acknowledgements

First and foremost, I would like to thank my supervisors Kevin Talbot, Martin Turner, and Elizabeth Gray for giving me the opportunity to work on this challenging but incredibly interesting and rewarding project at the forefront of ALS research. In addition to your invaluable guidance and advice, I particularly appreciated your trust and the independence I had in setting up iPSC microglia research in the lab. I have learnt an incredible amount designing and executing this project over the past three years. A huge thank you also to Sally Cowley, for sharing your deep knowledge and expertise in microglia with me and effectively acting as an unofficial supervisor. I would also like to acknowledge the support from various funders that have allowed me to pursue this project: the Clarendon Fund, St John's College Oxford, the MRC, NIHR, and the MNDA.

There are many people without whom I would have never been able to complete this thesis. First, I would like to thank everyone in the Talbot/Turner/Thompson labs; very special thanks ought to be given to: Jakub Scaber and Yinyan Xu, for going through the ups and downs inside and outside the lab together, the mutual support, and the daily (non-)science chats over lunch at the JR or College; Ana Candalija, for teaching me all about iPSC culture, motor neuron differentiation and pretty much everything else lab-related, and your continued advice and friendship (even from Spain); Antigoni Katsikoudi, for the countless hours of admiring microglial cells together and all the scientific exchange, in tissue culture or during formal dinners; Sumedha Nalluru, for all your enthusiasm and incredibly hard work during your MSc project that so greatly advanced the project; the other "elves" – special shoutouts to Lucy Farrimond and Emily Carroll for sharing the

ups and downs of a DPhil with me and your great help with the paper together with Benazir Amein; Elisa Giacomelli, for a very helpful and friendly collaboration; Kaitlyn Cramb for spending countless hours on the rig to patch my cells; Cathy Browne, for patiently teaching me the microglia differentiation protocol; Ruxandra Dafinca, for performing calcium imaging on the microglia; and the other friendly faces in the labs next door, for making our lab a great and supportive place to work in – Dmitry, Jade, Jodie, Max, and Jussi, to name a few.

I have been very lucky to have a support network outside the lab that has greatly enriched my DPhil experience. Thank you to all the friends I have made at St John's and in Oxford – in particular: Annabel, for the countless hours of friendly chat in the SCR and the close friendship that has emerged from it; and the German "Kaffeefreunde" Alaa, Sebastian, Lorika, and Maja. Ein großer Dank geht auch an meine Freunde in der Ferne: Loreen, Greta, Alex, Philipp, Aylin, Sophie, Fabian, Ramona und Lisa. Ganz besonders aber muss ich mich bei Steffi und Nico bedanken – für eure kontinuierliche Freundschaft, Zuneigung und Unterstützung.

Der größte Dank gilt meinen Eltern und Großeltern – danke, dass ihr meinen akademischen Werdegang immer voll unterstützt und mir die Freiheit und Unabhängigkeit gegeben habt, diesen doch vielleicht ein wenig unerwarteten Weg der Wissenschaft zu gehen. And, finally, Jack, thank you for everything, for being the incredible and kind person that you are, and for giving me the strength to finish this thesis.

Publications arising from this work

Vahsen, B.F., Gray, E., Thompson, A.G., Ansorge, O., Anthony, D.C., Cowley, S.A., Talbot, K., and Turner, M.R. (2021). Non-neuronal cells in amyotrophic lateral sclerosis - from pathogenesis to biomarkers. Nat Rev Neurol 17, 333-348.

Giacomelli, E., **Vahsen, B.F.,** Calder, E.L., Xu, Y., Scaber, J., Gray, E., Dafinca, R., Talbot, K., and Studer, L. (2022). Human stem cell models of neurodegeneration: From basic science of amyotrophic lateral sclerosis to clinical translation. Cell Stem Cell 29, 11-35.

Vahsen, B.F., Gray, E., Candalija, A., Cramb, K.M.L., Scaber, J., Dafinca, R., Katsikoudi, A., Xu, Y., Farrimond, L., Wade-Martins, R., James, W.S., Turner, M.R., Cowley, S.A., and Talbot. K. (2022). Human iPSC co-culture model to investigate the interaction between microglia and motor neurons. Sci Rep 12, 12606.

Vahsen, B.F., Nalluru, S., Farrimond, L., Carroll, E., Xu, Y., Cramb, K.M.L., Amein, B., Scaber, J., Katsikoudi, A., Candalija, A., Carcolé, M., Isaacs, A.M., Wade-Martins, R., Gray, E., Turner, M.R., Cowley, S.A., and Talbot, K. C9ORF72-ALS iPSC microglia are pro-inflammatory and induce apoptosis of co-cultured motor neurons via MMP9. *Under review*.

Table of Contents

List of Figures ..... **V**

List of Tables ..... **VII**

Abbreviations ..... **VIII**

1 Introduction: Amyotrophic lateral sclerosis and microglia **1**

1.1 Amyotrophic lateral sclerosis 1
1.1.1 Epidemiology 2
1.1.2 Clinical features 3
1.1.3 Genetic variants 5
1.1.4 Pathophysiology and pathology 6
1.1.5 *C9ORF72* and the hexanucleotide repeat expansion mutation 8
1.2 Microglia 14
1.2.1 Origin, role in brain physiology, markers, and states 15
1.2.2 Role in neurodegeneration 17
1.3 Microglia in ALS 18
1.3.1 Post mortem tissue, neuroimaging, and fluid biomarkers 19
1.3.2 Disease models 21
1.4 iPSC models for ALS 29
1.4.1 iPSC-derived spinal motor neurons 30
1.4.2 iPSC-derived microglia 31
1.4.3 Multicellular approaches 32
1.5 Aims of this thesis 33

2 Materials and methods **36**

2.1 Cell culture 36
2.1.1 Generation and culture of iPSC lines 36
2.1.2 Differentiation of iPSC-derived motor neurons 37
2.1.3 Differentiation of iPSC-derived macrophage/microglia precursors 39
2.1.4 Differentiation of iPSC-derived microglia 39
2.1.5 Co-culture of iPSC-derived motor neurons and microglia 40
2.1.6 Cell culture treatments 41
2.1.7 Multi-electrode array recordings 42
2.2 Analysis of RNA expression 43
2.2.1 RNA isolation 43
2.2.2 Measurement of RNA integrity 44
2.2.3 cDNA preparation and RT-qPCR 44

2.2.4 RNA-sequencing ... 45
2.2.5 Bioinformatic analysis of RNA-sequencing data ... 46
2.3 Analysis of protein expression ... 47
2.3.1 Protein extraction and quantification for Western blot ... 47
2.3.2 SDS-PAGE and Western blotting ... 48
2.3.3 Protein extraction and sample preparation for the analysis of Poly(GA) and Poly(GP) expression ... 50
2.4 Immunofluorescence, confocal microscopy, and image analysis ... 51
2.4.1 Immunofluorescence ... 51
2.4.2 Quantification of differentiation efficiency and marker expression ... 53
2.4.3 Quantification of apoptosis in MNs and microglia ... 53
2.4.4 Analysis of LAMP1-positive lysosomes in microglia ... 53
2.4.5 Quantification of neurite density in co-culture ... 54
2.4.6 Analysis of neuronal synaptophysin expression ... 54
2.5 Live cell microscopy and image analysis ... 55
2.5.1 Analysis of microglial motility ... 55
2.5.2 Analysis of phagocytosis ... 55
2.5.3 Analysis of clustering behaviour ... 56
2.6 Cytokine/chemokine analyses ... 57
2.6.1 Supernatant arrays ... 57
2.6.2 ELISA ... 58
2.7 Data analysis ... 59

3 Establishing and characterising a co-culture of iPSC-derived microglia and motor neurons ... 60

3.1 Introduction and aims ... 60
3.2 Differentiation of iPSC-derived microglia and spinal MNs, and optimisation of culture conditions for co-culture ... 61
3.3 Co-culture does not alter cleaved caspase 3 expression in iPSC microglia or motor neurons ... 66
3.4 Transcriptomic analysis demonstrates a microglial signature in iPSC microglia in monoculture and co-culture ... 67
3.5 Transcriptomic comparison of iPSC microglia differentiated in monoculture and co-culture ... 72
3.6 Co-culture supports a homeostatic microglial state ... 75
3.7 Key microglial markers are expressed in iPSC microglia in monoculture and co-culture ... 75
3.8 iPSC microglia in monoculture and co-culture express key ALS-associated genes ... 79
3.9 Co-cultured iPSC microglia show highly dynamic ramifications and are phagocytically competent ... 80

3.10 Co-cultured iPSC microglia change morphology and form clusters in response to pro-inflammatory stimulation 82

3.11 iPSC microglia in monoculture and co-culture release pro-inflammatory and anti-inflammatory cytokines 84

3.12 Discussion and conclusions 87

4 Phenotypic analysis of C9ORF72-ALS patient-derived iPSC microglia 93

4.1 Introduction and aims 93

4.2 Differentiation of C9ORF72-ALS patient-derived iPSCs into microglia 94

4.3 C9ORF72-ALS iPSC microglia show C9ORF72 haploinsufficiency and express dipeptide repeat proteins 97

4.4 C9ORF72-ALS iPSC microglia have a dysregulated transcriptome 100

4.5 C9ORF72-ALS iPSC microglia show a phagocytosis deficit and lysosomal impairment 105

4.6 C9ORF72-ALS iPSC microglia have a pro-inflammatory cytokine/chemokine profile and upregulate NFκB 108

4.7 C9ORF72-ALS iPSC microglia consistently upregulate expression and release of MMP9 111

4.8 Discussion and conclusions 115

5 Investigating effects of C9ORF72-ALS iPSC microglia on motor neurons in co-culture 125

5.1 Introduction and aims 125

5.2 Analysis of unstimulated co-cultures of C9ORF72-ALS iPSC microglia and healthy control motor neurons 126

5.2.1 Motor neuron and microglia markers are equally expressed, while pro-MMP9 expression is upregulated in unstimulated co-cultures 126

5.2.2 Unstimulated C9ORF72-ALS iPSC microglia do not cause overt neurotoxicity to healthy motor neurons in co-culture 128

5.2.3 Unstimulated C9ORF72-ALS iPSC microglia show a dysregulated supernatant profile and upregulate DPP4 release in co-culture with healthy MNs 131

5.3 Analysis of LPS-primed co-cultures of C9ORF72-ALS iPSC microglia and healthy control motor neurons 133

5.3.1 LPS-primed co-cultures express motor neuron and microglia markers and upregulate p-NFκB, pro-MMP9, and active MMP9 133

5.3.2 LPS-primed C9ORF72-ALS iPSC microglia induce apoptosis of healthy control motor neurons in co-culture in an MMP9-dependent manner 136

5.3.3 LPS-primed co-cultures show no differences in synaptophysin expression, neuronal activity, or neurite density 138

5.3.4 LPS-primed co-cultures have a dysregulated cytokine profile and upregulate DPP4 release in an MMP9-dependent manner 139

5.4 Discussion and conclusions 141

6 Discussion and conclusions 147

6.1 The contribution of microglia to C9ORF72-ALS pathophysiology 148

6.2 MMP9 as a therapeutic target in C9ORF72-ALS 150

6.3 Microglial release of MMP9 and DPP4 as biomarker candidates for C9ORF72-ALS 151

6.4 *C9ORF72* HRE loss-of-function versus gain-of-function effects on microglia 153

6.5 The utility of human iPSC microglia for modelling ALS 154

6.6 Closing remarks 155

7 Bibliography 157

List of Figures

Figure 1.1: Pathophysiological role of microglia, in crosstalk with astrocytes and oligodendrocytes, according to rodent models of ALS. 28
Figure 1.2: Physiological interactions between neurons, microglia, and astrocytes in the brain and spinal cord. 33
Figure 3.1: Differentiation protocols for iPSC macrophage/microglia precursors and spinal motor neurons, and adaptations for motor neuron-microglia co-culture. 63
Figure 3.2: iPSC motor neuron-microglia co-cultures express key motor neuron markers. 65
Figure 3.3: Analysis of cleaved caspase 3 expression in iPSC motor neurons and microglia shows no difference between monocultures and co-cultures. 67
Figure 3.4: Analysis of CD11b expression in iPSC microglia in monoculture and co-culture. 68
Figure 3.5: Analysis of *MYB*, *PU.1*, and *RUNX1* in iPSC microglia in monoculture and co-culture using our and previously published RNA sequencing datasets. 70
Figure 3.6: Transcriptomic analysis demonstrates a microglial signature for iPSC microglia in monoculture and co-culture. 71
Figure 3.7: Transcriptomic comparison of iPSC microglia in monoculture and co-culture. 74
Figure 3.8: iPSC microglia grown in co-culture with MNs have a more ramified morphology than in monoculture. 75
Figure 3.9: iPSC microglia in monoculture and co-culture express macrophage-/microglia markers at gene level. 77
Figure 3.10: iPSC microglia express macrophage-/microglia markers by immunofluorescent staining. 78
Figure 3.11: iPSC microglia express key ALS-associated genes. 79
Figure 3.12: iPSC microglia are motile and phagocytically competent in co-culture. 81
Figure 3.13: iPSC microglia in co-culture respond to stimulation with morphological changes and clustering behaviour. 83
Figure 3.14: iPSC microglia in monoculture and co-culture release cytokines and chemokines in unstimulated conditions and alter their cytokine profile in response to stimulation. 86
Figure 4.1: iPSC microglia from C9ORF72-ALS patients show expected microglial morphology, express key microglial markers, and respond to pro-inflammatory stimulation with LPS. 96
Figure 4.2: iPSC microglia from C9ORF72-ALS patients show C9ORF72 haploinsufficiency and express the DPRs Poly(GA) and Poly(GP). 99
Figure 4.3: RNA sequencing of C9ORF72-ALS iPSC microglia shows transcriptomic differences with controls. 102
Figure 4.4: RNA sequencing of C9ORF72-ALS iPSC microglia identifies dysregulation of pathways associated with immune cell activation, cytokines, lysosomes, and the extracellular matrix. 104

Figure 4.5: Setup of an assay to analyse phagocytosis in C9ORF72-ALS microglia. 105
Figure 4.6: C9ORF72-ALS iPSC microglia show a phagocytosis deficit. 106
Figure 4.7: C9ORF72-ALS iPSC microglia show aberrant lysosomal morphology. 108
Figure 4.8: C9ORF72-ALS iPSC microglia upregulate the pro-inflammatory cytokines *IL1A*, *IL1B*, *IL6*, and *IL10*. 109
Figure 4.9: C9ORF72-ALS iPSC microglia upregulate the NFκB pathway and show a numeric increase in NLRP3. 111
Figure 4.10: C9ORF72-ALS iPSC microglia consistently upregulated release and expression of MMP9. 114
Figure 5.1: Co-cultures of WT motor neurons with C9ORF72 iPSC microglia express MN and microglia markers and upregulate pro-MMP9. 127
Figure 5.2: Co-cultures of WT motor neurons with C9ORF72 iPSC microglia show no differences in microglia and MN numbers, neuronal expression of cleaved caspase 3, and neurite density. 129
Figure 5.3: Co-cultures of WT motor neurons with C9ORF72 iPSC microglia show no differences in synaptophysin expression and neuronal activity. 130
Figure 5.4: Co-cultures of WT motor neurons with C9ORF72 iPSC microglia have a dysregulated cytokine profile and upregulate DPP4 release. 132
Figure 5.5: LPS-primed co-cultures of WT MNs and C9ORF72 microglia express MN and microglia markers and upregulate pro-MMP9, active MMP9, and p-NFκB. 135
Figure 5.6: LPS-primed C9ORF72 microglia induce apoptosis in co-cultured healthy motor neurons via an MMP9-dependent mechanism. 137
Figure 5.7: LPS-primed C9ORF72 microglia do not alter synaptophysin expression, neuronal activity, or neurite density of co-cultured healthy motor neurons. 139
Figure 5.8: LPS-primed co-cultures of C9ORF72 microglia and healthy motor neurons have a dysregulated cytokine profile and upregulate DPP4 release in an MMP9-dependent manner. 140

List of Tables

Table 2.1: Human induced pluripotent stem cell lines used in this thesis. 37
Table 2.2: Cell numbers used for different MN monoculture experiments. 38
Table 2.3: Cell numbers used for different microglia monoculture experiments. 40
Table 2.4: Cell numbers used for different co-culture experiments. 41
Table 2.5: Primers used for RT-qPCR experiments. 44
Table 2.6: Primary antibodies and dilutions used for Western blotting. 50
Table 2.7: Primary antibodies and dilutions used for immunofluorescence. 52
Table 2.8: Different cytokines/chemokines measured using the Proteome Profiler Human XL Cytokine Array Kit. 57

Abbreviations

a.u.	arbitrary units
AD	Alzheimer's disease
ALS	amyotrophic lateral sclerosis
AMPA	α-amino-3-hydroxy-5-methyl-4-isoxazolepropionic acid
ANOVA	analysis of variance
BCA	bicinchoninic acid
BDNF	brain-derived neurotrophic factor
BMP	bone morphogenic protein
BSA	bovine serum albumin
C1QA	C1q A chain
C9	C9ORF72
C9ORF72	chromosome 9 open reading frame 72
C9ORF72 microglia	C9ORF72 HRE mutant microglia
CALHM2	calcium homeostasis modulator family member 2
CC3	cleaved caspase 3
CCL2/MCP-1	C-C motif chemokine ligand 2
CD11B/14/16/68	cluster of differentiation molecule 11B/14/16/68
ChAT	choline acetyltransferase
CHI3L1	chitinase-3-like protein 1
CHI3L2	chitinase-3-like protein 2
CHIT1	chitotriosidase 1
CNS	central nervous system
CRISPR	clustered regularly interspaced short palindromic repeats
CSF	cerebrospinal fluid
CSF1R	colony stimulating factor 1 receptor
CXCL5/9/10	chemokine (C-X-C motif) ligand 5/9/10
DAPI	4′,6-diamidino-2-phenylindole
DAPT	(2S)-N-[(3,5-Difluorophenyl)acetyl]-L-alanyl-2-phenyl]glycine 1,1-dimethylethyl ester
DEG	differentially expressed gene
DENN	differentially expressed in normal and neoplastic cells
DIV	day *in vitro*
DPP4	dipeptidyl peptidase 4
DPR	dipeptide repeat protein
EB	embryoid body
ECM	extracellular matrix
EDTA	ethylenediaminetetraacetic acid
ELISA	enzyme-linked immunosorbent assay
FTD	frontotemporal dementia

FUS	fused in sarcoma
GAPDH	glyceraldehyde 3-phosphate dehydrogenase
GAS6	growth arrest specific 6
GDF-15	growth/differentiation factor 15
GDNF	glial-derived neurotrophic factor
GO	Gene Ontology
GPR34	G protein-coupled receptor 34
GSEA	gene set enrichment analysis
HC	healthy control
HRE	hexanucleotide expansion
HRP	horseradish peroxidase
IBA1	ionized calcium-binding adapter molecule 1
IFN-γ	Interferon-γ
IL1B/1A/4/6/10/13/32	interleukin 1B/1A/4/6/10/13/32
iPSC	induced pluripotent stem cell
KO	knock-out
LAMP1	lysosomal-associated membrane protein 1
LPS	lipopolysaccharides
M-CSF	macrophage colony-stimulating factor
MACS	magnetic-activated cell sorting
MEA	multi-electrode array
MERTK	MER Proto-Oncogene, Tyrosine Kinase
MMP9	matrix metalloproteinase-9
MMP9I	MMP9 inhibitor I
MN	motor neuron
MND	motor neuron disease
MSD	Meso Scale Discovery
mSOD1	mutant SOD1
NES	normalized enrichment score
NFκB	nuclear factor kappa B
NLRP3	NLR family pyrin domain containing 3
NO	nitric oxide
ON	overnight
P2RY12	purinergic receptor P2Y12
PBS	phosphate-buffered saline
PC	principal component
PCA	principal component analysis
PCR	polymerase chain reaction
PD	Parkinson’s disease
PEI	polyethylenimine
PET	positron emission tomography

PFA	paraformaldehyde
PROS1	protein S complement
RA	retinoic acid
RabGEF	guanine exchange factor of Rab proteins
RFP	red fluorescent protein
RIN	RNA integrity number
RIPA	radioimmunoprecipitation
RM	repeated measurement
RT	room temperature
RT-qPCR	reverse transcription quantitative real-time PCR
SAG	smoothened agonist
SCF	stem-cell factor
SDS-PAGE	sodium dodecyl sulfate polyacrylamide gel electrophoresis
SEM	standard error of the mean
SMCR8	Smith–Magenis chromosome region 8
SOD1	superoxide dismutase 1
TARDBP/TDP-43	TAR DNA-binding protein 43
TBS-T	Tris-buffered saline/0.1% Tween-20
TMEM119	transmembrane protein 119
TNF-α	tumor necrosis factor α
TREM2	triggering receptor expressed on myeloid cells 2
TUJ1	class III beta-tubulin
VEGF	vascular endothelial growth factor
WDR41	WD repeat-containing protein 41
WT	wild-type

1 Introduction: Amyotrophic lateral sclerosis and microglia

This introduction is largely based on two previously published review articles:

Vahsen, B.F., Gray, E., Thompson, A.G., Ansorge, O., Anthony, D.C., Cowley, S.A., Talbot, K., and Turner, M.R. (2021). Non-neuronal cells in amyotrophic lateral sclerosis - from pathogenesis to biomarkers. Nat Rev Neurol 17, 333-348.

Giacomelli, E., **Vahsen, B.F.,** Calder, E.L., Xu, Y., Scaber, J., Gray, E., Dafinca, R., Talbot, K., and Studer, L. (2022). Human stem cell models of neurodegeneration: From basic science of amyotrophic lateral sclerosis to clinical translation. Cell Stem Cell 29, 11-35.

1.1 Amyotrophic lateral sclerosis

Amyotrophic lateral sclerosis (ALS) is an adult-onset neurodegenerative disease that was first described by Jean-Martin Charcot approximately 150 years ago (Finger, 2005). After Alzheimer's disease (AD) and Parkinson's disease (PD), ALS is the third most frequent neurodegenerative disorder (Talbot et al., 2018). ALS affects the upper and lower motor neurons (MNs), i.e., the MNs projecting from the cortex to the brainstem and spinal cord and the MNs connecting the brainstem and spinal cord with the muscles, respectively (Hardiman et al., 2017). There are other disease variants affecting only a subset of these MNs, for instance, primary lateral sclerosis or progressive muscular atrophy, which predominantly show degeneration of the upper or lower MNs, respectively (Hardiman et al., 2017; Kiernan et al., 2011). Some authors therefore define ALS as a subtype of the umbrella term motor neuron disease (MND), but MND is often used synonymously for ALS (Hardiman et al., 2017).

The initial presentation of ALS varies between patients, depending on the individual pattern of MN degeneration – some first present with muscle weakness of the limbs, termed spinal-onset disease, while others initially show bulbar-onset disease characterised by dysarthria and dysphagia, i.e., difficulties with speech and swallowing (Hardiman et al., 2017). Albeit a very heterogeneous disease, ALS has a rapid course in a large body of patients, ultimately resulting in death typically due to neuromuscular respiratory failure (Chio et al., 2011). ALS is currently incurable and there are only two licensed therapeutic options for ALS patients, riluzole (globally) and edaravone (in the US and Japan). Both only lead to very moderate improvements in survival and rate of progression (Kiernan et al., 2021). At present, a variety of drug candidates are in development or undergoing clinical trials.

1.1.1 Epidemiology

ALS is considered a rare disorder and its incidence varies between different populations. In populations of European genetic heritage, the incidence of ALS has been determined to be approximately 3 per 100,000 individuals (Chio et al., 2013; Hardiman et al., 2017; Kiernan et al., 2011; Marin et al., 2014). In contrast, the incidence is lower in east and south Asia with <1 case per 100,000 individuals (Chio et al., 2013; Hardiman et al., 2017). There are some regions with substantially higher incidence of ALS, for example, the island of Guam, where the incidence has significantly decreased over the past three decades, possibly due to local changes in environmental factors (Hardiman et al., 2017; Spencer et al., 1987). The incidence also appears to vary by sex, with a slightly higher male-to-female ratio in ALS patients, typically reported to be between 1 and 2 (Longinetti

and Fang, 2019). The prevalence of ALS is estimated to be 5-7/100,000 in Europe, but similarly varies between regions (Chio et al., 2013; Talbot et al., 2018). It is important to note that the rapidly fatal nature of ALS understates the overall risk for an individual to develop ALS during their lifetime and is the underlying reason for its low prevalence. The actual life-time risk of ALS is as high as approximately 1:350 (Al-Chalabi et al., 2017; Feldman et al., 2022; Ryan et al., 2019).

ALS is a clinically heterogenous disease, which is reflected by substantial variation in the age of onset and disease duration. In populations of European genetic heritage, the mean age of onset is approximately 62-63 years, with a mean interval of 12 months between disease onset and diagnosis (Chio et al., 2013; Kiernan et al., 2011; Westeneng et al., 2018). However, some patients are diagnosed with ALS at a young age, some their 20s (Turner et al., 2012). Familial forms of ALS typically have an earlier onset of disease compared with sporadic ALS (Mehta et al., 2019). Survival for ALS patients shows great variation, from several months to more than 10 years (Westeneng et al., 2018). However, the average survival from symptom onset is very short, being approximately three years in Europe, and slightly longer in central Asia (Hardiman et al., 2017; Westeneng et al., 2018).

1.1.2 Clinical features

The clinical presentation of ALS is varied in terms of onset and progression, but the defining feature is the concomitant presence of both upper and lower MN symptoms (Kiernan et al., 2011). Upper MN signs include spasticity, loss of

voluntary control of muscle and brisk tendon reflexes, while the disturbance of lower MNs can manifest as fasciculations, muscle wasting and weakness (Kiernan et al., 2011). Symptoms typically progress from a rather focal to more widespread disease. About 70% of patients have limb-onset disease with upper and lower MN signs in the limbs, while approximately 25% show a bulbar-onset with speech and swallowing difficulties (Kiernan et al., 2011). About 5% of ALS patients have initial trunk or respiratory involvement (Kiernan et al., 2011). The identification of these different phenotypes has important implications for the prognosis and survival of ALS patients. Predictors of longer survival are, for instance, younger age at symptom onset or limb-onset, while early respiratory muscle dysfunction or an older age at symptom onset correlate with reduced survival (Talbot, 2009). In addition to motor symptoms, up to 50% of ALS patients develop cognitive, principally behavioural, impairments over the disease course (Beeldman et al., 2018; Elamin et al., 2013; Hardiman et al., 2017; Phukan et al., 2012). Behavioural variant frontotemporal dementia (FTD) with deficits in social cognition and language with relative preservation of memory is present in 8-14% of ALS cases (Beeldman et al., 2018).

The progression of symptoms typically results in patients necessitating assistance with activities of daily living. The progressive impairment of respiratory function ultimately requires non-invasive or invasive ventilation. Several different staging system and rating scores have been developed to monitor and assess clinical function and progression, which are of particular importance for clinical trials. These include primarily the widely used Amyotrophic Lateral Sclerosis

Functional Rating Score-Revised (ALSFRS-R) (Cedarbaum et al., 1999) but also more recently developed scores such as the King's staging system (Roche et al., 2012). The ALSFRS-R quantifies functional deficits in 12 aspects of physical function, e.g., speech difficulties (from 48 = no deficits to 0 = no ability), whereas the King's staging system assesses the number of affected regions and therefore the anatomical spread of ALS (from Stage 1 = early disease with one region involved to Stage 5 = death).

1.1.3 Genetic variants

Approximately 90% of ALS patients have no family history of ALS or FTD, and these cases are therefore considered sporadic (Talbot et al., 2018). However, in approximately 10% of patients, ALS is a familial disease, mostly with an autosomal-dominant inheritance pattern, for which a causative genetic variant, in a multitude of different genes, can be identified in 70-80% (Al-Chalabi et al., 2017; Talbot et al., 2018). On the other hand, genetic variants are also found in a proportion of apparently sporadic ALS cases, suggesting that the penetrance of these mutations is highly variable (Talbot et al., 2018). At present, approximately 40 genes have been associated with ALS due to toxic gain-of-function or loss-of-function mutations (Feldman et al., 2022). In Europe, in both apparently sporadic and familial ALS, the commonest mutation is a dynamic hexanucleotide expansion (HRE) of GGGGCC (G_4C_2) repeats in the first intron of *C9ORF72* (chromosome 9 open reading frame 72) (DeJesus-Hernandez et al., 2011; Renton et al., 2011). HREs in *C9ORF72* account for 20-50% of familial and 3-5% of sporadic ALS, respectively (Kiernan et al., 2021), and also represent the most common genetic variant associated with FTD (DeJesus-Hernandez et al., 2011),

connecting ALS and FTD on a genetic level. In another 10-20% of familial and 1-2% of sporadic ALS cases, mutations are identified in *SOD1* (superoxide dismutase 1) (Rosen et al., 1993), while in 5% of familial and <1% of sporadic ALS (Sreedharan et al., 2008; Vance et al., 2009), mutations are found in *TARDBP* (encoding for the 43 kDa transactive response DNA binding protein TDP-43) and *FUS* (Fused In Sarcoma). Less commonly mutated genes include *MAT3*, *OPTN*, *UBQLN2*, *TBK1*, and *NEK1*, amongst others (Kiernan et al., 2021).

1.1.4 Pathophysiology and pathology

Research has primarily focused on understanding the role of ALS-associated gene variants, as a more tractable point of departure, hoping findings would ultimately be transferable into sporadic ALS. For this, a combination of human post mortem, biomarker and neuroimaging studies, animal models and, more recently, stem cell models has been employed. Focusing on their role in neurons, the pathophysiological processes associated with these gene variants can be broadly grouped into the following main categories: mitochondrial dysfunction and oxidative stress, impaired RNA metabolism, cytoskeletal or trafficking defects, and altered proteostasis or autophagy (Feldman et al., 2022; Mejzini et al., 2019; Rossi et al., 2016).

Despite all ongoing research efforts and the discovery of the aforementioned dysfunctional processes, the underlying cause of ALS is still not well understood. However, nuclear clearing and cytoplasmic aggregation of TDP-43 has been identified as the characteristic neuropathological hallmark in neuronal and non-

neuronal cells in approximately 97% of all ALS cases, both familial and sporadic, with the notable exception of the combined 3% of cases caused by mutations in the *FUS* and *SOD1* genes (Neumann et al., 2006). Importantly, 40-50% of FTD cases also show TDP-43 aggregation, reinforcing the notion that FTD and ALS show significant overlap clinically but also biologically and pathologically. More widely, the presence of protein inclusions is a common feature of neurodegenerative disorders, considering that aggregated α-synuclein and β-amyloid are also found in the related neurodegenerative disorders PD and AD, respectively. However, the underlying mechanisms for TDP-43 aggregation in ALS remain poorly understood (Suk and Rousseaux, 2020).

One of the puzzling features of ALS is the fact that it is an adult-onset disorder, even though gene mutations increasing the disease risk are already present at conception and, in fact, some mutation carriers do not develop the disease at all. Furthermore, the same mutation, for instance, the HRE in *C9ORF72*, can result in pleiotropic phenotypes, where patients can develop ALS, FTD, both, or no disease at all. To explain this phenomenon, a multi-step model has been proposed that includes six sequential steps ultimately leading to the manifestation of ALS (Al-Chalabi et al., 2014). According to this model, different mutated genes require a distinct number of other steps to be completed in addition to the gene mutation, providing an explanation for the different penetrance of mutations in different genes (Chio et al., 2018). This model suggests that a combination of environmental factors and genetics ultimately determine an individual's risk of developing ALS. For instance, mutations in *SOD1* seem to represent four out of the six total

steps, with the two additional steps likely provided by environmental factors (Chio et al., 2018). Environmental risk factors that have been associated with an increased ALS risk include cigarette smoking, physical trauma, or participation in professional sports (Alonso et al., 2010; Armon, 2009; Chio et al., 2018; Ingre et al., 2015). The model might also serve as an explanation as to why a specific population of neurons starts the apparent degenerative process first if these neurons are where all steps have been completed.

Another important aspect to consider regarding the pathophysiology of ALS is that the central nervous system (CNS) contains a diversity of cell types in addition to MNs. As ALS is primarily a disease of the MNs, research into ALS has been centred around improving understanding of how and why MNs selectively degenerate in ALS for decades. However, non-neuronal cells execute major functions in brain physiology, and there is now increasing appreciation that they also play a key role in ALS pathophysiology (reviewed by several recent review articles, for instance, (Beers and Appel, 2019; Clarke and Patani, 2020; Franklin et al., 2021; Serio and Patani, 2018) in addition to our review (Vahsen et al., 2021)). In particular, microglia have been implicated in ALS pathophysiology, and the evidence for their role from different model systems will be discussed below.

1.1.5 *C9ORF72* and the hexanucleotide repeat expansion mutation

The discovery of a dynamic HRE of GGGGCC (G_4C_2) repeats in the first intron of *C9ORF72* as the commonest genetic variant associated with ALS and FTD in Europe (DeJesus-Hernandez et al., 2011; Renton et al., 2011) was a milestone

in the more recent history of ALS research. Of note, FTD or ALS due to HREs in *C9ORF72* are very uncommon in the Middle East and Asia, suggesting a different genetic architecture (Balendra and Isaacs, 2018; Majounie et al., 2012; Woollacott and Mead, 2014). In the past 11 years since its discovery, much research has been done on the clinical phenotype and the underlying pathophysiology.

There is substantial heterogeneity in the age of onset and disease course in ALS/FTD patients with HREs in *C9ORF72*. The age of onset ranged from 27 to 83 years, while the disease duration showed a range from 1 to 22 years in previous studies (Balendra and Isaacs, 2018; Majounie et al., 2012; Woollacott and Mead, 2014). In rare cases, *C9ORF72* HREs can also cause other neurodegenerative phenotypes, more in keeping clinically with PD or AD (Balendra and Isaacs, 2018; Woollacott and Mead, 2014). HREs in *C9ORF72* are also found in healthy individuals, but in >95%, they do not exceed 11 repeats (Harms et al., 2013; Rutherford et al., 2012; van der Zee et al., 2013). There is no clear cut-off for a pathological repeat length, but 30 repeats is used as the threshold in most studies, and the repeat length can reach hundreds to thousands of repeats in C9ORF72-ALS/FTD patients (Balendra and Isaacs, 2018; Beck et al., 2013; Harms et al., 2013; Suh et al., 2015; van Blitterswijk et al., 2013). The HRE in *C9ORF72* is a heterozygous mutation transmitted with an autosomal-dominant inheritance pattern and age-dependent and incomplete penetrance, reaching almost 100% penetrance by the ninth decade (Murphy et al., 2017; Smeyers et al., 2021). There is conflicting evidence as to whether the size of the expansion

correlates with the age of disease onset (Smeyers et al., 2021). Furthermore, the repeat size seems to vary between different brain regions and can differ between the CNS and peripheral blood due to somatic instability of the mutation (Balendra and Isaacs, 2018).

The *C9ORF72* gene is found on the short arm of chromosome 9, and there is great homology between the human, mouse, and rat genes (Braems et al., 2020). *C9ORF72* has 11 exons and is transcribed into three different variants, termed V1-3, owing to different transcription start sites and alternative splicing (Balendra and Isaacs, 2018; Braems et al., 2020). The HRE is located in the first intron of variants 1 and 3 and in the promoter region of variant 2 (Balendra and Isaacs, 2018; Braems et al., 2020). Translation of these transcripts leads to two different isoforms: variant 1 is translated into a short isoform (222 amino acids, 24 kDa), while the long isoform stems from variants 2 and 3 (481 amino acids, 54 kDa) (Balendra and Isaacs, 2018; Braems et al., 2020).

Comparing its expression in different tissues, (Rizzu et al., 2016) found *C9ORF72* mRNA to be substantially more highly expressed in $CD14^+$ monocytes than in the CNS. Conversely, the C9ORF72 protein had the highest expression in the brain and spinal cord comparing different mouse tissues (Frick et al., 2018). Comparing different murine immune cells, C9ORF72 expression was the highest in macrophages and dendritic immune cells (O'Rourke et al., 2016), suggesting an important role in macrophage biology. C9ORF72 has been found in both the cytoplasm and nucleus, and has also been associated with various organelles,

including early and late endosomes, and lysosomes (Braems et al., 2020; Frick et al., 2018; Laflamme et al., 2019). However, several antibodies used in these studies have been shown to be non-specific, and thus the results have to be treated with caution (Laflamme et al., 2019). Using extensively validated antibodies, at least the presence of C9ORF72 in the cytosol and association with membranes including lysosomes (and phagosomes in macrophages) was confirmed (Laflamme et al., 2019).

C9ORF72 has been shown to have structural homology with 'differentially expressed in normal and neoplastic cells' (DENN) proteins, indicating that its physiological role is that of a guanine exchange factor for Rab proteins (RabGEF) (Levine et al., 2013). RabGEFs activate Rab proteins which are important for vesicular trafficking, and C9ORF72 has been connected with the autophagy process and the endo-lysosomal system by various research groups, in line with its subcellular localisation (Balendra and Isaacs, 2018; Braems et al., 2020; Smeyers et al., 2021). Specifically, C9ORF72 forms a complex with Smith–Magenis chromosome region 8 (SMCR8) and WD repeat-containing protein 41 (WDR41) (Sullivan et al., 2016), and this complex has been connected with the regulation of multiple Rab proteins, such as Rab5, Rab7, and Rab11, amongst others (Pang and Hu, 2021; Smeyers et al., 2021).

The HRE in *C9ORF72* has been shown to have three major pathophysiological consequences. Firstly, the expanded G_4C_2 repeats are transcribed into repetitive RNA bidirectionally, resulting in the formation of sense and antisense RNA foci

that exert gain-of-function toxicity through sequestration of RNA-binding proteins (Donnelly et al., 2013; Mizielinska et al., 2013; Smeyers et al., 2021). Secondly, through a mechanism termed repeat-associated non-ATG (RAN) translation, these repetitive RNAs can be translated to form five different dipeptide repeat proteins (DPRs). Sense RNA is translated into Poly-GR, Poly-GP, and Poly-GA, while antisense RNA leads to the translation of Poly-PR, Poly-GP, and Poly-PA (Lagier-Tourenne et al., 2013; Mori et al., 2013b; Zu et al., 2013). DPRs form TDP-43 negative, p62-positive cytoplasmic protein inclusions in addition to the canonical TDP-43 positive inclusions that are also found in C9ORF72-ALS (Balendra and Isaacs, 2018). Poly-GA represents the most frequent form of DPRs, followed by Poly-GP and Poly-GR (Mackenzie et al., 2015; Mori et al., 2013a; Mori et al., 2013b). Several model systems suggest that DPRs can cause neurodegeneration through gain-of-function toxicity-mediated disturbance of various cellular mechanisms such as translation, with the arginine-rich Poly-GR and Poly-PR deemed the most toxic (Balendra and Isaacs, 2018). However, in contrast with TDP-43 pathology, the burden of DPR inclusions does not generally seem to correlate with neurodegeneration in C9ORF72-ALS/FTD, and their contribution to aetiopathogenesis remains hotly debated (Balendra and Isaacs, 2018).

In addition to these gain-of-function mechanisms, the expanded repeats inhibit transcription of *C9ORF72*, resulting in C9ORF72 haploinsufficiency and loss-of-function (DeJesus-Hernandez et al., 2011). There is some variability across different studies regarding the degree of reduction in *C9ORF72* levels. Considering

the total *C9ORF72* transcript levels, an overall decrease of approximately 50% has been found in the frontal cortex due to significant decreases in V1 and V2 expression in a recent meta-analysis (Braems et al., 2020). On the other hand, overall C9ORF72 protein levels were found to be decreased by approximately 25% in the frontal cortex of C9ORF72-ALS/FTD patients across different studies (Braems et al., 2020). However, these results have to be interpreted with some caution, considering that many C9ORF72 antibodies employed to determine these expression patterns were found to be unreliable by (Laflamme et al., 2019). Furthermore, these data do not provide a detailed assessment of the degree of C9ORF72 haploinsufficiency in disease-relevant cell types.

Studies have also analysed the presence of the hallmarks of C9ORF72-ALS pathology in non-neuronal cells. RNA foci have been detected in both neuronal and non-neuronal cells including microglial cells in tissue from C9ORF72-ALS patients (Lagier-Tourenne et al., 2013; Mizielinska et al., 2013), but DPRs have thus far only been described in neuronal cells post mortem (Rostalski et al., 2019). To my knowledge, there are no studies that have specifically looked at whether C9ORF72 haploinsufficiency is found in non-neuronal cells in the CNS in post mortem tissue.

Since the discovery of these three main consequences of the HRE in *C9ORF72*, numerous studies have aimed to disentangle the contribution of cellular mechanisms to neurodegeneration in C9ORF72-ALS/FTD. To investigate the pathophysiological consequences of the *C9ORF72* HRE on MNs, cellular model

systems have been employed. MNs derived from human induced pluripotent stem cells (described as a model system for ALS in more detail in chapter 1.4) from patients carrying HRE mutations in *C9ORF72* replicate key pathological features including DPR expression, presence of RNA foci, and varying degrees of C9ORF72 haploinsufficiency (Almeida et al., 2019; Donnelly et al., 2013; Gendron et al., 2017; Sareen et al., 2013). TDP-43 mislocalisation and aggregation has not been conclusively described in MNs generated from C9ORF72-ALS patients *in vitro*, possibly due to the lack of cell maturity. Crucially, these models have allowed to investigate and unravel the downstream consequences of the *C9ORF72* HRE mutation on cellular pathways. The combined evidence from these studies has shown that the *C9ORF72* HRE mutation leads to MN cell death, impaired nucleocytoplasmic transport, sensitivity to glutamate toxicity, altered firing and electrophysiological activity, and dysregulated vesicular and synaptic trafficking in MNs (Giacomelli et al., 2022; Guo et al., 2017). Similarly, non-neuronal cells displayed different cellular phenotypes in experimental models for C9ORF72-ALS. While the discussion of phenotypes in C9ORF72-ALS astrocytes is beyond the scope of this introduction and was reviewed by us in detail in (Giacomelli et al., 2022) and (Vahsen et al., 2021), the findings regarding the role of microglia in C9ORF72-ALS are discussed in detail in chapter 1.3.

1.2 Microglia

Microglia, first described by Pio del Rio Hortega in 1919 (Sierra et al., 2019), represent one of the non-neuronal cell types in the CNS. Together with astrocytes, oligodendrocytes and others, they form a group of non-neuronal cell types

called glia (derived from the Greek word for 'glue'). The exact number of non-neuronal cell types in the CNS remains a matter of debate – while the prevailing dogma has been for a long time that glial cells vastly outnumber neurons in the CNS, recent evidence suggests a glia-neuron ratio closer to 1:1 (von Bartheld et al., 2016).

1.2.1 Origin, role in brain physiology, markers, and states

Microglia are the resident macrophages of the CNS, representing approximately 5-10% of glial cells in the CNS (Pelvig et al., 2008; von Bartheld et al., 2016). Originating from yolk sac-derived precursors in a process called primitive haematopoiesis, they migrate into the CNS during neurodevelopment (Ginhoux et al., 2010). Therefore, microglia have a different developmental origin from blood monocytes and blood macrophages, which originate from aorta-gonad-mesonephros region-derived definitive haematopoietic stem cells in a process termed definitive haematopoiesis (Alliot et al., 1999; Ginhoux et al., 2010; Ginhoux and Prinz, 2015). Yolk sac-derived macrophages can be distinguished from adult, definitive, blood monocyte-derived macrophages through the expression pattern of *MYB* (Buchrieser et al., 2017; Kierdorf et al., 2013; Vanhee et al., 2015). Whereas blood-monocyte derived macrophages are *MYB*-dependent, yolk sac-derived macrophages like microglia are considered to be *MYB*-independent. In the CNS, microglia maintain their population by self-renewal (Bruttger et al., 2015; Ginhoux et al., 2010).

Recent transcriptomic approaches have aimed at better defining microglia identity, in order to distinguish them from other CNS cells and brain-associated

macrophages. For instance, (Galatro et al., 2017) identified a core list of ~1300 signature genes for microglia extracted from human post mortem tissue. Although it is clear that microglial identity is best defined through their whole transcriptional identity (Li et al., 2019; Zhang et al., 2014), these efforts have led to the definition of three main markers that can be used to identify microglia for staining or reverse transcription quantitative real-time polymerase chain reaction (RT-qPCR) experiments: the cytoplasmic ionized calcium-binding adapter molecule 1 (IBA1), and the surface markers transmembrane protein 119 (TMEM119) and purinergic receptor P2Y12 (P2RY12). IBA1 is a more generic macrophage marker, together with additional macrophage markers such as cluster of differentiation molecule 11B (CD11B), MER Proto-Oncogene, Tyrosine Kinas (MERTK) or Triggering receptor expressed on myeloid cells 2 (TREM2), and is widely used in immunofluorescent staining experiments as it stains the whole cell. P2YR12 and TMEM119 are deemed to be largely microglia-specific and are associated with a homeostatic state (Bennett et al., 2016; Butovsky et al., 2014; Melief et al., 2012).

Historically, microglia were thought to be dormant cells under homeostatic conditions, but it is now commonly accepted that they are continuously active and constantly examine their CNS environment using highly motile processes called ramifications (Nimmerjahn et al., 2005). They execute crucial functions for the maintenance of the CNS and neuronal homeostasis, including surveillance, provision of nurture and support to neurons via secretion of soluble factors, synaptic pruning, and clearance of dead cells or misfolded proteins via phagocytosis (Colonna and Butovsky, 2017). According to an old concept, microglia can adopt a resting or

an activated state – if any disturbance to CNS homeostasis is detected by them, they would become activated, demonstrated by rapid changes in cell morphology, altered gene expression, and functional behaviour (Butovsky and Weiner, 2018; Li and Barres, 2018). Simplistically, the resting microglial state is often referred to as 'M0', while activation has classically been conceptualised as two opposing states: a pro-inflammatory 'M1' and an anti-inflammatory 'M2' phenotype (Hu et al., 2015; Mantovani et al., 2005; Ransohoff, 2016). 'M1' microglia were associated with the production of pro-inflammatory cytokines and the induction or exacerbation of neuron dysfunction, while 'M2' microglia were deemed neuroprotective (Cherry et al., 2014; Tang and Le, 2016). However, this polarisation is now viewed as an oversimplification, and microglial activation should rather be seen as a spectrum depending on the circumstances and environmental challenge. A recent initiative (Paolicelli et al., 2022) bringing together many leaders and experts in the microglia field has therefore called for a change of microglial terminology, suggesting that the dichotomy 'resting' versus 'active' should be avoided altogether. Their consensus statement calls for the combination of multiple different readouts, using morphological analysis tools and multiple 'omics' techniques coupled with functional experiments to define microglial states, aiming to avoid simplistic terms like 'M1', 'M2', or others.

1.2.2 Role in neurodegeneration

Microglial activation was described in post mortem tissue from AD, PD, ALS, and other neurodegenerative disease patients already in the 1980s (McGeer et al., 1988a; McGeer et al., 1988b; McGeer et al., 1987; McGeer et al., 1993). However, it was mainly in this century that microglia have received increasing

attention in the context of neurodegeneration, moving away from the highly neuron-centric research in the past. This shift has led to the discovery of key roles for microglia in neurodegenerative diseases through genetics and preclinical models. For instance, recent genome-wide association studies have provided a link with microglia in AD, as variants in *TREM2* increased the disease risk by 3-4-fold (Guerreiro et al., 2013; Jonsson et al., 2013). On a functional level, through evidence from various experimental models across the different neurodegenerative diseases, the involvement of microglia in neurodegeneration has been suggested to follow two themes. Firstly, aberrant or misfolded proteins, for example the β-amyloid found in AD, trigger microglial activation, resulting in initial attempts to clear away these agents. However, the properties and persistent production of these proteins elicit an aberrant microglial response with the production of pro-inflammatory cytokines, leading to neurodegeneration and neurotoxicity (Hickman et al., 2018). Secondly, the cell-autonomous expression of neurodegenerative disease-associated mutations within microglia themselves, for instance, variants in *TREM2*, negatively affect the intrinsic properties of microglia, such as their phagocytic or degradative ability, or trigger an upregulation of inflammatory pathways, resulting in neurotoxicity and neurodegeneration (Hickman et al., 2018). In the following section, I will review the current evidence for the pathophysiological role of microglia in ALS in more detail.

1.3 Microglia in ALS

Initial research efforts aimed to understand the role of microglia in human ALS using neuroimaging and post mortem techniques. With the stepwise discovery of

key genes associated with ALS, it has emerged that several of these, notably *SOD1*, *C9ORF72,* and *TARDBP*, have high expression in microglia (Boillee et al., 2006; O'Rourke et al., 2016; Yvanka de Soysa et al., 2022). Consequently, various preclinical models have been employed to study the cell-autonomous effect of variants in these genes on microglia as well as the non-cell-autonomous effects of microglia on neurons. In addition, these efforts have been complemented with fluid biomarker measurements, using cerebrospinal fluid (CSF), serum, and other biofluids, from human ALS patients.

1.3.1 Post mortem tissue, neuroimaging, and fluid biomarkers

Using positron emission tomography (PET) imaging with PK11195, a relative selective radiotracer for the 18 kDa translocator protein expressed by activated microglia, widespread cerebral activation of microglia was found in the motor cortex, pons, dorsolateral prefrontal cortex and thalamus of people with ALS (Turner et al., 2004). Microglial activation in the motor cortex correlated with the clinical burden of upper MN signs (Turner et al., 2004). Since this study was conducted before the majority of genetic variants associated with ALS, notably the HRE in *C9ORF72*, were discovered, it did not provide a detailed account of microglial activation across different mutations. Two more recent studies using PET with other radioligands (Corcia et al., 2012; Zurcher et al., 2015) also corroborated increased microglial activation in the motor cortex and other brain areas of people living with ALS. A recent study using PET on asymptomatic and symptomatic *SOD1* mutation carriers showed microglial activation in several cortical and subcortical areas, including the primary motor cortex at the symptomatic stage (Tondo et al., 2020). While these neuroimaging data have to be interpreted with

some caution due to the only relative selectivity of radiotracers, they suggest a key implication of microglia in people living with ALS, raising the question of whether microglial activation is beneficial or detrimental or a primary or secondary phenomenon in ALS.

Other studies have evaluated microglial activation in post mortem tissue. These experiments focus on end stages of the disease and might therefore be biased, but they allow for the analysis of pathophysiological processes with more cell-specificity and at single cell resolution in disease-relevant tissue. Examination of CNS tissue from sporadic and SOD1-ALS patients demonstrated elevated levels of macrophage/microglial transcripts and increased density of cluster of differentiation 68 (CD68)-positive macrophage/microglia cells close to MNs (Henkel et al., 2004). A more systematic analysis showed increased activation of IBA1- and CD68 positive microglia in frontotemporal areas of patients with ALS with dementia or impaired executive function – mostly sporadic in this study – which correlated with enhanced neuronal loss, TDP-43 pathology, and executive impairment (Brettschneider et al., 2012a). Furthermore, a correlation between IBA1 and CD68-positive microglial activation with disease progression and clinical upper MN deficits was demonstrated, with particularly pronounced microglial activation in *C9ORF72* HRE carriers (Brettschneider et al., 2012b). These post mortem findings reinforce the notion that microglial activation is a key feature of ALS.

In a complementary approach, several studies have analysed the release of biochemical markers associated with macrophages and microglia into the biofluids

of ALS patients including the CSF and serum. In particular, the release of three chitinases, chitotriosidase 1 (CHIT1), chitinase-3-like protein 1 (CHI3L1) and chitinase-3-like protein 2 (CHI3L2), has received substantial attention in recent years. There are other candidates, for instance, C-C motif chemokine ligand 2 (CCL2) that have been suggested as potential biomarkers, but I will focus here on the evidence for chitinase involvement in ALS, as their increased levels has been cross-validated by different groups. The CSF levels of the three chitinases showed a correlation with disease progression rate and the levels of phosphorylated neurofilament heavy chain, a marker for neuroaxonal damage (Thompson et al., 2018). CHIT1 is thought to be expressed in macrophages, while CHI3L1 appears to be predominantly expressed in astrocytes (Andres-Benito et al., 2018; Steinacker et al., 2018; Varghese et al., 2013; Vu et al., 2020). CHIT1 levels in the CNS were associated with faster disease progression rate and shortened survival and increased between the pre-symptomatic and symptomatic period in ALS patients (Gille et al., 2019; Thompson et al., 2019; Thompson et al., 2018). While the cellular source of these chitinases is at the moment not entirely clear, CHIT1 release might be an indication of macrophage/microglial activation in the CNS (Gaur et al., 2020). These data could therefore suggest that microglial activation represents more of a secondary response to neuronal image than a primary disease driver. Several preclinical models have provided further insights and will be reviewed in the following section.

1.3.2 Disease models

Aiming to answer if the observed microglial activation in ALS patients is beneficial or detrimental and a primary or secondary phenomenon, researchers have

employed multiple rodent models for ALS, investigating mutations in *SOD1*, *TARDBP*, and *C9ORF72*. Transgenic mice expressing a form of mutant SOD1 (mSOD1) have been widely made use of since the discovery of ALS-associated mutations in *SOD1* in the 1990s. They recapitulate some of the key features of human ALS, including progressive motor abnormalities and paralysis, and display protein aggregation, MN degeneration, and gliosis (Gurney et al., 1994; Philips and Rothstein, 2015; Turner and Talbot, 2008).

1.3.2.1 SOD1 models

Replicating findings in neuroimaging and post mortem, microglial activation is a key feature of mSOD1 models, and occurs well before the onset of clinical symptoms in some studies (Alexianu et al., 2001; Hall et al., 1998; Philips and Robberecht, 2011). Whereas some studies found that the selective expression of different forms of mSOD1 in MNs was insufficient to induce the degeneration of MNs (Lino et al., 2002; Pramatarova et al., 2001), others demonstrated that increasing the transgene expression in MNs elicited a mild ALS phenotype (Jaarsma et al., 2008; Wang et al., 2008). The expression of $SOD1^{G37R}$ in MNs determined disease onset and early disease progression in another study, while deletion of $SOD1^{G37R}$ from microglia did not substantially alter the early phases of the disease but slowed later disease progression (Boillee et al., 2006). Similarly, transplanted wild-type (WT) microglia slowed MN loss and prolonged disease duration and survival compared with $SOD1^{G93A}$ microglia (Beers et al., 2006). In keeping with these results, short hairpin RNA-mediated silencing of $SOD1^{G93A}$ in MNs had no effect on disease progression but delayed the onset of disease (Ralph et al., 2005). These data suggest that non-cell-autonomous

factors presented by microglia contribute to disease progression in ALS pathogenesis in mSOD1 models, more likely as a secondary toxic response to neuronal damage than a primary driver of disease. This view was corroborated by additional studies that looked at the specific expression of pro-inflammatory and anti-inflammatory markers and mediators in microglia from mSOD1 models at different stages of the disease. At disease onset, microglia isolated from $SOD1^{G93A}$ mice showed higher expression of markers associated with the neuroprotective 'M2' phenotype, while 'M1' marker expression was lower, compared with microglia at end-stage disease (Liao et al., 2012). Similarly, the $SOD1^{G93A}$ microglia isolated at disease onset were neuroprotective in co-culture with MNs, while at end-stage disease they caused neurotoxicity (Liao et al., 2012).

Several studies investigated the detailed molecular mediators of non-cell-autonomous microglial toxicity. Compared with cultured WT microglia, the release of reactive oxygen species and nitric oxide (NO) was increased in $SOD1^{G93A}$ microglia, while the release of the neurotrophic factor insulin-like growth factor 1 was reduced (Beers et al., 2006; Xiao et al., 2007) (Figure 1.1). Inhibiting inducible NO synthase using the L-NIL inhibitor increased MN survival in co-culture (Xiao et al., 2007). In addition, LPS-stimulated primary $SOD1^{G93A}$ microglia released more tumour necrosis factor α (TNF-α) compared with WT controls (Weydt et al., 2004). Similarly, when $SOD1^{G93A}$ microglia were treated with $SOD1^{G93A}$ recombinant protein, they showed increased release of TNF-α, superoxides, and interleukin 1b (IL1B) compared with WT SOD1, resulting in toxicity to MNs in co-culture in a toll-like receptor-dependent mechanism (Zhao et al., 2010). These data

from multiple studies suggest that mSOD1 microglia upregulate pro-inflammatory and potentially neurotoxic mediators, through a direct cell-autonomous effect of the mutation within microglia but also in response to mSOD1, which might be released from other cells *in vivo*. Knock-down of *Tnf-α* in mice expressing different forms of mSOD1 did not improve the disease course in mice, while inhibition of *Il1b* showed model-dependent improvements (Gowing et al., 2006; Meissner et al., 2010; Nguyen et al., 2001; Weydt et al., 2004). This suggests that other mediators are likely to contribute to the neurotoxic effect of mSOD1 microglia.

It is important to consider that most of these studies were conducted at a time when RNA sequencing was not yet widely available. Hence, they focused on the expression of specific pro-inflammatory or anti-inflammatory markers, which is likely to be a biased and is not considered a state-of-the-art approach in microglia research. To explore the properties of mSOD1 microglia in a more unbiased manner, one study analysed the transcriptome of $SOD1^{G93A}$ microglia by RNA sequencing (Chiu et al., 2013). As would be expected, this study demonstrated that the profile of $SOD1^{G93A}$ is complex, showing concurrent expression of neuroprotective and neurotoxic markers at different time points during disease progression including concomitant upregulation of the protective *Igf1* and *Grn* genes and the pro-inflammatory *Tnf-α*, *Il1b*, and *Mmp12* genes, amongst others. This study shows that the profile of mSOD1 microglia is dysregulated in a more complex manner than the assessment of a few markers can reliably reflect and suggests that ‘omics experiments should be conducted to accurately determine the profile of microglia in models for ALS in future studies. Although most evidence

regarding the role of microglia in ALS comes from mSOD1 models, there are additional recent studies that have investigated TDP-43 and C9ORF72 models, which I will discuss below.

1.3.2.2 TDP-43 models

One focus of studies on microglia in TDP-43 models for ALS has been the microglial response to WT or mutant TDP-43. Primary microglia responded to both WT and mutant TDP-43 with the upregulation of pro-inflammatory markers such as TNF-α and IL1B in an nuclear factor kappa B (NFκB) and NLR family pyrin domain containing 3 (NLRP3) inflammasome-dependent manner, but mutant TDP-43 elicited a stronger response (Deora et al., 2020; Zhao et al., 2015). Similarly, TDP-43 aggregates added to primary microglia were taken up and induced the release of pro-inflammatory mediators such as IL1b (Leal-Lasarte et al., 2017). In co-culture, microglia caused toxicity to MNs after the addition of mutant TDP-43^{A315T} (Zhao et al., 2015) (Figure 1.1). These findings show substantial overlap with the pro-inflammatory markers expressed in mSOD1 microglia. However, they do not provide information on the role of TDP-43 in microglia including the potential effects of TDP-43 aggregates or expression of mutant TDP-43. Aggregated TDP-43 is found in microglia in ALS patients in post mortem tissue (Nolan et al., 2020), but its effect on human microglia function remains currently unclear. Interestingly, conditional knock-out (KO) of *Tardbp* in mice lead to increased clearance of amyloid-β and enhanced loss in an AD model (Paolicelli et al., 2017), indicating a role for TDP-43 in microglial phagocytosis.

Other models have analysed the microglial response to TDP-43 proteinopathy in neurons. In mice with reversible induction of TDP-43 aggregates in neurons, progressive motor dysfunction and MN loss was observed, but this was associated with only subtle microglial changes (Spiller et al., 2018). When expression of mutant TDP-43 in neurons was halted, this led to a drastic proliferation of microglia, clearance of TDP-43 aggregates in neurons, and functional improvements. Depletion of microglia using PLX3397, a colony stimulating factor 1 receptor (CSF1R)/kit inhibitor, prevented functional recovery, indicating a neuroprotective effect of microglia in this model. However, whether this also holds true for a human and more physiological model with concomitant neuronal and microglial dysfunction, remains unclear.

1.3.2.3 C9ORF72 models

C9ORF72 is very highly expressed in microglia (O'Rourke et al., 2016; Yvanka de Soysa et al., 2022). Initial studies have therefore primarily focused on the effects of C9ORF72 haploinsufficiency on microglia. For this, *C9orf72* KO mice have been developed. While they do not develop clinical symptoms of ALS or neurodegeneration, they have an inflammatory phenotype (Choi et al., 2019a; Jiang et al., 2016; O'Rourke et al., 2016). Specifically, progressive lymphadenopathy, splenomegaly, and upregulation of pro-inflammatory cytokines was observed in peripheral immune cells (Burberry et al., 2016; Jiang et al., 2016; O'Rourke et al., 2016). Looking specifically at microglia, upregulation of microglial activation pathways, increased levels of IL1b and IL6, and accumulation of lysosomal markers was found (Lall and Baloh, 2017; Lall et al., 2021; O'Rourke et al., 2016). The upregulation of pro-inflammatory cytokines, in particular, IL1B in

microglia is therefore a common theme across SOD1, TDP-43, and C9ORF72 rodent models for ALS (Figure 1.1). A more detailed assessment of *C9orf72* KO microglia found a loss of homeostatic genes such as *P2ry12* with a transition to an inflammatory state and an enhanced type I interferon signature (Lall et al., 2021). *C9orf72* KO microglia caused enhanced synapse loss *in vivo and* in co-culture with murine neurons but reduced amyloid accumulation in the 5XFAD model of AD (Lall et al., 2021). These findings suggest a role for C9ORF72 in inflammatory pathways but must be treated with some caution. A substantial majority of findings were only present in *C9orf72*$^{-/-}$ but not in *C9orf72*$^{+/-}$ mice, the latter of which show a more similar reduction in C9ORF72 expression compared with human ALS patients with HREs in *C9ORF72*.

Different groups have aimed to investigate mouse models for gain-of-function toxicity of the HRE in *C9ORF72*. However, no overt MN phenotype or neurodegeneration was found in transgenic mice that express the *C9orf72* HRE driven from a bacterial artificial chromosome despite widespread production of DPRs and RNA foci (O'Rourke et al., 2015; Peters et al., 2015). Other studies have investigated the expression of selective forms of DPRs. Overexpression of neuronal Poly(GA) in mice led to neurodegeneration and activation of microglia, with upregulation of interferon-associated genes and cytokine pathways (LaClair et al., 2020; Schludi et al., 2017; Zhou et al., 2020). Treatment with an antibody against poly(GA) attenuated motor deficits and microglial activation, suggesting it might neutralise neuronal secretion of poly(GA) and thereby attenuate a harmful microglial response (Zhou et al., 2020). These models indicate a secondary toxic

response of microglia to DPR-induced neuronal degeneration or release of aggregates, which is in line with the pro-inflammatory response of microglia to mutant TDP-43 and SOD1 (Figure 1.1). However, the studies so far do not answer the question of the cell-autonomous consequences of DPR or RNA foci expression within microglia. Furthermore, it remains unclear if authentic human microglia that are assumed to concomitantly show *C9ORF72* HRE induced loss-of-function and gain-of-function toxicity replicate these phenotypes.

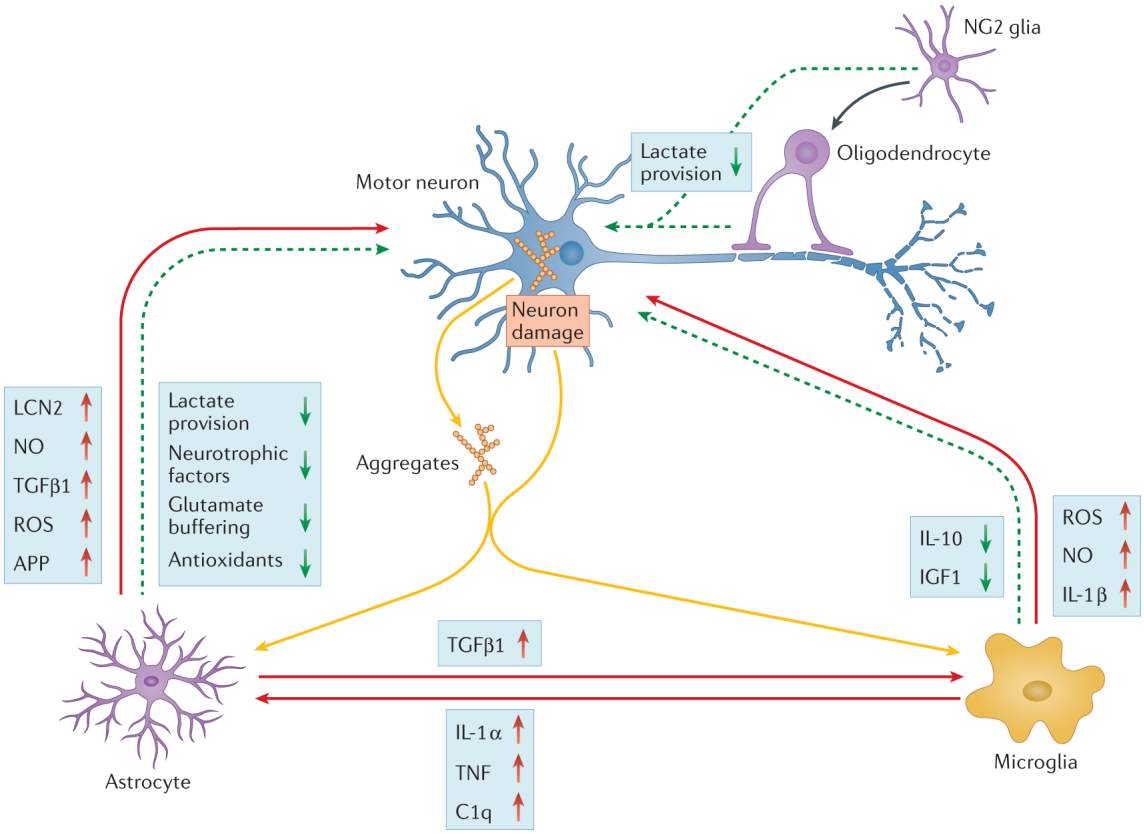


Figure 1.1: Pathophysiological role of microglia, in crosstalk with astrocytes and oligodendrocytes, according to rodent models of ALS. Neuronal damage associated with dysfunction and aggregation of proteins, such as SOD1 and TDP-43, as well as with aggregate release has been implicated in the activation of astrocytes and microglia (yellow arrows). Glial cells are thought to acquire neurotoxic properties, comprising both gain-of-function toxicity (red arrows) and loss of supportive functions (green dashed arrows), in response to the expression of ALS-associated mutations in genes such as *SOD1*, *TARDBP* and *C9ORF72*. The neurotoxicity is exacerbated by crosstalk between different cell types. The mechanisms depicted are derived from different models and have not all been identified in every model. Figure and figure legend from (Vahsen et al., 2021), with kind permission from Springer Nature.

Of note, it is important to consider that microglia in the CNS do not act in isolation, and there is substantial crosstalk between microglia, neurons, and other glial cells such as astrocytes and oligodendrocytes (Figure 1.1), but also peripheral immune cells, for instance, T-cells. Reviewing studies for the involvement of these additional cell types in ALS models goes beyond the scope of this thesis, but there are plenty of experimental data supporting an implication of other non-neuronal cells in ALS pathophysiology (Vahsen et al., 2021).

1.4 iPSC models for ALS

Species-specific differences between rodent and human cells make it difficult to interpret the results from animal models for ALS, while the complex and multicellular pathophysiology of ALS poses significant challenges for modelling ALS *in vitro*. With the advent of human induced pluripotent stem cells (iPSCs) in 2006 (Takahashi and Yamanaka, 2006), this has changed dramatically. iPSCs are generated by reprogramming somatic cells, very often obtained as fibroblasts through skin biopsy, into a pluripotent state. This conversion can be achieved through the introduction of only four factors, Oct3/4, Sox2, c-Myc, and Klf4 (Takahashi and Yamanaka, 2006). This ground-breaking discovery and milestone in stem cell research was recognised with the Nobel Prize in Physiology or Medicine to Shinya Yamanaka and John Gurdon in 2012. iPSCs can now be used to generate virtually all types of human cells including MNs and non-neuronal cells, furthering our understanding of brain development, biology, and pathophysiology. In the following sections, I will provide an overview of iPSC MN and microglia models for ALS.

1.4.1 iPSC-derived spinal motor neurons

Soon after the concept of iPSCs was first described by Takahashi and Yamanaka, the first protocols for the successful generation of iPSC-derived spinal MNs were reported (Dimos et al., 2008; Hu and Zhang, 2009). These protocols are of divergent duration and complexity but generally follow human embryonic development and involve several defined developmental steps. First, neural induction of iPSCs is performed by inhibiting transforming growth factor β and bone morphogenic protein (BMP) signalling, which is commonly referred to as dual-SMAD inhibition (Chambers et al., 2009). For this, small molecules such as SB431542 and LDN193189, to inhibit activin-nodal and BMP signalling, respectively are harnessed (Neely et al., 2012). To promote neuroepithelial proliferation and posterior identity, SMAD inhibition is often complemented with activation of Wnt signalling, for instance, using CHIR99021 (Li et al., 2011). Hereafter, a caudal and ventral identity is achieved through application of retinoic acid (RA) and sonic hedgehog protein or smoothened agonist (SAG) (Maury et al., 2015; Wichterle et al., 2002). In a final step, the differentiating neuronal precursors are dissociated, replated, and postmitotic maturation and neurite outgrowth is induced. For this step, the medium is supplemented with different neurotrophins, such as brain-derived neurotrophic factor (BDNF) and glial-derived neurotrophic factor (GDNF) (Dimos et al., 2008; Hu and Zhang, 2009). The MN identity of the resulting neurons can be determined by transcriptomic comparison with human post mortem MNs or, in a simplified approach, by assessing the expression of the transcription factors HB9 and ISLET1. More mature MNs express choline acetyltransferase (ChAT) and the vesicular acetylcholine neurotransmitter transporter (Amoroso et al., 2013;

Karumbayaram et al., 2009). In addition, these assessments can be complemented with functional read-outs for neuronal identity, for instance, patch clamping electrophysiology, multi-electrode array (MEA) recordings, or calcium imaging.

1.4.2 iPSC-derived microglia

It required more time for the field to develop protocols for the differentiation of iPSC microglia, probably due to the more complex developmental microglial ontogeny. However, since the first protocol was published in 2016 (Muffat et al., 2016), multiple protocols have become available that allow for the generation of iPSC microglia using paradigms of diverging complexity to mimic the embryonic development of microglia. These protocols can either make use of embryoid bodies (EBs) (Haenseler et al., 2017; Muffat et al., 2016; van Wilgenburg et al., 2013) or be performed in monolayers, e.g., (Abud et al., 2017; Douvaras et al., 2017) and other protocols. As an example, I will describe the protocol from the Cowley Lab (Haenseler et al., 2017; van Wilgenburg et al., 2013) here in more detail. First, iPSCs are patterned into EBs corresponding to the mesoderm and then haemogenic endothelium using a cocktail of BMP4, vascular endothelial growth factor (VEGF), and stem-cell factor (SCF) (Haenseler et al., 2017; van Wilgenburg et al., 2013). By addition of cytokines such as macrophage colony-stimulating factor (M-CSF) and IL-3, these EBs further differentiate into yolk sac-like structures containing primitive haematopoietic stem cells, which give rise to *MYB*-independent and *RUNX1*- and *PU.1*-dependent myeloid precursor cells (Buchrieser et al., 2017; Haenseler et al., 2017; van Wilgenburg et al., 2013). These myeloid precursors cells can be differentiated into microglia-like cells upon

engagement of CSF1R using IL-34 (Haenseler et al., 2017). The identity of the resulting microglial cells can be determined by transcriptomic comparison with *bona fide* microglial cells from human samples obtained during brain surgery or post mortem tissue (with the caveat that the processing of these human samples might have an effect on the microglial identity), analysis of a subset of the microglial marker genes as outlined in chapter 1.2.1, and investigation of expected physiological functions such as phagocytosis and cytokine release.

1.4.3 Multicellular approaches

In addition to monocultures, the iPSC field is now moving towards establishing multicellular cultures of different cell types. There is ample crosstalk, and the different cell types have numerous interactions through contact-dependent or contact-independent mechanisms (Figure 1.2). For example, it has previously been shown that a homeostatic iPSC microglial identity in culture is supported in co-culture with cortical neurons (Haenseler et al., 2017). In addition to generating a more physiological *in vitro* system, the striking advantage of multicellular cultures is the opportunity to analyse non-cell-autonomous phenotypes such as potential neuroprotective or neurotoxic microglial effects on MNs in culture.

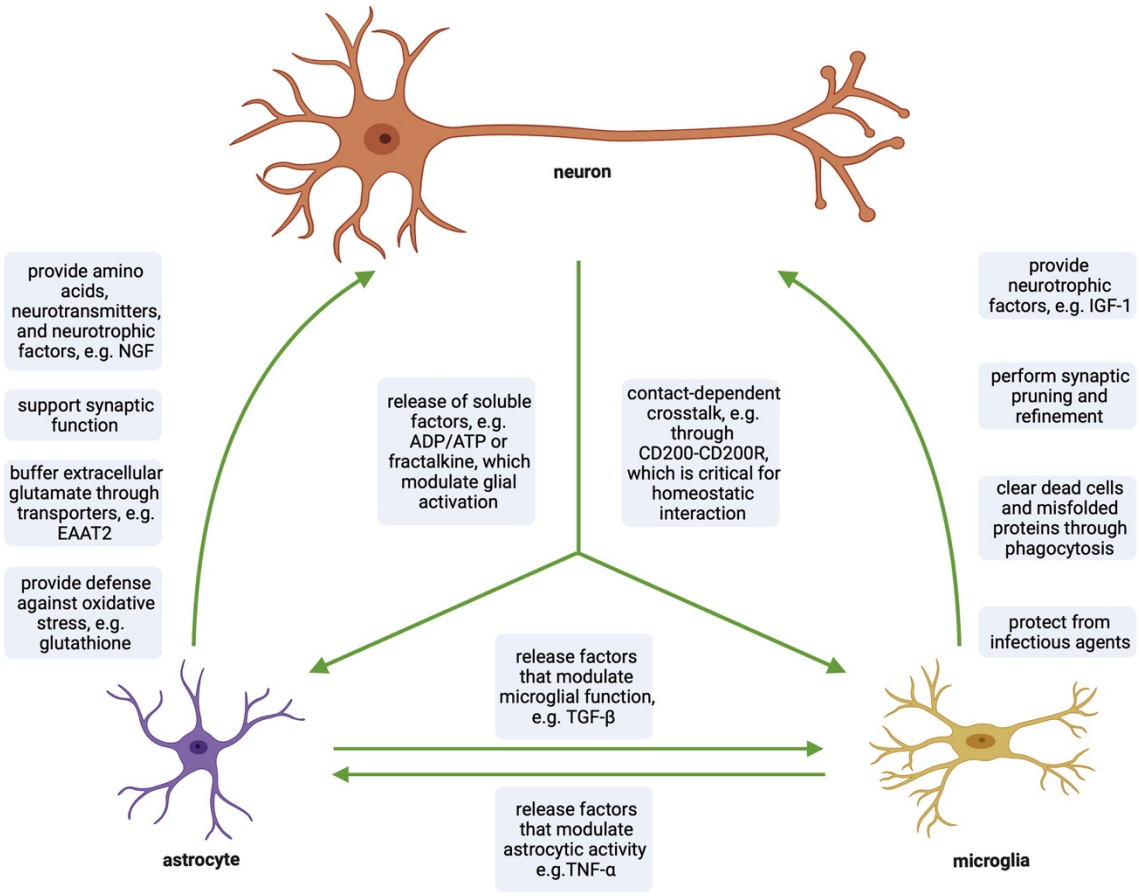


Figure 1.2: Physiological interactions between neurons, microglia, and astrocytes in the brain and spinal cord. Neuronal and glial cells interact through various contact-dependent and -independent mechanisms under homeostatic conditions. Figure and figure legend from (Giacomelli et al., 2022) with kind permission from Cell Press.

1.5 Aims of this thesis

There are several gaps in the state of knowledge in iPSC research and our understanding of microglia in ALS pathophysiology that I endeavoured to address in this DPhil thesis. Studies investigating the involvement of microglia in the ALS field have heavily relied on human post mortem, bioimaging, or preclinical rodent models, all of which have their limitations. Since murine and human microglia have distinct features and gene signatures, the investigation of human microglial cells is warranted. Conveniently, the first papers and protocols for the differentiations of iPSC-derived microglial cells had just been published before my DPhil project commenced, allowing me to generate iPSC microglia to study the cell-

autonomous effects of ALS-associated mutations in a more physiological model. Using the protocol developed by the Cowley Lab (Haenseler et al., 2017; van Wilgenburg et al., 2013), I aimed to differentiate iPSC microglia derived from ALS patients carrying HREs in *C9ORF72* to perform a comprehensive phenotypic analysis. While data from macrophages and microglia from *C9orf72* KO mice predicted a pro-inflammatory state due to C9ORF72 haploinsufficiency, it was unclear if human microglia would display a similar phenotype. To assess this in an unbiased manner rather than relying on the expression of a few pro-inflammatory or anti-inflammatory markers, I aimed to perform RNA sequencing for iPSC microglia generated from multiple C9ORF72-ALS patient and control lines.

Furthermore, co-culture models of iPSC microglia and different neuronal types had just been developed and published prior to my DPhil project. However, a human cell model with which to study microglia-MN crosstalk was not available. Such a system is imperative to study non-cell-autonomous effects of microglia on an ALS-relevant neuronal cell type. Therefore, I aimed to combine the differentiation protocols for iPSC MNs and iPSC microglia to establish a novel co-culture paradigm. I would then thoroughly assess both cell types in co-culture to ensure that both iPSC microglia and MNs retained their identity and function.

Finally, I aimed to combine both experimental set ups, using the novel co-culture model to investigate non-cell-autonomous effects of C9ORF72-ALS patient derived microglia on MNs in co-culture. To assess whether microglia modulated MN function, I endeavoured to use multiple readouts of MN survival and synaptic

function. I expected these experiments to provide an answer as to whether C9ORF72-ALS patient derived microglia directly contribute to MN degeneration. If microglial toxicity was present, I would investigate the underlying molecular mechanisms and, if possible, perform targeted drug treatments aiming to rescue the toxic effects of microglia.

Based on this, the two main hypotheses of this DPhil thesis were:

1. The presence of the HRE in *C9ORF72* induces a pro-inflammatory phenotype in iPSC microglia derived from C9ORF72-ALS patients;
2. C9ORF72-ALS patient-derived iPSC microglia cause non-cell-autonomous toxicity to MNs in co-culture.

Therefore, the specific aims of my DPhil thesis were the following:

1. To establish a co-culture model of iPSC-derived microglia and MNs (chapter 3);
2. To perform a phenotypic analysis of iPSC microglia derived from ALS patients carrying HRE mutations in *C9ORF72* (chapter 4);
3. To investigate non-cell-autonomous effects of *C9ORF72* ALS patient-derived iPSC microglia on MNs in co-culture (chapter 5).

2 Materials and methods

2.1 Cell culture

2.1.1 Generation and culture of iPSC lines

Three iPSC lines derived from three different ALS patients (one iPSC clone each) carrying a HRE mutation in *C9ORF72*, generated from skin biopsy fibroblasts, were used for experiments in this thesis: C9-01-07, C9-02-02, and C9-04-12. As controls, an isogenic line for C9-02-02, termed 59-2, previously generated through clustered regularly interspaced short palindromic repeats (CRISPR)/Cas9 genome editing using homology directed repair (Ababneh et al., 2020), as well as four gender- and age-matched healthy control iPSC lines, SFC840-03-03, SFC841-03-01, SFC856-03-04, and OX3-06, were used in this thesis. Additionally, an iPSC line with constitutive expression of red fluorescent protein (RFP) under continuous puromycin selection was used for some live imaging experiments. To improve the readability of the thesis, the disease and control lines were numbered according to the gender and age matching. An overview of the lines, their allocated number, the publications in which they were characterised, and demographics can be found in Table 2.1. iPSCs were cultured in mTeSR™1 (StemCell Technologies) or OXE8 medium (Vaughan-Jackson et al., 2021) on Geltrex™ (Thermo Fisher)-coated tissue culture plates with daily medium changes. Passaging was done as clumps using ethylenediaminetetraacetic acid (EDTA) in phosphate-buffered saline (PBS) (0.5 mM). Cells were initially expanded at low passage to create a master stock to ensure consistency. Cell

stocks tested negative for mycoplasma using the MycoAlert™ Mycoplasma Detection Kit (Lonza).

Table 2.1: Human induced pluripotent stem cell lines used in this thesis. PMID: PubMed ID.

iPSC line	abbreviation	gender	age	mutation/modification	PMID
OX3-06	HC-1	male	49	-	29604226
SFC856-03-04	HC-2a	female	78	-	28827786
SFC840-03-03	HC-2b	female	67	-	26905200
SFC841-03-01	HC-3	male	36	-	27097283
AH016-3 Lenti_IP_RFP	-	male	80	red fluorescent protein (RFP)	28591653
C9-01-07	C9-1	male	72	*C9ORF72* (~970 G_4C_2 repeats)	32330447
C9-02-02	C9-2	female	58	*C9ORF72* (~1000 G_4C_2 repeats)	27097283
C9-04-12	C9-3	male	39	*C9ORF72* (>500 G_4C_2 repeats)	32330447
59-2	ΔC9-2	female	58	isogenic control (2 G_4C_2 repeats)	32504093

2.1.2 Differentiation of iPSC-derived motor neurons

iPSCs were differentiated to MNs using a modified, previously published protocol (Ababneh et al., 2020; Dafinca et al., 2020; Dafinca et al., 2016; Vahsen et al., 2022). Briefly, neural induction of iPSC monolayers at ~70-90% confluency was performed using DMEM-F12/Neurobasal 50:50 medium supplemented with N2 (1X), B27 (1X), 2-Mercaptoethanol (1X), Antibiotic-Antimycotic (1X, all ThermoFisher), Ascorbic Acid (0.5 µM), Compound C (1 µM, both Merck), and Chir99021 (3 µM, R&D Systems). After two days in culture, RA (1 µM, Merck) and SAG (500 nM, R&D Systems) were additionally added to the medium. Two days later, Compound C and Chir99021 were removed from the medium. After another five days in culture, neural precursors were dissociated using accutase

(ThermoFisher), and split 1:3 onto Geltrex™-coated tissue culture plates in medium supplemented with Y-27632 dihydrochloride (10 µM, R&D Systems). After one day, Y-27632 dihydrochloride was removed from the medium, and the cells were cultured for another eight days with medium changes every other day. For terminal maturation, the cells were dissociated on day *in vitro* (DIV) 18 using accutase and plated onto coverslips, tissue culture plates or dishes coated with polyethylenimine (PEI, 0.07%, Merck) and Geltrex™ or PDL (Sigma-Aldrich)/ Laminin (R&D Systems)/ Fibronectin (Corning) at the densities indicated in Table 2.2. For this step, the medium was additionally supplemented with BDNF (10 ng/mL), GDNF (10 ng/mL), Laminin (0.5 µg/mL, all ThermoFisher), Y-27632 dihydrochloride (10 µM), and (2S)-N-[(3,5-Difluorophenyl)acetyl]-L-alanyl-2-phenyl]glycine 1,1-dimethylethyl ester (DAPT) (10 µM, R&D Systems). Three days later, Y-27632 dihydrochloride was removed from the medium. After another three days, DAPT was removed from the medium. Full medium changes were then performed every three days. For MNs differentiated in co-culture medium or co-culture, all steps were performed similarly until three days after the terminal re-plating (D21). MNs were then cultured in co-culture medium or co-culture as described in 2.1.5.

Table 2.2: Cell numbers used for different MN monoculture experiments.

purpose of experiment	plate format	cells per well [n]	volume of medium per well [mL]
Protein extraction/ supernatant arrays	6 well	1,000,000/ 500,000	2
Immunofluorescence	24 well	200,000/ 100,000	0.5

2.1.3 Differentiation of iPSC-derived macrophage/microglia precursors

iPSCs were differentiated to macrophage/microglia precursors as described previously (Karlsson et al., 2008; van Wilgenburg et al., 2013). Briefly, embryoid body (EB) formation was induced by seeding iPSCs into Aggrewell 800 wells (STEMCELL Technologies) in OXE8 (Vaughan-Jackson et al., 2021) or mTeSR™1 medium supplemented with BMP4 (50 ng/mL), VEGF (50 ng/mL, both Peprotech), and SCF (20 ng/mL, Miltenyi Biotec). After four to seven days with daily ¾ medium changes, EBs were transferred to T175 flasks (~150 EBs each) and differentiated in X-VIVO15 (Lonza), supplemented with IL-3 (25 ng/mL, R&D Systems), M-CSF (100 ng/mL), GlutaMAX (1X, both ThermoFisher), and 2-Mercaptoethanol (1X). Fresh medium was added weekly. After approximately one month, precursors emerged into the supernatant and could be harvested weekly. Harvested cells were passed through a cell strainer (40 µM, Falcon or Greiner) and either lysed directly for RNA extraction or differentiated to microglia in monoculture or co-culture as described below.

2.1.4 Differentiation of iPSC-derived microglia

Macrophage/microglia precursors harvested as described in 2.1.3 were counted using a Countess 3 Automated Cell Counter (ThermoFisher) and then plated in co-culture medium (see 2.1.5) in tissue culture plates or dishes coated with PEI (0.07%) and Geltrex™ or PDL / Laminin / Fibronectin using the densities listed in Table 2.3. Microglia were differentiated in monoculture using the co-culture medium described in 2.1.5 for approximately 14 days, with half medium changes every 2-3 days, and then either collected for RNA/protein extraction or used for

live imaging or assays as described below. Half medium changes were performed every 2-4 days.

Table 2.3: Cell numbers used for different microglia monoculture experiments.

purpose of experiment	plate format	cells per well [n]	volume of medium per well [mL]
Protein/RNA extraction, supernatant array	6 well	1,000,000/ 500,000/	2
Immunofluorescence	24 well	200,000/ 100,000	0.5
Live imaging	confocal dish	200,000/ 100,000	2
Assay	96 well	32 000/ 16 000	0.2
RNA sequencing	10 cm dish	6,000,0000	15

2.1.5 Co-culture of iPSC-derived motor neurons and microglia

Three days after the final re-plating of differentiating MNs (DIV21), macrophage/microglia precursors were harvested as described in 2.1.3 and resuspended in co-culture medium comprised of Advanced DMEM-F12 (ADMEM-F12, ThermoFisher) supplemented with GlutaMAX (1X), N2 (1X), Antibiotic-Antimycotic (1X), 2-Mercaptoethanol (1X), Interleukin-34 (IL-34, 100 ng/mL, Peprotech/BioLegend), BDNF (10 ng/mL), GDNF (10 ng/mL), and Laminin (0.5 µg/mL). MNs were quickly rinsed with PBS, and macrophage/microglia precursors re-suspended in co-culture medium were added to each well in a 1:1 ratio with the MNs. Co-cultures were then maintained for at least 14 days before assays were conducted as described below. Half medium changes were performed every 2-4 days.

Table 2.4: Cell numbers used for different co-culture experiments.

purpose of experiment	plate format	cells per well for each cell type [n]	volume of medium per well [mL]
Protein extraction, supernatant array	6 well/ 12 well	1,000,000/ 500,000/	2/ 1
Immunofluorescence	24 well	200,000/ 100,000	0.5
Live imaging	confocal dish	200,000/ 100,000	2
CD11b-MACS and RNA sequencing	10 cm dish	6,000,0000	15

2.1.6 Cell culture treatments

2.1.6.1 Induction of an 'M1'/'M2'-phenotype in monocultures and co-cultures for comparative supernatant analyses

All medium was aspirated from the wells, and fresh co-culture medium containing lipopolysaccharides (LPS, 100 ng/mL, Sigma) and Interferon-γ (IFN-γ, 100 ng/mL, ThermoFisher) to induce an 'M1' phenotype, or IL-4 (40 ng/mL, R&D Systems) and IL-13 (20 ng/mL, Peprotech) for an 'M2' phenotype, respectively, were added to the cells for 18 h. Cells treated with co-culture medium only were used as an unstimulated ('M0') vehicle control. Supernatant from MNs, microglial monocultures, and co-cultures was collected and used for supernatant analyses as described in 2.6. Alternatively, cells cultured in live imaging dishes were used for live imaging as described in 2.4.

2.1.6.2 Induction of an 'M1'-phenotype in disease monocultures

To assess the response of C9ORF72-ALS microglia to pro-inflammatory stimulation, all medium was aspirated from the wells and LPS (100 ng/mL) diluted in co-

culture medium or co-culture medium alone as vehicle control was added to the cells. 48 h later, cells were fixed for immunofluorescence as described in 2.4, RNA and protein were collected as detailed in 2.2 and 2.3, and culture supernatants were processed for supernatant analyses as described in 2.6.

2.1.6.3 Induction of an 'M1'-phenotype in disease co-cultures

To assess co-cultures after pro-inflammatory stimulation, half of the medium was removed from each well on DIV 25 of the co-culture protocol, and LPS (100 ng/mL) diluted in co-culture medium or co-culture medium alone as vehicle control was added to the cells. Repetitive treatments with LPS were performed every 3-4 days for a total of 10 days.

2.1.6.4 Treatment with an MMP9 inhibitor

To inhibit MMP9 in LPS-primed co-cultures, treatments with LPS (100 ng/mL) were performed as described in 2.1.6.3. In addition, MMP9 inhibitor I (MMP9I, 3 μM, 444278, Merck) or DMSO in equal concentration (0.3%) as vehicle control were added in parallel.

2.1.7 Multi-electrode array recordings

On DIV 18, healthy control MNs generated as described above were plated in CytoView MEA 48 well black plates (M768-tMEA-48B, Axion BioSystems). On DIV 21, microglia precursors generated as described in 2.1.3 were added in a 1:1 ratio. Half medium changes were performed every 2-4 days. For LPS-stimulated co-cultures, treatments were performed from DIV 25 as described above and repeated every 3-4 days. MEA recordings were obtained using the Maestro system

(Axion Biosystems). Plates were allowed to settle down for 5 min before 2-15 min recordings of neural activity were obtained. Analysis was performed using the AXIS software v2.5.2 (Axion BioSystems) using SD > 5.5 as the threshold for the detection of neuronal activity. The mean firing rate per well was calculated by averaging all active electrodes per well (defined as > 1 spike per min).

2.2 Analysis of RNA expression

2.2.1 RNA isolation

RNA was isolated either from macrophage/microglia precursors lysed directly after the harvest or from microglia differentiated in monoculture or co-culture for at least 14 days. Microglia in monoculture were rinsed with PBS and directly lysed in the dish or plate. For both precursors and microglia in monoculture, RNA was extracted using an RNAeasy Mini Plus kit (Qiagen) according to the manufacturer's instructions. Co-cultures were first dissociated by 15 min incubation with papain (P4762, Sigma-Aldrich) diluted in accutase (20 U/mL) and gentle trituration based on a previously published protocol (Thiry et al., 2020). The cell suspension was then passed through a cell strainer (70 µm, Falcon) to remove cell clumps. To extract co-cultured microglia from co-cultures, magnetic-activated cell sorting (MACS) was then performed using CD11b-MACS beads (130-093-634, Miltenyi Biotec) according to the manufacturer's instructions. The panned cell population was lysed for RNA extraction using an RNAeasy Micro kit (Qiagen) according to the manufacturer's instructions. In addition, RNA from human fetal microglia and blood monocytes from three different healthy genetic backgrounds was re-used from a previous study (Haenseler et al., 2017).

2.2.2 Measurement of RNA integrity

Before sample submission, RNA was quality controlled by analysing the RNA integrity number (RIN) using an RNA 6000 Nano Kit (Agilent Technologies) according to the manufacturer's instructions. All samples used for sequencing displayed RIN values > 8.5.

2.2.3 cDNA preparation and RT-qPCR

Equal amounts of RNA (30-100 ng) were reverse-transcribed to complementary DNA (cDNA) using the High-Capacity cDNA Reverse Transcription Kit (ThermoFisher) according to the manufacturer's instructions. RT-qPCR for all samples in triplicates was performed with Fast SYBR™ Green Master Mix (ThermoFisher) according to the manufacturer's instructions using a LightCycler® 480 PCR System (Roche). The primers (ChAT from Eurofins Genomics, all others from ThermoFisher) used are listed in Table 2.5. Quantification of the relative fold gene expression of samples was performed using the $2^{-\Delta\Delta Ct}$ method with normalization to the *GAPDH* or *TBP* reference genes as indicated in each figure legend and the mean gene expression of the healthy or isogenic control microglia for each experiment.

Table 2.5: Primers used for RT-qPCR experiments.

Gene	Forward primer sequence	Reverse primer sequence
C1QA	GTGACACATGCTCTAA-GAAG	GACTCTTAAGCACTGGATTG
C9ORF72 (ALL)	CCCACTTCATAGAG-TGTGTGTTG	TTCCATTCTCTCTGTGCCTTC
C9ORF72 V1 (short)	GAAATCACACAG-TGTTCCTGAAGAA	ATCTGCTTCATCCAGCTTTTATGA

C9ORF72 V2+3 (long)	CATGGCTCAGGATAC-GATCA	GGAAGGCTTTCACTAGAG-TGTCTC
ChAT	CGTG-GACAACATCAGATCG	ATGGCCATGACTGTGTATGC
CXCL10	GTGGCATTCAAGGAG-TACCTC	TGATGGCCTTCGATTCTGGATT
GAPDH	CTGGGCTACACTGAG-CACC	AAGTGGTCGTTGAGGGCAATG
GAS6	CGAAGAAACTCAA-GAAGCAG	AGACCTTGATCTCCATTAGG
GPR34	GAAGACAATGA-GAAGTCATACC	TGTTGCTGAGAAGTTTTGTG
MERTK	AGGACTTCCTCAC-TTTACTAAG	TGAACCCAGAAAATGTTGAC
MMP9	GGGACGCAGA-CATCGTCATC	TCGTCATCGTCGAAATGGGC
P2RY12	AAGAGCACTCAA-GACTTTAC	GGGTTTGAATGTATCCAGTAAG
PROS1	AAAGATGTG-GATGAATGCTC	TCACATTCAAAATCTCCTGG
TBP	GAGAGTTCTGG-GATTGTACCG	ATCCTCATGATTACCGCAGC
TMEM119	AGTCCTGTAC-GCCAAGGAAC	GCAGCAACAGAAGGATGAGG
TREM2	TCTGAGAGCTTCGAG-GATGC	GGGGATTTCTCCTTCAAGA

2.2.4 RNA-sequencing

Further processing of samples for RNA-sequencing and the generation and initial processing of the data was performed by the Oxford Genomics Centre at the Wellcome Centre for Human Genetics. Briefly, input material was normalised to 100 ng prior to library preparation. Polyadenylated transcript enrichment and strand specific library preparation was completed using NEBNext Ultra II mRNA kit (NEB) following manufacturer's instructions. Libraries were amplified (14 cycles) on a Tetrad (Bio-Rad) using in-house unique dual indexing primers (based

on (Lamble et al., 2013)). Individual libraries were normalised using Qubit, and the size profile was analysed on the 2200 or 4200 TapeStation. Individual libraries were normalised and pooled together accordingly. The pooled library was diluted to ~10 nM for storage. The 10 nM library was denatured and further diluted prior to loading on the sequencer. Paired end sequencing was performed using a NovaSeq6000 platform (Illumina, NovaSeq 6000 S2/S4 reagent kit, v1.5, 300 cycles), generating a raw read count of a minimum of 30M reads per sample.

2.2.5 Bioinformatic analysis of RNA-sequencing data

The analysis of the raw data was performed using custom Python and R scripts. For comparison of the microglial identity of the samples, macrophage/microglia precursors from four different healthy control iPSC lines and microglia differentiated in monoculture or co-culture from the same lines were subjected to RNA sequencing analysis (12 samples in total). Furthermore, the RNA sequencing data (GSE89189) from (Abud et al., 2017) and the dataset (GSE85839) from (Muffat et al., 2016) were downloaded and processed in parallel. Quality control of fastq files was performed using FastQC (https://www.bioinformatics.babraham.ac.uk/projects/fastqc/) and MultiQC (Ewels et al., 2016). Paired-end reads were mapped to the human GRCh38.p13 reference genome (https://www.gencodegenes.org) using HISAT2 v2.2.1 (Kim et al., 2019). Mapping quality control was done using SAMtools (Li et al., 2009) and Picard (http://broadinstitute.github.io/picard/) metrics. The counts table was obtained using FeatureCounts v2.0.1 (Liao et al., 2014). Normalization of counts and differential expression analysis was performed using DESeq2 v1.28.1 (Love et al., 2014), including the biological gender and differentiation in the model, as appropriate, and with

the Benjamini-Hochberg method for multiple testing correction. Exploratory data analysis was performed following variance-stabilizing transformation of the counts table, using heat maps, hierarchical clustering, and principal component analysis (PCA). Log_2 fold change (log_2 fc) shrinkage was performed using the ashr package v2.2-47 (Stephens, 2017). Genes with $| log_2 fc | > 2$ and adjusted p-value < 0.01 were defined as differentially expressed and interpreted with annotations from the Gene Ontology (GO) database using clusterProfiler v3.16.1 (Yu et al., 2012) to perform over-representation analyses. For the analysis of C9ORF72 patient-derived microglia, microglia were differentiated from three C9ORF72-ALS patient lines and three age- and gender-matched healthy control lines. For each line, three independent differentiations from three different harvests from the differentiation factories were performed. RNA sequencing (36 samples in total) and further processing of the raw data was performed as described above. However, log_2 fc shrinkage was performed using the 'normal' approach. Genes with $| log_2 fc | > 0.5$ and adjusted p-value < 0.05 were defined as differentially expressed. Gene set enrichment analyses (GSEA) using the whole transcriptome ranked by log_2fc were interpreted with annotations from the GO database using clusterProfiler v3.16.1.

2.3 Analysis of protein expression

2.3.1 Protein extraction and quantification for Western blot

The medium was aspirated from all wells, and the cells were quickly rinsed with PBS. Cells were then either collected as a cell suspension or lysed directly in the well. In suspension, they were transferred to Eppendorf cups and centrifugated

at 4°C and 500 x g for 5 min. The supernatants were discarded, and pellets were stored at -80°C until further utilisation. To extract the proteins, frozen cell pellets were resuspended in 100-200 µL of radioimmunoprecipitation (RIPA) buffer (ThermoFisher) supplemented with cOmplete™ protease and PhosSTOP™ phosphatase inhibitor cocktails (both Merck). Alternatively, 60-200 µL of cold lysis buffer, depending on the plate format, were added directly to the wells. The samples were transferred to Eppendorf cups and stored at -80°C until thawed at a different time. 10 motor-driven 1-second impulses with pellet pestles were used to homogenise the lysates. After incubation on ice for 30 min, lysates were then centrifuged at 12,000 rpm and 4°C for 15 min. The supernatants were transferred to new Eppendorf cups and stored at -80°C until further utilisation. The protein content of each lysate was determined using the Pierce™ bicinchoninic acid (BCA) protein assay kit (ThermoFisher) according to the manufacturer's instructions. Bovine serum albumin (BSA) diluted in distilled water to 8 defined concentrations (0.025-2.0 µg/µL) was used as reference standard.

2.3.2 SDS-PAGE and Western blotting

For sodium dodecyl sulfate polyacrylamide gel electrophoresis (SDS-PAGE), protein samples were immediately prepared in distilled water, NuPAGE™ lithium dodecyl sulfate loading buffer, and NuPAGE™ sample reducing agent (both ThermoFisher) to a final concentration of 0.33-1.0 µg/µL. Samples were denatured and reduced by 5 min incubation at 95°C. 10-25 µL of each sample and 4-5 µL of protein ladder were loaded onto pre-cast NuPAGE™ Bis-Tris 4-12% gradient gels (ThermoFisher) with 12, 17, or 20 wells. Samples were separated by SDS-PAGE using 2-(N-morpholino)ethanesulfonic acid (MES) running buffer

(both ThermoFisher) at 50-130 V. When the 10 kDA band of the protein ladder reached the end of the gels, the electrophoresis was stopped, and the proteins were transferred to nitrocellulose membranes at 20-25 V for 7 min using an iBlot 2 Dry blotting system (both ThermoFisher). After blocking with 5% milk or 5% BSA in Tris-buffered saline/0.1% Tween-20 (TBS-T, ThermoFisher) at RT for 1 h, membranes were incubated with primary antibodies diluted in 3% milk or 3% BSA in TBS-T at 4°C overnight (ON). The primary antibodies used are listed in Table 2.6. Membranes were then washed three times with TBS-T for 5-7 min. This was followed by incubation with corresponding horseradish peroxidase (HRP)-coupled secondary antibodies at room temperature (RT) for 1 h. The following HRP-coupled secondary antibodies were used: sheep anti-mouse HRP (NA931V), donkey anti-rabbit HRP (NA934V, both GE Healthcare), or donkey anti-goat HRP (PA128664, ThermoFisher). Hereafter, membranes were washed three times with TBS-T for 5-7 min. Enhanced chemiluminescence solutions (Millipore) were mixed 1:1 and applied to the membranes for 1 min. The signal was visualized using a ChemiDoc™ MP imaging system (Bio-Rad). Signal accumulation images were taken to determine the optimal exposure time. Band intensities were quantified using Fiji (Schindelin et al., 2012), and target protein band intensities were normalised to the band intensities of the housekeeping genes β-actin or glyceraldehyde 3-phosphate dehydrogenase (GAPDH). After development, membranes were washed two times with TBS-T for 5 min, followed by 10 min of incubation with Restore™ PLUS stripping buffer (ThermoFisher). After two additional 5-min-washes with TBS-T, membranes were blocked and incubated with new primary antibodies.

Table 2.6: Primary antibodies and dilutions used for Western blotting.

target	species	dilution	catalogue number	company
b-actin	mouse	1:5000	AM4302	ThermoFisher
C9ORF72	mouse	1:500	GTX634482	GeneTex
C9ORF72	mouse	1:1000	GTX632041	GeneTex
ChAT	goat	1:1000	ab144P	Sigma-Aldrich
GAPDH	mouse	1:1000	Nb300221	Novus Biologicals
IBA1	rabbit	1:1000	019-19741	FUJIFILM Wako
IL1B	mouse	1:1000	8516	ThermoFisher
LAMP1	mouse	1:1000	15665	Cell Signaling
MMP9	rabbit	1:1000	ab76003	Abcam
NFκB	rabbit	1:1000	C22B4	Cell Signalling
NLRP3	rabbit	1:500	D4D8T	Cell Signalling
p-NFκB	rabbit	1:500	3033T	Cell Signalling

2.3.3 Protein extraction and sample preparation for the analysis of Poly(GA) and Poly(GP) expression

For the analysis of Poly(GA) and Poly(GP) expression, protein was extracted using a protocol developed by the Isaacs Lab (University College London, UK). All medium was aspirated from the plates, and the cells were quickly rinsed with PBS. The plates were placed on ice, and 150-200 μL of lysis buffer consisting of RIPA buffer (Sigma-Aldrich) supplemented with 2x complete Mini, EDTA free protease inhibitor cocktail (Merck) and 2% SDS (ThermoFisher) were added. After 10 min of incubation, the samples were transferred to Eppendorf tubes and homogenised using a sonicator (30%, 3 x 10 s pulses, 5 s intervals, ThermoFisher). The lysates were centrifuged at 17,000 x g and 16°C for 20 min, and the supernatants were transferred to new Eppendorf cups and stored at -80°C until further

utilisation. The protein content was determined by BCA as described in 2.3.1 and the concentration of each sample was adjusted to 0.6-1.0 mg/mL in lysis buffer, using equal concentrations for the different samples per experiment. The expression of Poly(GA) and Poly(GP) was then determined by Mireia Carcolé in the Isaacs Lab using an Meso Scale Discovery (MSD) enzyme-linked immunosorbent assay (ELISA) assay.

2.4 Immunofluorescence, confocal microscopy, and image analysis

2.4.1 Immunofluorescence

Cells cultured on coverslips were either rinsed with PBS and fixed with 4% paraformaldehyde (PFA) in PBS for 15 min at RT or, alternatively, pre-fixed with 2% PFA in PBS for 2 min and then fixed with 4% PFA in PBS for 15 min at RT. After a washing step with PBS, cells were left in PBS, sealed with Parafilm and stored at 4°C until further utilisation. Cells were permeabilised and blocked with 5% donkey serum and 0.2% Triton X-100 in PBS for 1 h at RT. Hereafter, the permeabilization/blocking solution was replaced with primary antibodies diluted in 1% donkey serum and 0.1% Triton X-100 in PBS and incubated at 4°C ON. The primary antibodies used are listed in Table 2.7. After three washes with PBS-0.1% Triton X-100 for 5 min each, the coverslips were incubated with corresponding fluorescent secondary antibodies Alexa Fluor® 488/568/647 donkey or goat anti-mouse/rabbit/rat/goat/guineapig/chicken (all 1:1000, ThermoFisher or Abcam). Coverslips were then washed twice with PBS-0.1% Triton X-100 for 5 min each

and incubated with 4′,6-diamidino-2-phenylindole (DAPI, 1 μg/mL, Sigma-Aldrich) in PBS for 10 min. After an additional 5 min-washing step with PBS-0.1% Triton X-100, the coverslips were mounted onto microscopy slides using ProLong™ Diamond or Glass Antifade Mountant (ThermoFisher). Confocal microscopy was performed using an LSM 710 (Zeiss) or a Fluoview FV1000 (Olympus) microscope.

Table 2.7: Primary antibodies and dilutions used for immunofluorescence.

target	species	dilution	catalogue number	company
CD11b	rat	1:100	101202	BioLegend
ChAT	goat	1:100	ab144P	Abcam
cleaved caspase 3	rabbit	1:400	9661S	Cell Signaling
IBA1	rabbit	1:500	019-19741	FUJIFILM Wako
IBA1	goat	1:500	ab5076	Abcam
ISLET1	mouse	1:50	40.2D6	Developmental Studies Hybridoma Bank
LAMP1	mouse	1:100	15665	Cell Signaling
synaptophysin	guineapig	1:500	101004	Synaptic Systems
synaptophysin	rabbit	1:200	ab14692	Abcam
TDP-43	mouse	1:500	60019-2-1g	Proteintech
TMEM119	rabbit	1:100	ab185337	Abcam
TREM2	rat	1:100	MAB17291-100	R&D Systems
TUJ1	mouse	1:1000	801201	Biolegend
TUJ1	rabbit	1:500	802001	Biolegend
TUJ1	chicken	1:500	GTX85469	GeneTex

2.4.2 Quantification of differentiation efficiency and marker expression

z-stacks of three randomly selected visual fields were taken for each coverslip at 20x or 40x magnification. For MNs in different medium compositions and in monoculture and co-culture, the ratios of class III beta-tubulin (TUJ1)-positive, ChAT-positive, ISLET1-positive, ChAT-positive/ TUJ1-positive, and ISLET1-positive/ TUJ1-positive cells were quantified using Fiji in a blinded fashion. For microglia in monoculture and co-culture, the ratios of CD11b-positive/ IBA1-positive, TMEM119-positive/ IBA1-positive, and TREM2-positive/ IBA1-positive cells were quantified.

2.4.3 Quantification of apoptosis in MNs and microglia

z-stack images of three to five randomly selected visual fields were taken at 40x magnification for each coverslip. For the analysis of apoptosis in MNs, neuron numbers were determined by counting the number of TUJ1-positive cells per view field and the ratio of cleaved caspase 3 (CC3)-positive/ TUJ1-positive cells (in 16-104 TUJ1-positive cells per view field) were manually quantified using Fiji in a blinded fashion. To quantify apoptosis in microglia in monoculture and co-culture, the expression of CC3 in IBA1-positive microglia (in 3-33 IBA1-positive cells per view field) was manually quantified using Fiji in a blinded fashion.

2.4.4 Analysis of LAMP1-positive lysosomes in microglia

z-stack images of four to five randomly selected visual fields were taken at 100x magnification for each coverslip. Maximum intensity projections were generated in Fiji, and a macro was employed for automatic and unbiased analysis. An auto

threshold was applied to the lysosomal-associated membrane protein 1 (LAMP1) staining, and the number and area of LAMP1-positive particles was determined for each view field using the ‘analyze particles’ function. The resulting data for each view field was then normalised to the number of DAPI-positive nuclei per view field.

2.4.5 Quantification of neurite density in co-culture

z-stacks of four to five randomly selected and equally distributed (top left, top right, centre, bottom left, and bottom right of the well) view fields showing neurites but avoiding neuronal somas were obtained at 60x magnification for each coverslip. Maximum intensity projections were generated in Fiji, and a macro was employed for automatic and unbiased analysis. An auto threshold was applied to the TUJ1 staining, and the neurite density for each view field was determined by measuring the area of TUJ1-positive neurites per view field using the ‘analyze particles’ function in Fiji.

2.4.6 Analysis of neuronal synaptophysin expression

z-stack images of four to five randomly selected visual fields were taken at 60x magnification for each coverslip. Maximum intensity projections were generated in Fiji. Using a macro, an auto threshold was applied to the synaptophysin staining to analyse dot-like structures, and the number and area of synaptophysin particles was determined for each view field using the ‘analyze particles’ function in Fiji.

2.5 Live cell microscopy and image analysis

2.5.1 Analysis of microglial motility

AH016-3 Lenti-IP-RFP-microglia were co-cultured with healthy control MNs in PEI- and Geltrex™-coated glass bottom dishes for confocal microscopy (VWR). The RFP signal was used to identify microglia in co-culture. To visualize microglial movement, images of the RFP signal and brightfield were taken every ~30 s for 1 h at 20x magnification using a Cell Observer spinning disc confocal microscope (Zeiss) equipped with an incubation system (37°C, 5% CO_2).

2.5.2 Analysis of phagocytosis

To assess the phagocytic capacity of co-cultures, AH016-3 Lenti-IP-RFP-microglia were co-cultured with healthy control MNs in PEI- and Geltrex™-coated glass bottom dishes for confocal microscopy (VWR). The RFP signal was used to identify microglia in co-culture. Co-cultures were rinsed with Live Cell Imaging Solution (1X, ThermoFisher), and pHrodo™ Green Zymosan Bioparticles™ Conjugates (P35365, ThermoFisher) diluted in Live Cell Imaging Solution (50 μg/mL), which become fluorescent upon phagocytic uptake, were added. The dish was immediately transferred to the spinning disc confocal microscope, and stitched images (3x3, 20x magnification) were acquired every 5 min for 2 h.

To compare the phagocytic activity of C9ORF72 and control microglia in monoculture, live cells in culture plates were stained with Hoechst diluted in Live Cell Imaging Solution (1:10,000, ThermoFisher) for 10 min at 37°C and 5% CO_2. After

two washing steps with Live Cell Imaging Solution, pHrodo™ Red Zymosan Bioparticles™ Conjugates (P35364, ThermoFisher) diluted in Live Cell Imaging Solution (50 μg/mL) were added to each well. In selected conditions, cells were pretreated with the phagocytosis/degradation inhibitors Cytochalasin D (10 µM, C2618, Merck), Bafilomycin A1 (1 µM, 1334, R&D Systems) or DMSO (vehicle) for 1 h before the addition of phagocytosis particles. The phagocytosis particles were then added to the cells together with the respective phagocytosis inhibitors diluted in Live Cell Imaging solution. The cells were maintained at 37°C for 150 min, and then images were acquired using an Invitrogen™ EVOS™ XL Core Cell Imaging System (ThermoFisher) equipped with a 10x objective. Quantification of the phagocytosis signal was performed using an analysis macro in Fiji. The number of microglial cells was quantified by counting the number of Hoechst-positive cells. A threshold was applied to the phagocytosis signal, and the number and area of the internalised phagocytosis particles was quantified using the 'analyze particles' function. The resulting values per view field were normalised to the number of Hoechst-positive cells.

2.5.3 Analysis of clustering behaviour

To analyse the clustering of microglia upon pro-inflammatory and anti-inflammatory stimulation, RFP-positive microglia in co-culture with MNs were imaged directly before the addition of 'M1'/'M2' inducing agents, and 9 h and 18 h post-stimulation using the Cell Observer spinning disc confocal microscope at 10x magnification. The number of individual microglial cells and size of microglial clusters was quantified using the "analyze particle" function in Fiji.

2.6 Cytokine/chemokine analyses

2.6.1 Supernatant arrays

Culture supernatants were collected and spun down at 1200 x g for 10 min at 4°C. For the comparison of cytokines in microglial and MN monocultures and co-cultures, pooled samples from different replicates for the same condition as indicated in the respective figure legends were analysed using the Proteome Profiler Human XL Cytokine Array Kit (ARY022B, R&D Systems) according to the manufacturer's instructions. The kit allows for the parallel measurement of 105 different cytokines/chemokines (for details, see Table 2.8). C9ORF72 microglia in monoculture and co-culture were analysed using the Proteome Profiler Human XL Cytokine Array Kit or the Proteome Profiler Human Protease/Protease Inhibitor Array Kit (ARY025, R&D Systems). The signal was visualized on a ChemiDoc™ MP imaging system (Bio-Rad) and analysed using ImageStudioLite (LI-COR). The two datapoints per target on each membrane were averaged, and data was plotted as arbitrary units using the pheatmap function in RStudio or normalised to the control condition for each target.

Table 2.8: Different cytokines/chemokines measured using the Proteome Profiler Human XL Cytokine Array Kit.

Adiponectin/Acrp30	IFN-gamma	CCL2/MCP-1
Angiogenin	IGFBP-2	CCL7/MCP-3
Angiopoietin-1	IGFBP-3	M-CSF
Angiopoietin-2	IL-1 alpha/IL-1F1	MIF
Apolipoprotein A1	IL-1 beta/IL-1F2	CXCL9/MIG
BAFF/BLyS/TNFSF13B	IL-1ra/IL-1F3	CCL3/CCL4 MIP-1 alpha/beta
BDNF	IL-2	CCL20/MIP-3 alpha
CD14	IL-3	CCL19/MIP-3 beta

CD30	IL-4	MMP-9
CD31/PECAM-1	IL-5	Myeloperoxidase
CD40 Ligand/TNFSF5	IL-6	Osteopontin (OPN)
Chitinase 3-like	IL-8	PDGF-AA
Complement Component C5/C5a	IL-10	PDGF-AB/BB
Complement Factor D	IL-11	Pentraxin 3/TSF-14
C-Reactive Protein/CRP	IL-12 p70	CXCL4/PF4
Cripto-1	IL-13	RAGE
Cystatin C	IL-15	CCL5/RANTES
Dkk-1	IL-16	RBP4
DPPIV/CD26	IL-17A	Relaxin-2
EGF	IL-18 BPa	Resistin
CXCL5/ENA-78	IL-19	CXCL12/SDF-1 alpha
Endoglin/CD105	IL-22	Serpin E1/PAI-1
EMMPRIN	IL-23	SHBG
Fas Ligand	IL-24	ST2/IL1 R4
FGF basic	IL-27	CCL17/TARC
KGF/FGF-7	IL-31	TFF3
FGF-19	IL-32 alpha/beta/gamma	TfR
Flt-3 Ligand	IL-33	TGF-alpha
G-CSF	IL-34	Thrombospondin-1
GDF-15	CXCL10/IP-10	TIM-1
GM-CSF	CXCL11/I-TAC	TNF-alpha
CXCL1/GRO alpha	Kallikrein 3/PSA	uPAR
Growth Hormone (GH)	Leptin	VCAM-1
HGF	LIF	VEGF
ICAM-1/CD54	Lipocalin-2/NGAL	Vitamin D BP

2.6.2 ELISA

To analyse the expression of specific cytokines and chemokines in cell culture supernatants, cell culture supernatants were processed as described in 2.6.1 and then analysed using the Human Chitinase 3-like 1 Quantikine ELISA Kit (DC3L10), Human Serpin E1/PAI-1 Quantikine ELISA Kit (DSE100), DPPIV/CD26 Quantikine ELISA Kit (DC260B), Human MMP-9 Quantikine ELISA

Kit (DMP900), Human CXCL10/IP-10 Quantikine ELISA Kit (DIP100), and Human Active MMP-9 Fluorokine E Kit (F9M00, all R&D Systems) according to the manufacturer's instructions.

2.7 Data analysis

Statistical analyses were conducted using GraphPad Prism 9 software. Two groups were compared using two-tailed unpaired t-tests, and multiple group comparisons were done by one-way analysis of variance (ANOVA) with Dunnett's and Tukey's *post-hoc* test or two-way ANOVA with Tukey's *post-hoc* test and repeated measurements (RM) if appropriate. The statistical test and number of *in vitro* experiments and different lines used for each analysis are indicated in each figure legend. For comparisons between C9ORF72 patient-derived iPSC lines and healthy controls, different lines and differentiations for each condition were pooled to investigate the overall difference between C9ORF72 patients and controls. For the comparison between the isogenic control line and its C9ORF72 patient-derived donor line, multiple differentiations for one line were pooled. Data are presented as single data points and means ± standard error of the mean (SEM). The definition of each data point is provided in the figure legends. Differences were considered significant when $P < 0.05$ (*$P < 0.05$; **$P < 0.01$; ***$P < 0.001$; ****$P < 0.0001$; ns.: not significant). GraphPad Prism 9 or RStudio were used to plot data. Some schematics were created with BioRender.com. Final assembly and preparation of all figures was done in Adobe Illustrator.

3 Establishing and characterising a co-culture of iPSC-derived microglia and motor neurons

The data in this chapter have been published in:

Vahsen, B.F., Gray, E., Candalija, A., Cramb, K.M.L., Scaber, J., Dafinca, R., Katsikoudi, A., Xu, Y., Farrimond, L., Wade-Martins, R., James, W.S., Turner, M.R., Cowley, S.A., and Talbot. K. (2022). Human iPSC co-culture model to investigate the interaction between microglia and motor neurons. Sci Rep 12, 12606.

3.1 Introduction and aims

Numerous studies have analysed the role of microglia in different *in vitro* and *in vivo* animal models for ALS. However, it is now becoming increasingly clear that substantial differences exist between rodent and human microglia. For instance, many microglial neurodegenerative disease-associated genes do not have appropriate orthologues in mice (Mancuso et al., 2019), posing significant challenges for the study of these genes using rodent models. Modelling disease-associated mutations appropriately in rodents is not a simple task; for instance, the biochemistry of HREs in *C9ORF72* is complex and the development of an accurate animal model has not yet been achieved. iPSC technology provides a means to overcome these obstacles, allowing for the generation of patient-derived cells, while simultaneously retaining the genetic background of the donor. Differentiated disease-relevant cells can be used to study the effect of disease-associated genetic variants on cellular pathways and function.

Several protocols for the differentiation of iPSC-derived microglia had just been published prior to my DPhil project, allowing for the study of comparably authentic

human microglial cells. iPSC microglia are becoming an increasingly popular tool for the study of neurodegenerative diseases, and a first publication investigating the effect of an ALS-associated mutation in the *FUS* gene on iPSC microglia has just been published (Kerk et al., 2022). Monoculture setups are ideal for the study of cell-autonomous microglial phenotypes. Co-cultures, on the other hand, allow for the investigation of non-cell-autonomous effects of microglia on neurons. Furthermore, it was previously shown that co-culture and transplantation approaches support a homeostatic microglial state due to the interaction with a more physiological environment (Giacomelli et al., 2022; Haenseler et al., 2017). The first main aim of this chapter was therefore to establish an ALS-relevant co-culture model by optimising and combining our previously published differentiation protocol for iPSC-derived spinal MNs with iPSC microglia. For the differentiation of iPSC-derived microglia, I adopted the previously published protocol from the Cowley Lab (Sir William Dunn School of Pathology, University of Oxford) (Haenseler et al., 2017; van Wilgenburg et al., 2013). The second main aim was to perform a comprehensive characterisation of this iPSC MN-microglia co-culture paradigm to assess the identity and function of both cell types in co-culture.

3.2 Differentiation of iPSC-derived microglia and spinal MNs, and optimisation of culture conditions for co-culture

The previously published protocol from (van Wilgenburg et al., 2013) allows for the reliable and reproducible generation of large amounts of macrophage/microglia precursors. iPSCs are initially expanded and then differentiated into EBs in AggreWell™ plates, after which the EBs are transferred to larger tissue culture

flasks (Figure 3.1A). Upon the addition of M-CSF and IL-3, the EBs develop into yolk-sac like structures, which start to release precursor cells into the supernatant after some weeks (Figure 3.1A). These precursors can be collected and then terminally differentiated into microglia. I first established the differentiation of microglia precursors and then focused on optimising our MN differentiation protocol for co-culture with microglia.

In our previously published differentiation protocol for spinal MNs (Ababneh et al., 2020; Dafinca et al., 2020; Dafinca et al., 2016), we first promote neural identity using Compound C and Chir99021 and then induce caudalisation and ventralisation via addition of RA and SAG (Figure 3.1B). On DIV 18, MNs are dissociated, counted, and re-plated at defined cell numbers. Final post-mitotic maturation is achieved by additional treatment with BDNF, GDNF, and DAPT (Figure 3.1B). Assays and experiments are then typically conducted on DIV 30 as per our previous studies (Ababneh et al., 2020; Dafinca et al., 2020). Intending to mimic spinal cord development and combine the precursors of both cell types as early as possible without disturbing MN differentiation, I opted to differentiate MNs in monoculture with no changes to the protocol until DIV 21, at which time point the neurons typically already display robust neurite branching. On DIV 21, I aimed to add in the macrophage/microglia precursors and then mature both cell types in co-culture until at least DIV 35 (Figure 3.1B), as 14 days were found to be an optimal co-culture duration in the previous study of the Cowley Lab (Haenseler et al., 2017).

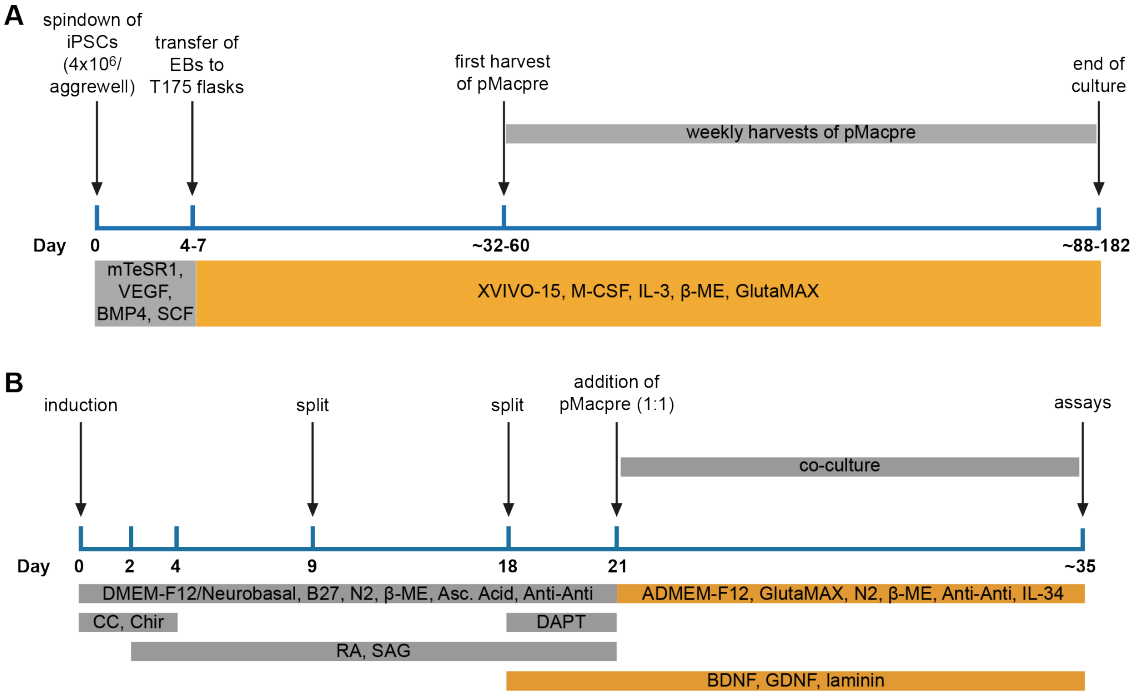


Figure 3.1: Differentiation protocols for iPSC macrophage/microglia precursors and spinal motor neurons, and adaptations for motor neuron-microglia co-culture. A) Schematic overview of differentiation protocol for iPSC macrophage/microglia precursors. iPSCs were spun down, and embryoid body (EB) formation was induced using VEGF, BMPF, and SCF over the course of 4-7 days. EBs were then transferred to large tissue culture flasks and macrophage/microglia precursor (pMacpre) formation was induced with M-CSF and IL-3. After about 4-8 weeks, pMacpre emerged into the supernatant and were harvested weekly for terminal differentiation into microglia. Differentiation factories were maintained for several weeks and up to 6 months. **B)** Schematic overview of differentiation protocol for iPSC MNs and co-culture with microglia. iPSCs are differentiated to spinal MNs in monolayers. Neural identity is promoted by Compound C (CC) and Chir99021 (Chir). Ventralisation and caudalisation is achieved using RA and SAG. On DIV 18, MNs are dissociated and replated, and terminal differentiation is performed through addition of BDNF, GDNF, and DAPT. In our previously established MN monoculture differentiation protocol, DAPT was removed after seven days, and cells were kept until DIV 30 (Ababneh et al., 2020; Dafinca et al., 2020; Dafinca et al., 2016). Here, the medium composition was optimised for co-culture, and therefore changed on DIV 21 to allow for compatibility with microglia. Cells were kept at least until DIV 35. Figure adapted from (Vahsen et al., 2022).

First, I sought to optimise the MN culture medium for compatibility with both cell types, aiming to retain the identity of MNs while simultaneously removing constituents of the culture medium that could negatively impact on the identity or function of microglia. I sequentially excluded four immunomodulatory constituents, namely B27 supplement, RA, SAG, and DAPT, from the culture medium on DIV 21 (Figure 3.1B). In parallel, I replaced the DMEM-F12/Neurobasal 50:50 background medium with ADMEM-F12 plus GlutaMAX and added in IL-34, to

establish optimal culture conditions for microglia differentiation and survival as described previously (Haenseler et al., 2017) (Figure 3.1B). Differentiating MNs in monoculture using a battery of different compositions where one immunomodulatory medium constituent was either added or removed, I observed no difference compared with full MN medium (data not shown). Encouraged by this observation, I differentiated MNs and microglia precursors in parallel, plated the microglia precursors on top of the MNs on DIV 21, and maintained them in co-culture using the newly defined co-culture medium (Figure 3.2A) After 14 days, the resulting co-cultures showed clear expression of the microglia marker IBA1 and the MN marker ChAT (Figure 3.2A). To assess if the co-culture medium *per se* affected MN marker expression, I differentiated MN monocultures in our full MN medium and in the newly defined co-culture medium, changing the medium composition on DIV 21. Quantifying the neuron marker TUJ1 and the two MN markers ChAT and ISLET1, I observed similar expression in MNs in both media, confirming that MN identity was not affected by the change in medium composition (Figure 3.2B, C). For the comparison of MN identity in monocultures and co-cultures, one has to factor in that the total number of cells is different between monocultures and co-cultures. Therefore, to compare monocultures and co-cultures, I did not quantify the percentage of ChAT and ISLET1-positive cells but rather their expression in TUJ1-positive neuronal cells. Again, I observed similar expression for MNs in monoculture, differentiated in MN medium and co-culture medium, and co-cultured MNs (Figure 3.2D), confirming that co-culture does not alter MN identity.

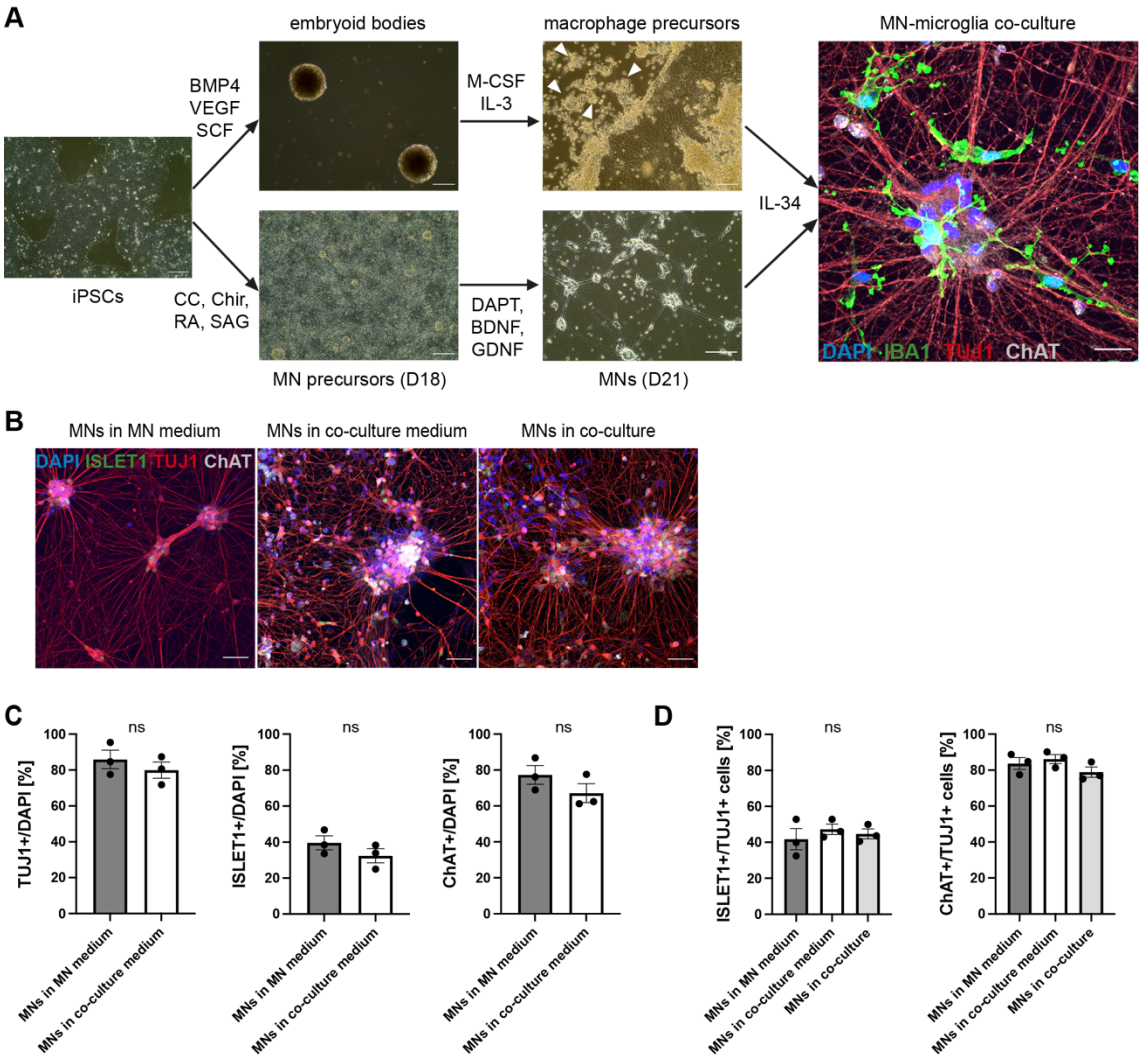


Figure 3.2: iPSC motor neuron-microglia co-cultures express key motor neuron markers. **A)** Exemplar images of iPSCs, key steps for the differentiation protocol for both lineages, and the resulting co-cultures, which are positive for the MN marker ChAT and the microglial marker IBA1. White arrowheads indicate macrophage/microglia precursors. Scale bars: 200 µm (left and centre images), 25 µm (right image). **B)** Exemplar images of MNs in MN medium (left), co-culture medium (centre), and co-culture with microglia (right), stained for the MN markers ISLET1 and ChAT. Scale bars: 50 µm. **C)** Quantification of the expression of TUJ1, ISLET1, and ChAT in all cells in MN monocultures in MN or co-culture medium. **D)** Quantification of ISLET1 and ChAT expression in TUJ1-positive neurons in MN medium, co-culture medium, and co-culture with microglia. Single data points from n=3 lines from different healthy donors. One-way ANOVA and Tukey's multiple comparisons test. Figure adapted from (Vahsen et al., 2022).

Of note, as part of our publication describing and characterising the MN-microglia co-culture, we also assessed the properties of MNs differentiated in MN medium, co-culture medium, and co-culture using calcium imaging and patch-clamp electrophysiology (Vahsen et al., 2022). The data confirmed the expected neuronal properties in MNs and demonstrated that the co-culture medium and co-culture

did not have a negative impact on MN function but, in fact, showed a tendency to increase the activity of MNs (Vahsen et al., 2022).

In summary, these data show the successful differentiation of iPSC macrophage/microglia precursors and MNs, and the successful combination of both cell types in a co-culture system.

3.3 Co-culture does not alter cleaved caspase 3 expression in iPSC microglia or motor neurons

To evaluate if changes to the medium composition, or co-culture, affected the survival of MNs or microglia, I then analysed the expression of the apoptosis marker CC3 in MNs and microglia in monocultures and co-cultures. Comparing the expression of CC3 in TUJ1-positive neuronal cells, I found no significant differences between MNs in monoculture grown in MN medium and co-culture medium or in co-culture with microglia (Figure 3.3A, B). Similarly, quantifying the expression of CC3 in IBA1-positive microglia in monocultures and co-cultures, I found no differences (Figure 3.3C, D).

Together, these results demonstrate that changes to the medium composition or co-culture do not induce apoptosis in MNs or microglia.

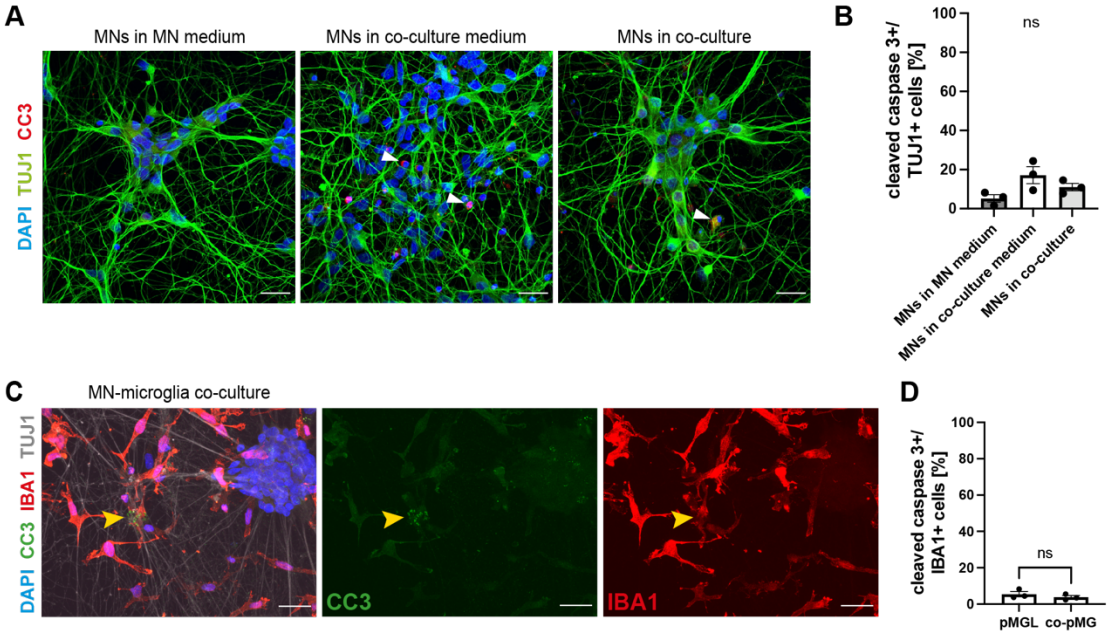


Figure 3.3: Analysis of cleaved caspase 3 expression in iPSC motor neurons and microglia shows no difference between monocultures and co-cultures. A) Exemplar images of expression of the apoptosis marker cleaved caspase 3 (CC3) in TUJ1-positive neurons in MN medium (left), co-culture medium (centre), and co-culture with microglia (right). White arrowheads indicate CC3-positive cells. Scale bars: 25 µm. **B)** Quantification of CC3 expression in TUJ1-positive neurons in MN medium, co-culture medium, and co-culture with microglia. **C)** Exemplar images of CC3 expression in IBA1-positive microglia in co-culture. Yellow arrowheads indicate CC3-positive cells. Scale bars: 25 µm. **D)** Quantification of CC3 expression in IBA1-positive microglia in monoculture and co-culture. Scale bars: 25 µm. Single data points from n=3 lines from different healthy donors. One-way ANOVA and Tukey's multiple comparisons test (**B**) and two-tailed unpaired t-test (**D**). Figure adapted from (Vahsen et al., 2022).

3.4 Transcriptomic analysis demonstrates a microglial signature in iPSC microglia in monoculture and co-culture

Next, I sought to evaluate the identity of microglia differentiated in monoculture and co-culture with MNs. Microglial identity cannot be easily defined by the expression of a small set of markers. Hence, I opted to perform an RNA sequencing analysis to compare the transcriptome of our differentiated cell with post mortem human microglial cells, previously published iPSC-derived microglia, and other immune cell types. For microglial monocultures, RNA was simply extracted from the whole well of the culture plate, while co-cultured microglia first had to be enriched. The macrophage/microglia marker CD11b was clearly and highly

expressed in microglia in co-culture (Figure 3.4A, B), rendering it suitable to pull down co-cultured microglia, as performed previously (Haenseler et al., 2017). I therefore employed magnetic-activated cell sorting (MACS) with magnetic beads against CD11b to extract the microglia from co-cultures.

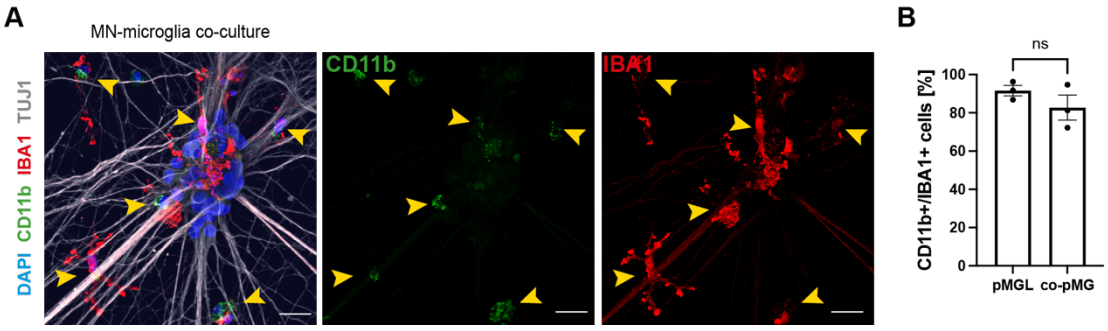


Figure 3.4: Analysis of CD11b expression in iPSC microglia in monoculture and co-culture. **A)** Exemplar images of expression of CD11b in IBA1-positive microglia in co-culture. Yellow arrowheads indicate examples of CD11b-positive cells. Scale bars: 25 µm. **B)** Quantification of CD11b expression in IBA1-positive microglia in monoculture and co-culture with MNs. Single data points from n=3 lines from different healthy donors. Two-tailed unpaired t-test. Figure adapted from (Vahsen et al., 2022).

I dissociated co-cultures using a papain/accutase mix and enriched co-cultured microglia using CD11b-MACS. RNA extracted from the panned population was then subjected to RNA sequencing analysis, along with microglia cultured in monocultures and macrophage/microglia precursor cells. Of note, microglia in monoculture and co-culture were differentiated in parallel from the same harvest of precursors to avoid transcriptomic differences due to potential batch effects between the different cell types. The main aim of this experiment was to compare the identity of our cells with primary human microglia, other iPSC-derived microglia grown in monoculture and co-culture, and blood monocytes, the latter of which would be expected to differ in their transcriptome compared with microglia. To this end, I obtained and reanalysed the RNA sequencing datasets from two seminal iPSC microglia publications (Abud et al., 2017; Muffat et al., 2016), which sequenced iPSC-derived microglia but also blood monocytes and *bona fide*

human microglia. Comparisons between different datasets have inherent limitations due to differences in sample processing; however, I performed identical mapping, processing, and downstream analyses for all three datasets to optimise the comparability of the sequencing analyses.

First, I compared the expression of *MYB*, *PU.1*, and *RUNX1*, as *bona fide* microglial cells are thought to develop from yolk-sac precursors in an *MYB*-independent and *RUNX1*- and *PU.1*-dependent manner (Buchrieser et al., 2017). *MYB* expression was almost absent in our iPSC myeloid cells, similar to primary fetal and adult human microglia (Figure 3.5). In contrast, *PU.1* and *RUNX1* were highly expressed (Figure 3.5), providing reassurance that the ontogeny of our cells is in keeping with their assumed primitive haematopoietic origin, in line with previous observations for cells differentiated with this protocol (Buchrieser et al., 2017). I then performed exploratory analyses for the RNA sequencing dataset using PCA and heatmaps with hierarchical clustering, both using the top 500 most variable genes with biggest variance. The PCA plot of principal component 1 (PC) 1 versus PC 2 broadly showed three groups (Figure 3.6A). $CD14^+$ and $CD16^+$ blood monocytes from (Abud et al., 2017) formed a group and separated out from a second group containing the iPSC-derived microglia in monoculture and co-culture with rat neurons from (Abud et al., 2017). A more diffuse third group contained the primary fetal and adult human microglia, all of the myeloid/microglial cells generated in this study, and monocultured microglia from (Muffat et al., 2016). Whereas the microglia I differentiated in monoculture were more closely aligned with the microglial monocultures from (Muffat et al., 2016) on PC 1, co-

culture with MNs shifted them towards the *bona fide* human microglial cells. Unsupervised hierarchical clustering broadly confirmed these observations (Figure 3.6B). Blood monocytes clustered together with the microglia cultured in monoculture and co-culture with rat neurons from (Abud et al., 2017). 3 of the 4 microglial monoculture samples clustered with the monocultured microglia from (Muffat et al., 2016), while the precursors and co-cultured microglia differentiated with our protocol clustered with the fetal and adult human microglia.

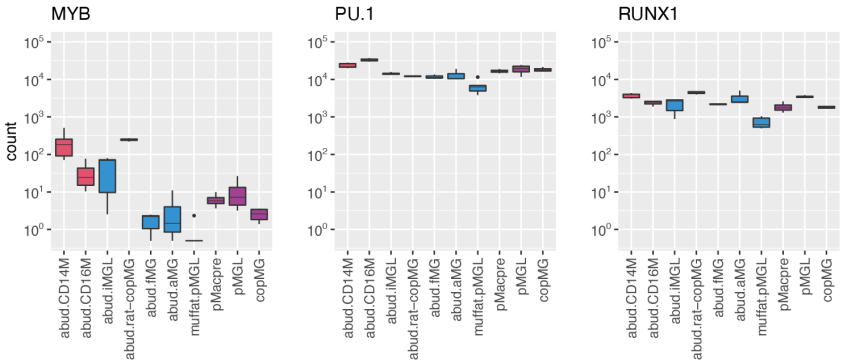


Figure 3.5: Analysis of *MYB*, *PU.1*, and *RUNX1* in iPSC microglia in monoculture and co-culture using our and previously published RNA sequencing datasets. Macrophage/microglia precursors (pMacpre) and microglia in monoculture (pMGL) and co-culture with MNs (co-pMG, after CD11b-MACS) were generated in this study and integrated with samples from (Abud et al., 2017) (microglia in monoculture: abud.iMGL, microglia in co-culture with rat neurons: abud.rat-copMG, CD14+ blood monocytes: abud.CD14M, CD16+ blood monocytes: abud.CD16M, fetal primary human microglia: abud.fMG, adult primary human microglia: abud.aMG) and (Muffat et al., 2016) (microglia in monoculture: muffat.pMGL). Box plots of normalized DESeq2 counts for *MYB*, *PU.1*, and *RUNX1* gene expression in RNA sequencing (n=6 samples for abud.iMGL, abud.rat-copMG and muffat.pMGL, n=5 samples for abud.CD16M, n=4 samples for abud.CD14M, pMacpre, pMGL and co-pMG, n=3 samples for abud.aMG and abud.fMG). Figure adapted from (Vahsen et al., 2022).

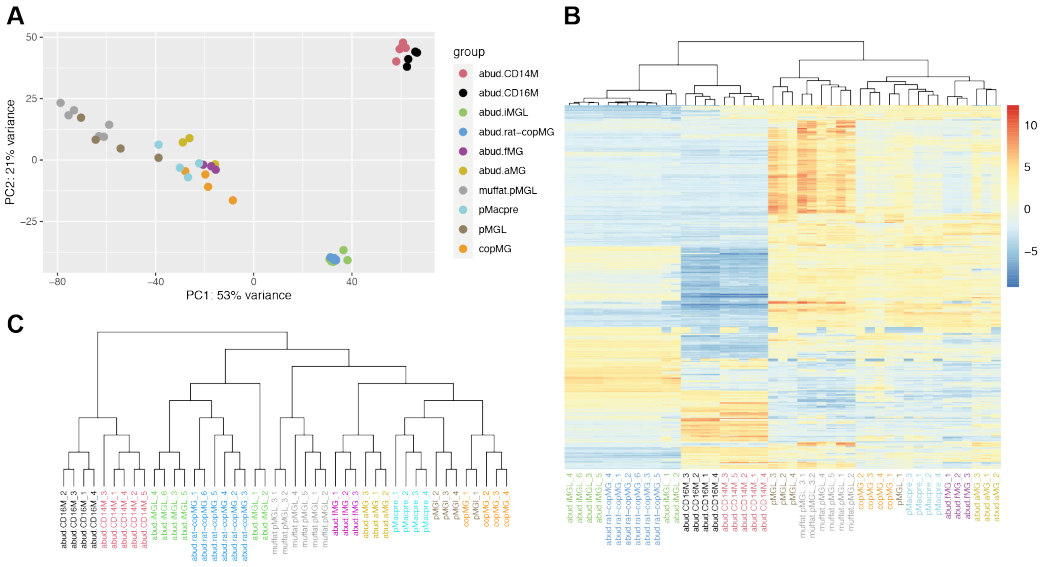


Figure 3.6: Transcriptomic analysis demonstrates a microglial signature for iPSC microglia in monoculture and co-culture. A) PCA plot of VST-transformed RNA sequencing samples based on top 500 most variable genes with biggest variance. Macrophage/microglia precursors (pMacpre) and microglia in monoculture (pMGL) and co-culture with MNs (co-pMG) were generated from four different healthy control lines in this study and integrated with samples from (Abud et al., 2017) (microglia in monoculture: abud.iMGL, microglia in co-culture with rat neurons: abud.rat-copMG, CD14+ blood monocytes: abud.CD14M, CD16+ blood monocytes: abud.CD16M, fetal primary human microglia: abud.fMG, adult primary human microglia: abud.aMG) and (Muffat et al., 2016) (microglia in monoculture: muffat.pMGL). **B)** Heatmap of relative VST-transformed values across samples based on top 500 most variable genes with biggest variance with unsupervised hierarchical clustering between samples. **C)** Dendrogram of unsupervised hierarchical clustering of relative VST-transformed values of samples based on set of ~1300 microglial genes identified by (Galatro et al., 2017). n=6 samples for abud.iMGL, abud.rat-copMG and muffat.pMGL, n=5 samples for abud.CD16M, n=4 samples for abud.CD14M, pMacpre, pMGL and co-pMG, n=3 samples for abud.aMG and abud.fMG. Figure adapted from (Vahsen et al., 2022).

In a previous publication, (Galatro et al., 2017) identified a set of ~1300 microglial key genes. I also used this list of genes to compare the microglial identity of our samples with the datasets from (Abud et al., 2017) and (Muffat et al., 2016) using hierarchical clustering (Figure 3.6C). This analysis yielded similar results to the PCA and heatmap based on the top 500 genes with biggest variance (Figure 3.6A, B). The blood monocytes formed a separate cluster from all other cell types. A separate cluster was formed by the microglia in monoculture and co-culture from (Abud et al., 2017). The microglia from (Muffat et al., 2016) separated out

from another cluster, which was further subclustered into the *bona fide* primary human microglia and all of the myeloid cells I generated in this study. 3 of the 4 co-culture microglia samples formed a separate cluster from the precursors and monoculture microglia.

In summary, these data confirm the microglial identity of the iPSC-derived microglia differentiated in monoculture and co-culture with MNs in this thesis.

3.5 Transcriptomic comparison of iPSC microglia differentiated in monoculture and co-culture

Having confirmed the microglial identity of the iPSC microglia, I aimed to compare our microglia grown in monoculture and co-culture to understand if the different culture environments altered the microglial transcriptome. Using differential expression analysis, I identified 1566 differentially expressed genes (DEGs) (Figure 3.7A). I then performed pathway analysis using GO terms to see if specific pathways were enriched in microglial monoculture or co-culture. The genes upregulated in co-culture showed enrichment of the GO term “regulation of neurotransmitter levels” and three cytokine-associated terms (Figure 3.7B). Further exploring the DEGs associated with these pathways I found some genes, such as *SYT4* (synaptotagmin 4) (Figure 3.7C), which have high expression in neurons and could be differentially expressed due to possible phagocytic engulfment of neuronal material by microglia or low-level neuronal contamination of the CD11b-MAC-sorted co-culture microglial population. However, homeostatic microglia-

specific genes, including *LAG3* (lymphocyte activating 3*)* and *IRF4* (interferon regulatory factor 4), were also up-regulated in co-culture (Figure 3.7C).

I also investigated the enrichment of pathways for the genes downregulated in co-culture. For these, the highest enrichment score was for extracellular matrix (ECM)-associated GO terms (Figure 3.7D). Amongst the DEGs associated with this term, several genes were associated with collagen- and cell-to-matrix-interaction, including *COL4A1* (Collagen type IV alpha 1), *FN1* (Fibronectin 1) and *FBN1* (Fibrillin-1), and matrix metalloproteinases such as *MMP16* (Matrix metalloproteinase-16) (Figure 3.7E).

Together, these data indicate that microglia in co-culture are characterised by a specific transcriptome.

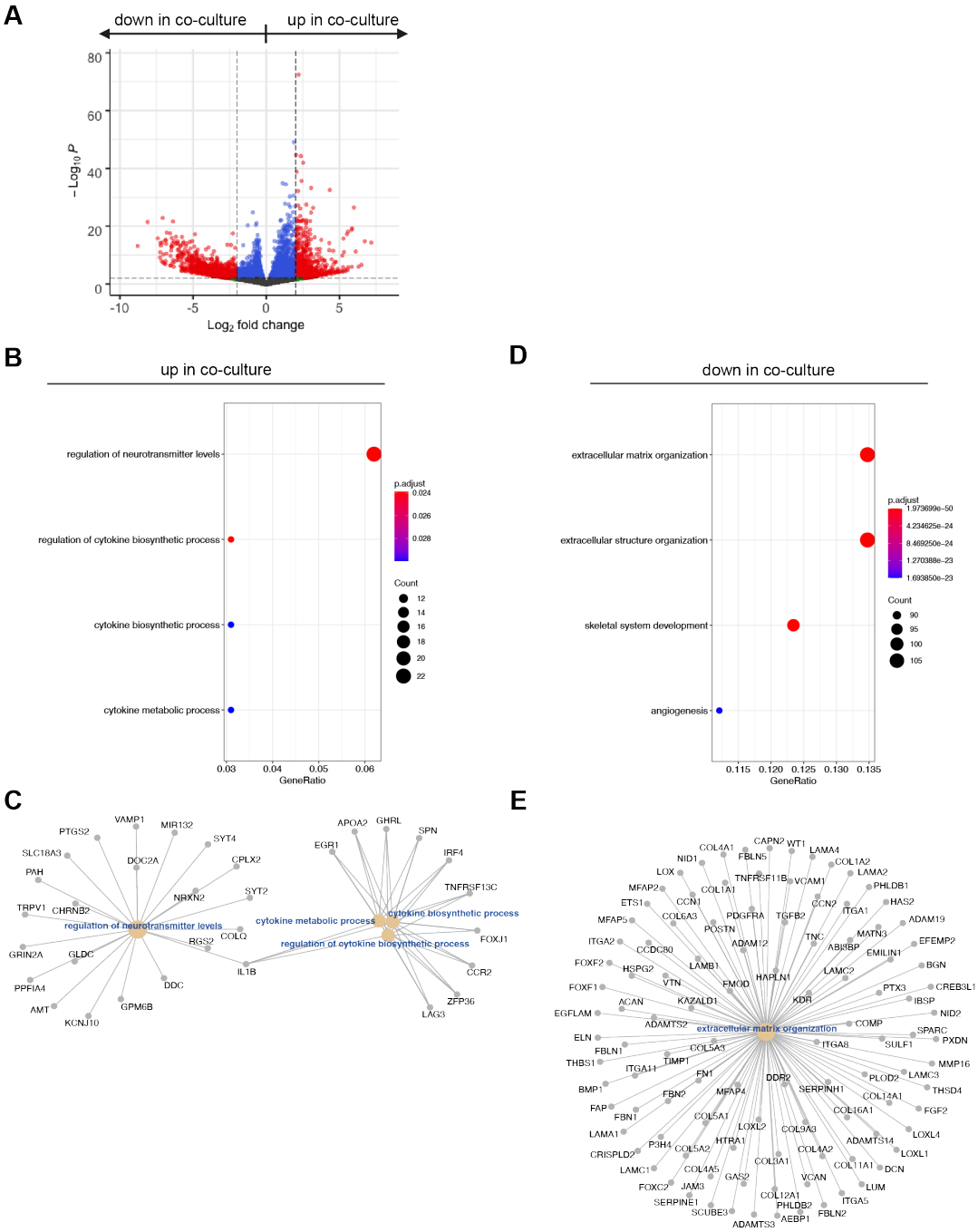


Figure 3.7: Transcriptomic comparison of iPSC microglia in monoculture and co- culture. **A)** Volcano plot of all differentially expressed genes (DEGs) between monocultures and co-cultures. Genes with | log2 fc | > 2 and adjusted p-value < 0.01 were defined as DEGs and are depicted in red. Up-regulated DEGs: 726, down-regulated DEGs: 843. **B)** Dot plot showing top 4 enrichment terms using pathway enrichment for Gene Ontology (GO) terms for genes up-regulated in co-culture. **C)** Cnet plot showing DEGs associated with the enriched GO terms in B. **D)** Dot plot showing top 4 GO enrichment terms for genes down-regulated in co-culture. **E)** Cnet plot showing DEGs associated with the enriched GO term “extracellular matrix organization”. Figure adapted from (Vahsen et al., 2022).

3.6 Co-culture supports a homeostatic microglial state

To follow up on the differences between microglial monocultures and co-cultures indicated by the RNA sequencing analysis, I assessed the microglial morphology in monoculture and co-culture. For this analysis, I used 3DMorph, a previously published tool for the automated analysis of microglial morphology (York et al., 2018). Compared with microglia in monoculture, microglia co-cultured with MNs showed similar branch length but an increased number of branch points and end-points (Figure 3.8A-D). These results reflect an increased ramified state in co-culture and corroborate that co-culture supports a homeostatic microglial identity.

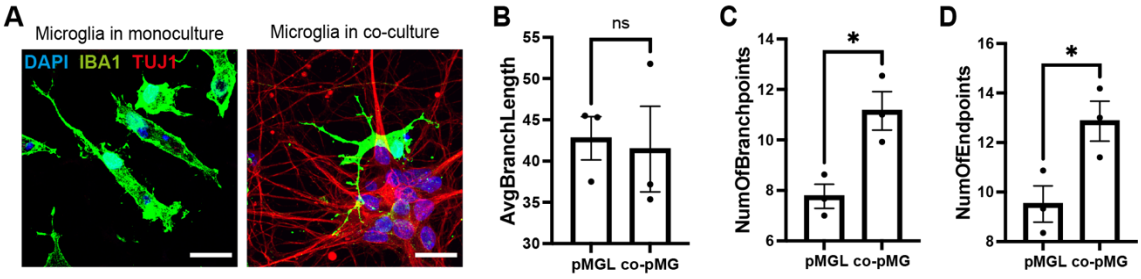


Figure 3.8: iPSC microglia grown in co-culture with MNs have a more ramified morphology than in monoculture. A) Exemplar images of microglial ramifications in monoculture (left) and co-culture with MNs (right). Scale bars: 20 µm. **B-D)** Quantification of the average branch length (**B**), number of branch points (**C**), and number of end points (**D**) for microglia in monoculture and co-culture using 3DMorph demonstrates significantly enhanced ramifications in co-culture (n=3 lines from different healthy donors). Two-tailed unpaired t-test. Figure adapted from (Vahsen et al., 2022).

3.7 Key microglial markers are expressed in iPSC microglia in monoculture and co-culture

I then sought to compare the expression of key myeloid/microglial markers associated specifically with microglia but not with blood monocytes as defined by previous studies (Bennett et al., 2016; Butovsky et al., 2014; Melief et al., 2012), namely *P2RY12*, *MERTK*, *TREM2*, *TMEM119*, Protein S (*PROS1*), complement C1q A chain (*C1QA*), growth arrest specific 6 (*GAS6*), and G protein-coupled

receptor 34 (*GPR34*). Using the RNA-seq dataset, I found clear expression and enrichment of *P2RY12*, *MERTK*, *TREM2*, *TMEM119*, *PROS1*, *C1QA*, *GAS6*, and *GPR34* (Figure 3.9A). Compared with the classical $CD14^+$ blood monocytes, *TREM2*, *MERTK*, *C1QA*, *PROS1*, *GAS6*, and *GPR34* were particularly enriched across the different iPSC-derived and primary microglial cells (Figure 3.9A).

I then aimed to validate the expression of the key myeloid/microglial markers and performed RT-qPCR analysis using a different set of samples. I differentiated iPSC macrophage/microglia precursors, microglial monocultures and CD11b-MAC-sorted co-cultured microglia, and compared them with $CD14^+$ blood monocytes, fetal primary human microglia, and, additionally, monocultured MNs differentiated in co-culture medium as another negative control (Figure 3.9B). In general, I found substantial overlap between the RNA-sequencing analysis and RT-qPCR data. Notably, most myeloid/microglial genes showed strong enrichment in all myeloid cells compared with MNs, with the notable exception of *PROS1* and *GAS6* (Figure 3.9B). Particularly, *TMEM119* and *TREM2* were highly enriched in the microglial cells compared with blood monocytes. Furthermore, most genes showed similar expression in the iPSC-derived microglial cells and fetal human microglia. *TMEM119* was most highly expressed in the primary microglia (Figure 3.9B), in line with the RNA-seq results (Figure 3.9A). I also confirmed MN identity by RT-qPCR for *ChAT*, which showed strong enrichment in MNs and moderate expression in the MAC-sorted co-culture microglia, likely as a result of low neuronal contamination of the sorted microglial population (Figure 3.9C).

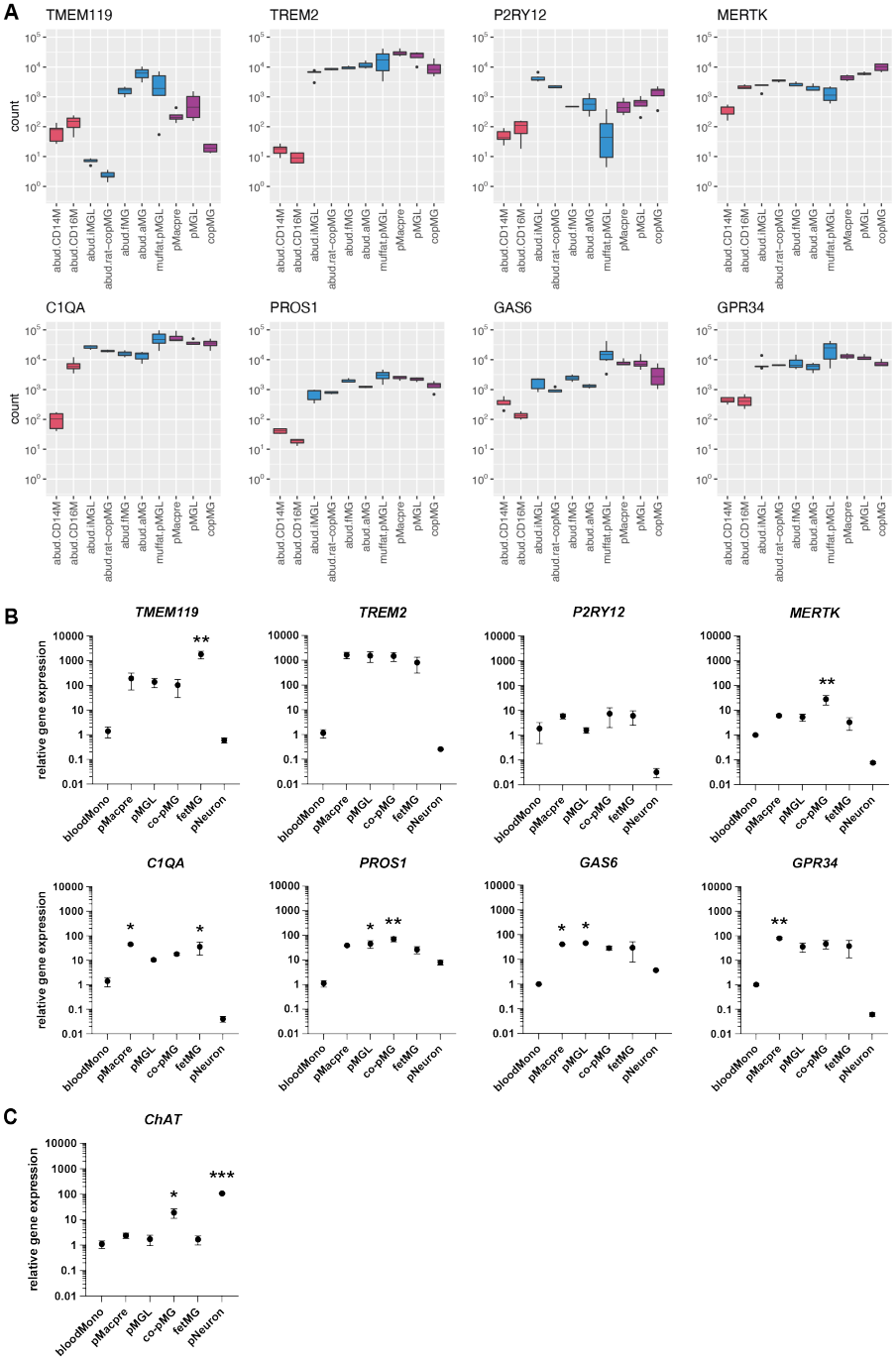


Figure 3.9: iPSC microglia in monoculture and co-culture express macrophage-/microglia markers at gene level. A) Box plots of normalized DESeq2 counts from RNA sequencing analysis for 8 key microglial genes (n=6 samples for abud.iMGL, abud.rat-copMG and muffat.pMGL, n=5 samples for abud.CD16M, n=4 samples for abud.CD14M, pMacpre, pMGL and copMG, n=3 samples for abud.aMG and abud.fMG). Red: blood monocytes from (Abud et al., 2017); blue: iPSC microglia and primary human microglia from (Abud et al., 2017) and (Muffat et al., 2016); purple: microglial samples sequenced in this thesis. **B, C)** Quantification of the relative gene expression of multiple macrophage/microglia markers and the MN marker ChAT by RT-qPCR in iPSC-derived microglia/macrophage precursors (pMacpre), microglia in monoculture (pMGL) and co-culture after CD11b-MACS (co-pMG), MNs in monoculture differentiated in co-culture medium (pNeuron) (all n=3 lines from different healthy donors), human feetal microglia (fetMG, n=3 donors), and human blood monocytes (bloodMono, n=3 healthy donors). Relative expression was calculated using the $2^{-\Delta\Delta Ct}$ method, with *GAPDH* as an endogenous control and normalization to bloodMono. One-way ANOVA and Dunnett's multiple comparisons test versus bloodMono (**B, C**). Figure adapted from (Vahsen et al., 2022).

In addition, I assessed the expression pattern of the two key microglial markers TMEM119 and TREM2 by immunofluorescent staining. Co-cultures showed clear, localized, and high expression of both markers within microglia in mono-culture and co-culture (Figure 3.10A, B).

In summary, these data confirm the microglial identity of our iPSC-derived micro-glial cells in monoculture and co-culture.

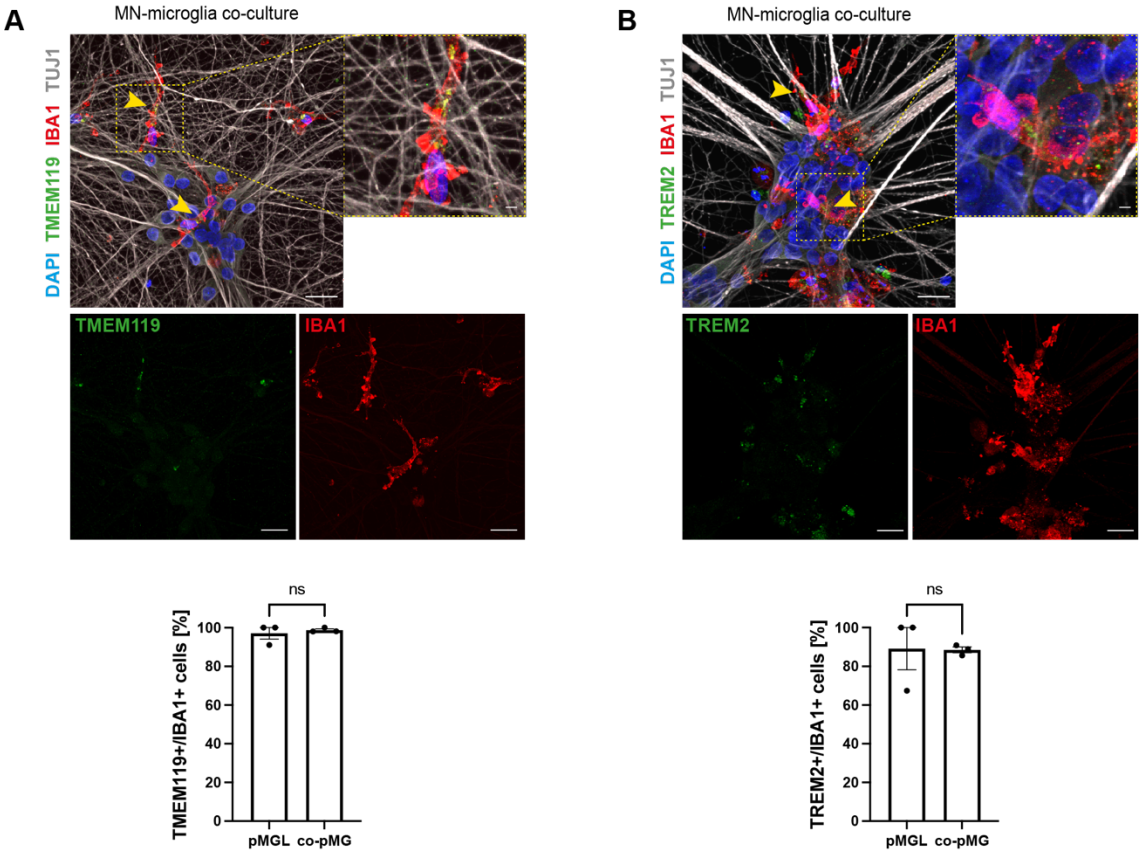


Figure 3.10: iPSC microglia express macrophage-/microglia markers by immunofluorescent staining. A, B) Top: Exemplar images of microglia in co-culture with MNs. Yellow arrowheads and close-ups indicate co-expression of the microglia markers TMEM119 (**A**) and TREM2 (**B**) in IBA1-positive microglia. Scale bars (including insets): 25 µm. Bottom: Quantification of the expression of TMEM119 and TREM2 in IBA1-positive microglia in monoculture and co-culture with MNs. Single data points from n=3 lines from different healthy donors. Two-tailed unpaired t-test. Figure adapted from (Vahsen et al., 2022).

3.8 iPSC microglia in monoculture and co-culture express key ALS-associated genes

In addition, I analysed the expression of key ALS-associated genes across the different myeloid samples in the RNA sequencing datasets (Figure 3.11). *C9ORF72*, *SOD1*, *TARDBP*, and *FUS*, the four commonest genes in which ALS-associated variants are found, had high expression in all analysed cell types. Interestingly, the levels of *C9ORF72* were slightly higher in blood monocytes than in the different microglial cells, and its expression increased in co-culture. I also evaluated the expression of *CHIT1*, *CHI3L1*, *CHI3L2*, and *MCP-1*, four putative biomarkers for ALS (Thompson et al., 2018; Vahsen et al., 2021). Intriguingly, the expression of *CHIT1*, *CHI3L1*, and *MCP-1*, but not *CHI3L2*, was strongly enriched in most microglial cells compared with blood monocytes (Figure 3.11).

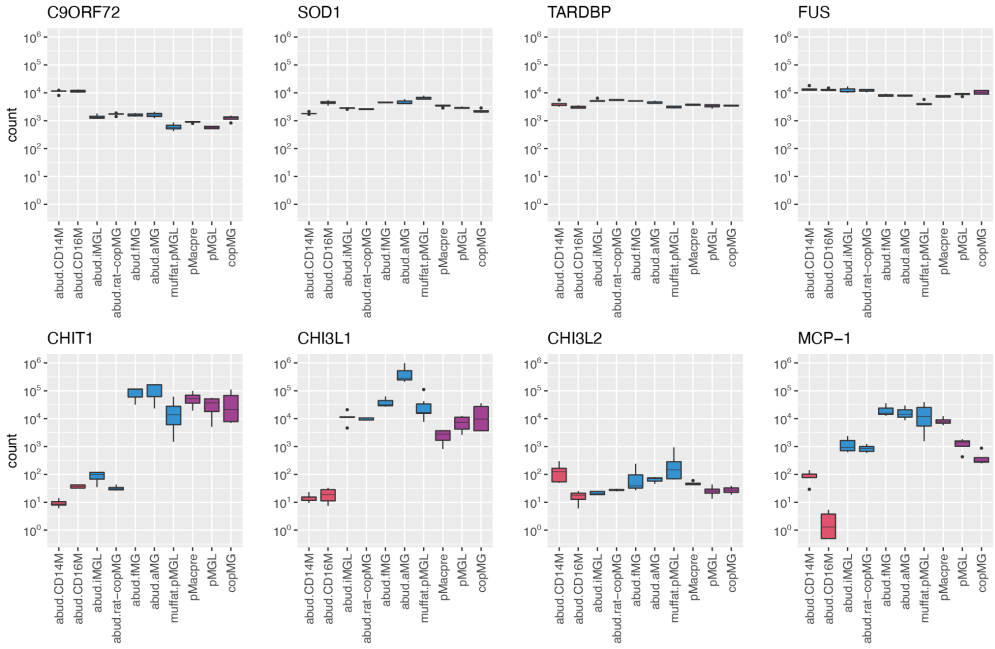


Figure 3.11: iPSC microglia express key ALS-associated genes. Box plots of normalized DESeq2 counts for 8 ALS-associated genes in RNA sequencing (n=6 samples for abud.iMGL, abud.rat-copMG and muffat.pMGL, n=5 samples for abud.CD16M, n=4 samples for abud.CD14M, pMacpre, pMGL and copMG, n=3 samples for abud.aMG and abud.fMG). Figure adapted from (Vahsen et al., 2022). Red: blood monocytes from (Abud et al., 2017); blue: iPSC microglia and primary human microglia from (Abud et al., 2017) and (Muffat et al., 2016); purple: microglial samples sequenced in this thesis.

These results confirm that human microglia have high expression of key ALS-associated genes, as postulated in a recent review (Yvanka de Soysa et al., 2022). Furthermore, microglia are likely to be a key source of ALS-associated biomarkers and iPSC microglia represent a suitable model to study their release *in vitro*.

3.9 Co-cultured iPSC microglia show highly dynamic ramifications and are phagocytically competent

After demonstrating the microglial gene signature of iPSC microglia in monoculture and co-culture, I set out to investigate their functional properties. *Bona fide* microglia are constantly active, continuously scanning the surrounding environment using their highly ramified processes, and show phagocytic competency.

To analyse the motility of co-cultured microglia, I performed live imaging experiments using microglia differentiated from an iPSC line with stable expression of RFP, which allows for easy identification and distinction from neurons in co-culture. Performing live-imaging, I found highly ramified microglial cells in co-culture (Figure 3.12A). Imaging with 1 image every ~30 s over the course of one hour demonstrated very dynamic remodelling of their ramifications (Figure 3.12A). Co-cultured microglia were constantly active and interacted closely with neurons and their neurites, mostly maintaining their territories. These results show that iPSC microglia in co-culture with MNs are motile.

I then evaluated the phagocytic competence of microglia in co-culture performing live imaging over the course of 2 h. For these experiments, I used pHrodo-labelled yeast particles which – due to progressive lysosomal acidification – become fluorescent after phagocytic uptake. Upon addition of these particles to the cultures, co-cultured microglial cells demonstrated increasing visibility of fluorescent dots (Figure 3.12B), confirming that microglia are phagocytically competent in co-culture.

In summary, these data confirm that iPSC microglia in co-culture with MNs have dynamic ramifications and are phagocytically competent.

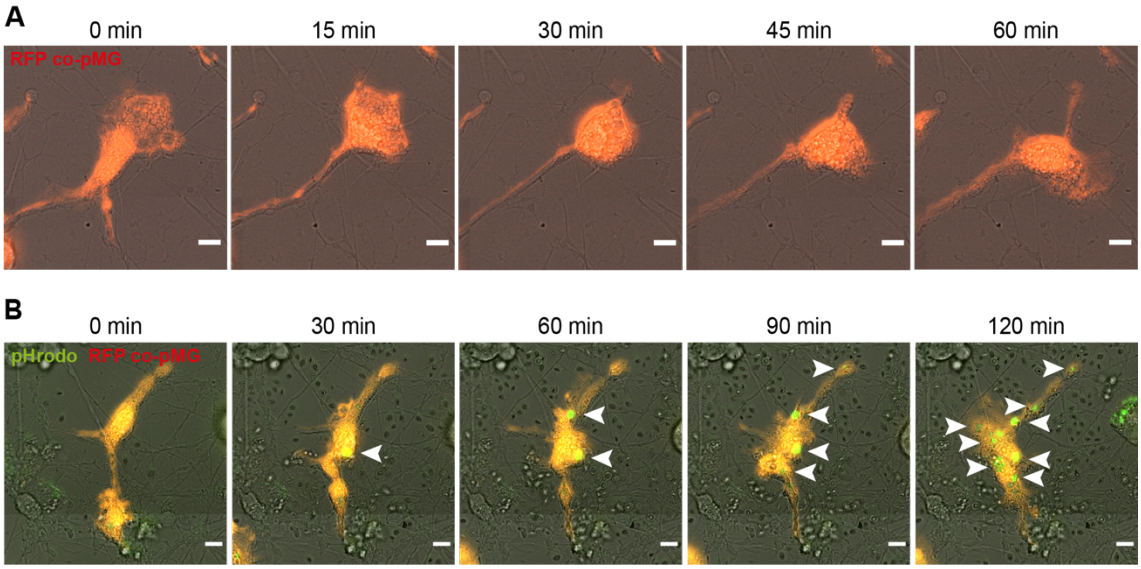


Figure 3.12: iPSC microglia are motile and phagocytically competent in co-culture. A) Live imaging of RFP-expressing microglia in co-culture (co-pMG) over 60 min shows highly dynamic remodelling of microglial ramifications. Scale bar: 10 µm. **B)** Live imaging of RFP-expressing co-pMG over 120 min after addition of pHrodo green zymosan bioparticles shows progressive phagocytic uptake. White arrowheads: phagocytosed particles. Scale bar: 10 µm. Figure adapted from (Vahsen et al., 2022).

3.10 Co-cultured iPSC microglia change morphology and form clusters in response to pro-inflammatory stimulation

Hereafter, I evaluated if co-cultured microglia responded to pro-inflammatory and anti-inflammatory stimulation. I stimulated co-cultures of microglia, again generated from an iPSC line with stable RFP expression, and MNs with LPS/ IFN-γ or IL-4/IL-13 to induce contrasting phenotypes (simplistically termed 'M1' or 'M2', respectively, versus 'M0'). I then performed live imaging to assess the morphological response to stimulation.

After 18 h of stimulation, co-cultured RFP-expressing microglia showed amoeboid morphology and clustering in pro-inflammatory (LPS/IFN-γ) conditions (Figure 3.13A, B). In contrast, no overt morphological changes were observable after induction with IL-4/IL-13 (Figure 3.13C). I then performed another live-imaging experiment to study changes in clustering more closely. In this experiment, I imaged co-cultures before treatment and 9 h and 18 h after the addition of LPS/IFN-γ or IL-4/IL-13 (Figure 3.13D). I expected that pro-inflammatory stimulation would lead to increased microglial cluster formation, resulting in a reduced number of individual cells and increased size of individual clusters. First, I quantified the number of individual microglial cells and the size of microglial clusters before stimulation, which showed no difference (Figure 3.13E, F). However, after 9 and 18 hours of stimulation with LPS/IFN-γ, I observed a significant increase in cluster size, compared with unstimulated or IL-4/IL-13 conditions (Figure 3.13E). In

keeping with this result, the number of individual microglial cells was significantly reduced after 9 and 18 hours of treatment with LPS/IFN-γ (Figure 3.13F).

In summary, these results demonstrate that microglia in co-culture with MNs display the dynamic behaviour expected of microglial cells, by actively responding to stimulation with morphological changes and clustering behaviour,

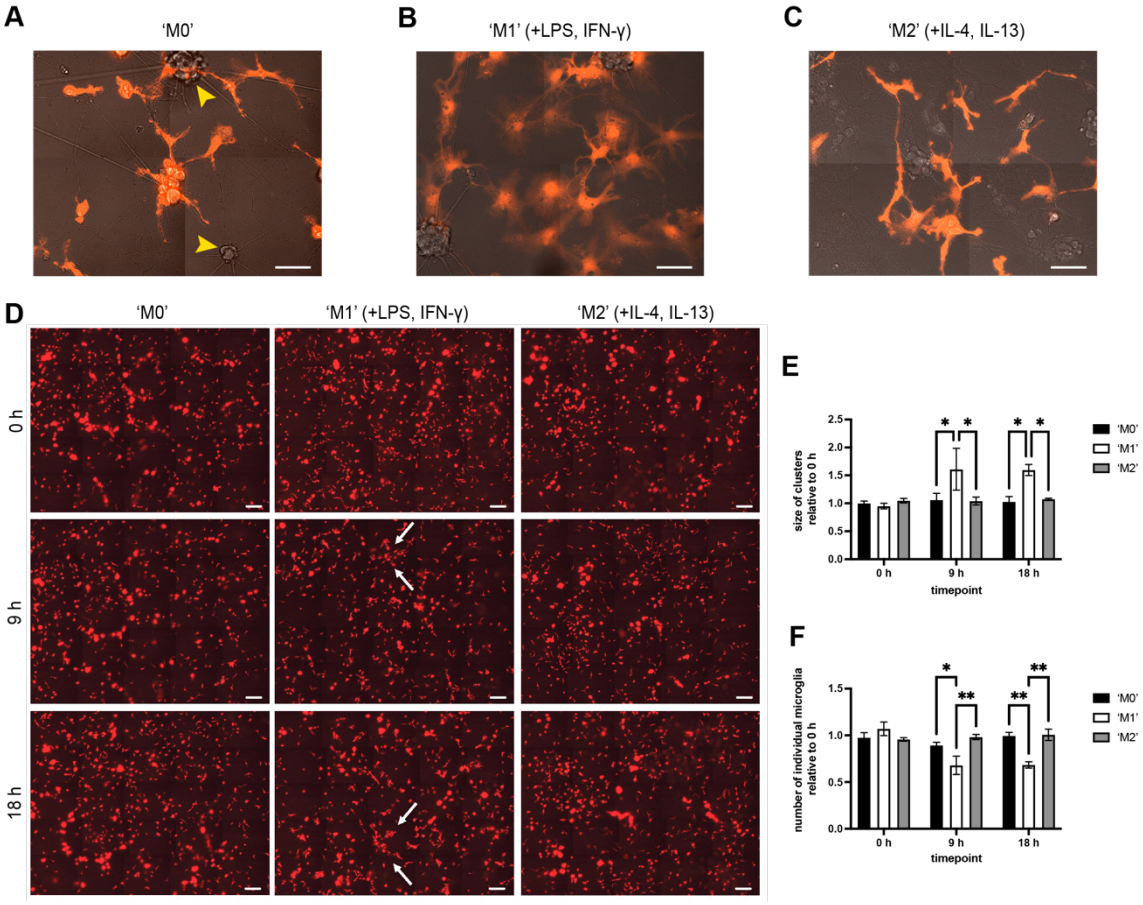


Figure 3.13: iPSC microglia in co-culture respond to stimulation with morphological changes and clustering behaviour. A-C) Exemplar live-imaging pictures of RFP microglia in co-culture with MNs. Cells were either treated with vehicle ('M0', **A**), LPS/IFN-γ to induce a pro-inflammatory phenotype ('M1', **B**) or IL-4/IL-13 to induce an anti-inflammatory phenotype ('M2', **C**). Yellow arrowheads indicate exemplar MN clusters in co-culture. Scale bar: 50 µm. **D)** Representative live-imaging images of RFP microglia in co-culture before stimulation (0 h), and after 9 h and 18 h of treatment with LPS/IFN-γ or IL-4/ IL-13. White arrows indicate examples of microglial clusters. Scale bar: 250 µm. **E)** Quantification of the size of microglial clusters in co-culture at different time points after stimulation relative to 0 h-time point (n=3 lines from different healthy donors). **F)** Quantification of the number of individual microglial cells in co-culture at different time points after stimulation relative to 0 h-time point (n=3 lines from different healthy donors). Two-way repeat measurement ANOVA and Tukey's multiple comparisons test (**E, F**). Figure adapted from (Vahsen et al., 2022).

3.11 iPSC microglia in monoculture and co-culture release pro-inflammatory and anti-inflammatory cytokines

Finally, I evaluated if microglia in monoculture and co-culture released cytokines and chemokines. For this, I used a membrane-based supernatant proteome array, allowing for the detection of 105 different cytokines and chemokines. I used microglial monocultures, MN monocultures, and co-cultures, all of which were differentiated in the same co-culture medium in unstimulated conditions ('M0') or after stimulation with LPS/IFN-γ ('M1') or IL-4/IL-13 ('M2').

Unstimulated MNs released only a small number of cytokines, for instance, IGFBP-2 or osteopontin, while stimulation with LPS/IFN-γ induced the release of a few additional cytokines including IP-10/CXL10 (chemokine (C-X-C motif) ligand 10) (Figure 3.14A). IL-4/IL-13 treatment did not result in substantial changes. In contrast, both unstimulated and stimulated microglial monocultures and co-cultures secreted many more cytokines. LPS/IFN-γ led to the release of several key inflammatory mediators, for instance, IL6, CCL5 (chemokine (C-C motif) ligand 5), CXCL9, and TNF, in microglial monocultures and co-cultures with MNs (Figure 3.14A, B). Co-cultures showed a moderately attenuated secretion profile, compared with microglial monocultures. For instance, CHI3L1 or serpin E1 release was reduced in co-cultures compared with monocultures (Figure 3.14A). *Serpin E1* was also downregulated in co-cultured microglia compared with monocultures in the RNA-seq analysis (Figure 3.7E).

To validate the apparent differences in serpin E1 and CHI3L1 release into the supernatant, I performed ELISAs on supernatants from MNs in monoculture, microglia in monoculture, and co-cultures, using pooled unstimulated and treated sample to compare the overall differences (Figure 3.14C, D). Indeed, I found substantial release of serpin E1 from monocultured microglia by ELISA, which was abolished in co-culture (Figure 3.14C). Similarly, ELISA validation for CHI3L1 showed no release from MNs but a substantial secretion from microglia in monoculture, which was at lower levels in co-culture supernatants (Figure 3.14D).

In summary, these data confirm that microglia in monoculture and co-culture release multiple cytokines and chemokines in unstimulated conditions and respond to stimulation with an altered secretion profile.

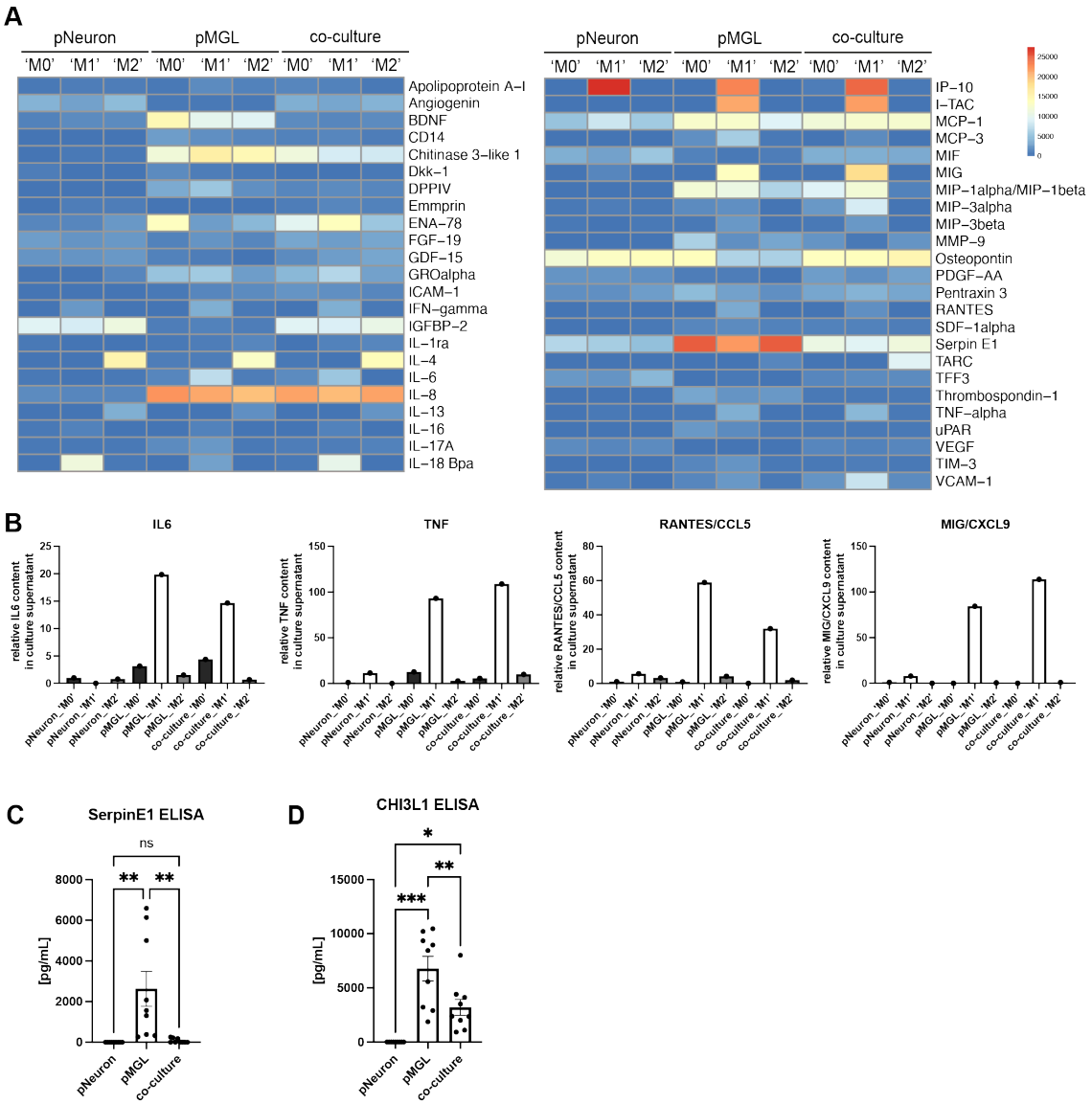


Figure 3.14: iPSC microglia in monoculture and co-culture release cytokines and chemokines in unstimulated conditions and alter their cytokine profile in response to stimulation. **A)** Cytokine release into the culture supernatant from MNs in monoculture (pNeuron), microglia in monoculture (pMGL), and co-cultures was measured using the Proteome Profiler Human XL Cytokine Array Kit. Cells were either treated with co-culture medium as vehicle ('M0'), LPS/IFN-γ ('M1') or IL-4/IL-13 ('M2') for 18 h. Pooled supernatant from n=3 lines from different healthy donors was used for each condition. Data represent the mean of two technical replicates per condition and are presented as a heatmap of arbitrary units (a.u.), where blue indicates low expression and red reflects high release. Only cytokines with a minimum expression of 1000 a.u. in at least one condition are shown. **B)** Relative expression of IL6, TNF, RANTES/CCL5, and MIG/CXCL9 determined by Proteome Profiler Human XL Cytokine Array Kit in the culture supernatant from pNeuron, pMGL, and co-culture. Samples treated with vehicle ('M0'), LPS/IFN-γ ('M1'), or IL-4/IL-13 ('M2') for 18 h, pooled from n=3 lines from different healthy donors for each condition, **C, D)** Quantification of Serpin E1 (**C**) or CHI3L1 (**D**) release into the culture supernatant by ELISA in pNeuron, pMGL, and co-culture. Pooled samples either treated with vehicle ('M0'), LPS/IFN-γ ('M1'), or IL-4/IL-13 ('M2') for 18 h (all n=3 lines from different healthy donors). One-way ANOVA and Tukey's multiple comparisons test (**C, D**). Figure adapted from (Vahsen et al., 2022).

3.12 Discussion and conclusions

In this chapter, I have demonstrated the successful differentiation of iPSC-derived macrophage/microglia precursors and terminal differentiation to microglia in monoculture and co-culture with MNs. I have established a novel co-culture system of iPSC-derived microglia and MNs, allowing for the study of MN-microglia cross-talk in an authentic human model system. MNs in co-culture expressed key MN markers, while co-cultured microglia fulfilled multiple established criteria for microglial cell identity. Their transcriptome resembled *bona fide* human microglia, they expressed key microglial markers assessed by RNA-sequencing, RT-qPCR and immunofluorescence, had highly dynamic ramifications, were phagocytically competent, and released a battery of cytokines, both in unstimulated conditions and upon stimulation. Of particular interest for ALS research, microglia in monoculture and co-culture expressed key ALS-associated genes such as *C9ORF72*. In addition, disease-relevant biomarkers such as CHI3L1 were expressed and released from microglia. Microglial monocultures represent a valid microglia model, allowing the study of cell-autonomous phenotypes in a simplified system. Co-culture, on the other hand, supports a homeostatic microglial state and is best suited for the investigation of non-cell-autonomous effects.

In recent years, various methods for the differentiation of iPSC-derived microglia have been published, and there is great overlap between the functional properties of these cells (Giacomelli et al., 2022). However, thus far, only the protocol from the Cowley Lab has been shown to produce *MYB*-independent and *PU.1*-and *RUNX1*-dependent primitive macrophages, previously demonstrated through

gene KO (Buchrieser et al., 2017). In this thesis, I have provided further evidence for this finding using RNA sequencing – *MYB* expression was almost absent in the iPSC-derived myeloid cells generated using our macrophage/microglia differentiation protocol and thereby similar to primary human microglial cells, while *PU.1* and *RUNX1* were highly expressed. It is arguably difficult to compare sequencing datasets from different sources due to differences in sample processing. However, when I integrated our RNA-sequencing data with the datasets from two seminal protocols for the differentiation of microglial cells (Abud et al., 2017; Muffat et al., 2016), I limited batch effects, which could be caused by different versions of the software packages or the genome used for alignment, due to simultaneous bioinformatic processing of the raw data. Direct comparison indicates that our monocultured microglia transcriptomically resembled the microglia from the established protocol from (Muffat et al., 2016), while co-cultured microglia were closer to the *bona fide* primary human microglia previously sequenced by (Abud et al., 2017). It is noteworthy that the transcriptome of the microglial cells generated by (Abud et al., 2017), in monoculture and co-culture, appeared to be closer to blood monocytes according to the RNA sequencing comparison in this thesis. Based on these observations, the differentiation protocols established by (Muffat et al., 2016) and ourselves seem more suitable to accurately model actual human microglial cells. Importantly, our differentiation protocol is relatively simple and highly efficient, allowing for easy scaling up of production for large-scale and drug screening experiments (Haenseler et al., 2017).

The combined findings from the earlier study from the Cowley Lab (Haenseler et al., 2017) and this thesis show that iPSC microglial monocultures are a viable, simple, and reliable model to study microglial function. Microglial monocultures allow for the study of cell-autonomous phenotypes in neurodegenerative disease research. The main focus of this chapter, however, was to establish the co-culture of microglia and spinal MNs. Many other microglia differentiation protocols have also shown compatibility with neurons, either through direct co-culture or by transplantation into animals (reviewed by us in (Giacomelli et al., 2022)), but, to my knowledge, this is the first human model system to investigate microglia-spinal MN crosstalk.

As one would expect, and has been demonstrated by other protocols, co-culture supported a homeostatic microglial state, with increased ramifications and higher expression of some homeostatic genes. In fact, in our published methods paper, we also demonstrated that co-cultured microglia had a reduced response to ADP in calcium imaging (Vahsen et al., 2022), lending further evidence to co-culture supporting a homeostatic microglial state. Interestingly, MN-microglia co-cultures had a slightly different and attenuated secretion profile compared with microglial monocultures. Serpin E1 release was lower in co-culture supernatants compared to iPSC microglia monoculture supernatants. In contrast, in the previous study from the Cowley Lab (Haenseler et al., 2017), serpin E1 secretion was upregulated in co-cultures of cortical neurons and microglia. This observation suggests that microglia in co-culture specifically respond to the neuronal subtype with which they are cultured and could represent an indication of heterogenous

microglial populations in different areas of the CNS. Microglial heterogeneity across the neuroaxis is increasingly being explored as a concept in neuroscience (Masuda et al., 2020), but is yet to be investigated in the context of iPSC microglia. While generic protocols for the differentiation of iPSC neurons and astrocytes initially set the stage in iPSC research, there is now a battery of more refined differentiation methods for many different subtypes of neurons, and protocols that generate different subtypes of astrocytes, e.g., spinal astrocytes (Soubannier et al., 2022), are now emerging (Giacomelli et al., 2022). In comparison, the first iPSC microglia differentiation protocols were only published in 2016 (Muffat et al., 2016) and 2017 (Abud et al., 2017). iPSC microglia therefore still represent a comparably new concept, which can be expected to be more widely implemented over the next few years. It will be important to factor in microglial heterogeneity in future protocols to establish more refined and more accurate differentiation methods.

With regards to ALS research, RNA sequencing in this chapter demonstrated that several key ALS-associated genes, notably *C9ORF72,* are expressed in microglia in monoculture and co-culture. This observation sets the stage for exploiting iPSC microglia in monoculture and co-culture with MNs as a suitable model to study cell-autonomous and non-cell-autonomous phenotypes using patient-derived cells in the next chapters of this thesis. In this context, it is of particular interest that I found several candidate ALS biomarkers to be highly expressed in the microglial cells, including *CHIT1* and *CHI3L1*, by RNA sequencing. I confirmed CHI3L1 release from microglia in monoculture and co-culture through a

supernatant array and ELISA. CHI3L1 is one of the prime candidates to serve as a biomarker in ALS (Gray et al., 2020; Thompson et al., 2019; Thompson et al., 2018; Vahsen et al., 2021) but has previously been hypothesised to be primarily released by astrocytes (Thompson et al., 2018; Vahsen et al., 2021). Future studies should also evaluate microglia as a potential source for increased CHI3L1 secretion in ALS.

Another limitation of the experiments conducted and discussed in this chapter that ought to be considered is the relatively short culture duration. I chose to perform the characterisation experiments on DIV 35, as 14 days of co-culture are a sufficiently long interval for the microglia to adopt a microglial identity. Because of this, I cannot make a comprehensive statement about the identity and function of both cell types in culture after pro-longed culture intervals. In some pilot experiments, I was able to maintain co-cultures of both cell types without substantial morphological changes until at least DIV 50, but the characterisation of both cell types at different time points was beyond the scope of this thesis. I chose not to include anti-mitotic drugs in this protocol to simplify the experimental paradigm, but treatments with drugs such as Mitomycin C might prove beneficial if one were interested in more mature cultures. It is to be expected that longer culture durations would increase the electrophysiological maturity of MNs and, from a disease modelling perspective, might be required to uncover phenotypes associate with cellular ‘ageing’.

In future studies, it will be of interest to further develop this model to include additional non-neuronal cell types, such as astrocytes or oligodendrocytes, for which iPSC differentiation protocols are already readily available. In particular, the combination of iPSC-derived MNs, microglia, and astrocytes would be of considerable interest for ALS research. The combination of more cell types will probably result in a more physiological model but, on the other hand, will also lead to more culture variability and complexity.

Taken together, the microglia-spinal MN co-culture developed in this thesis has great potential to serve as a new tool to further our understanding of MN-microglial crosstalk and the microglial component of ALS. Its use for disease modelling in ALS research will be demonstrated in chapter 5 of this thesis.

4 Phenotypic analysis of C9ORF72-ALS patient-derived iPSC microglia

4.1 Introduction and aims

Widespread microglial activation has been particularly observed in patients with HREs in *C9ORF72*, the commonest genetic cause of ALS (Talbot et al., 2018), and correlated with disease progression (Brettschneider et al., 2012a; Brettschneider et al., 2012b). Mechanistically, in neurons, the HRE in *C9ORF72* has been shown to result in both loss-of-function and gain-of-function toxicity, specifically, C9ORF72 haploinsufficiency and the formation of RNA foci and DPRs (DeJesus-Hernandez et al., 2011; Mori et al., 2013b). C9ORF72 is highly expressed in myeloid cells (O'Rourke et al., 2016; Yvanka de Soysa et al., 2022), but the consequences of the HRE in *C9ORF72* for microglial function are less clear. *C9orf72* KO has had pronounced effects on myeloid cells and microglia in mice, resulting in a pro-inflammatory state with increased release of pro-inflammatory cytokines such as IL-1b (Lall et al., 2021; McCauley et al., 2020; O'Rourke et al., 2016). Therefore, it is currently assumed that C9ORF72 loss-of-function through haploinsufficiency drives microglial dysfunction in C9ORF72-ALS. However, whether human C9ORF72 HRE mutant microglia (C9ORF72 microglia) endogenously display the cellular pathological features associated with the HRE in *C9ORF72* and show a cell-autonomous disease phenotype is currently unclear. Having successfully established differentiation protocols for iPSC microglia in monoculture and co-culture in chapter 3, the next aim of my thesis was to

generate microglial monocultures derived from C9ORF72-ALS patients and investigate whether the presence of the HRE in *C9ORF72* resulted in a disease phenotype in microglia. To do so, I aimed to first assess whether C9ORF72 haploinsufficiency and DPR formation, two hallmarks of the HRE in *C9ORF72,* were present in C9ORF72 iPSC microglia. The second aim was to perform RNA sequencing to identify whether C9ORF72 microglia showed transcriptomic differences and dysregulated pathways compared with controls. If enrichment of dysregulated pathways was present, I aimed to progress to functional experiments, additionally guided by the phenotypes described by (Lall et al., 2021; McCauley et al., 2020; O'Rourke et al., 2016) in *C9orf72* KO mice-derived macrophages and microglia.

4.2 Differentiation of C9ORF72-ALS patient-derived iPSCs into microglia

Using the differentiation protocol established in the previous chapter, I generated iPSC microglia from three different C9ORF72-ALS patients, three gender- and age-matched healthy donors, and one isogenic control line, previously obtained through CRISPR-mediated homology directed repair of the *C9ORF72* HRE and characterised before (Ababneh et al., 2020) (Figure 4.1A). For all downstream experiments, I compared the pooled three C9ORF72-ALS lines with the pooled three healthy control lines; the isogenic line was compared with its donor C9ORF72 (C9-2) line. All lines readily differentiated into iPSC microglia and showed typical microglial morphology under the light microscope (Figure 4.1B) and after immunofluorescent staining against IBA1 (Figure 4.1C). Similarly, IBA1

was equally expressed by Western blotting in all lines (Figure 4.1D). Differentiated microglial cells also expressed the key microglial marker TMEM119 by immunofluorescent staining and RT-qPCR (Figure 4.1C, E). Furthermore, the *P2RY12* gene, a marker for homeostatic microglia, was expressed in differentiated microglial cells (Figure 4.1F). Pro-inflammatory treatment with LPS led to a substantial reduction in *P2RY12* expression, confirming the expected microglial response to pro-inflammatory stimulation (Figure 4.1F). Interestingly, *P2RY12* expression was also reduced in unstimulated C9ORF72 microglia compared with controls, reaching statistical significance for the C9ORF72-healthy control microglia comparison (Figure 4.1F). This observation provides first evidence for a pro-inflammatory profile in C9ORF72 microglia.

Together, these data demonstrate the successful differentiation and stimulation of iPSC microglia derived from three different C9ORF72-ALS patients and corresponding healthy and isogenic control lines.

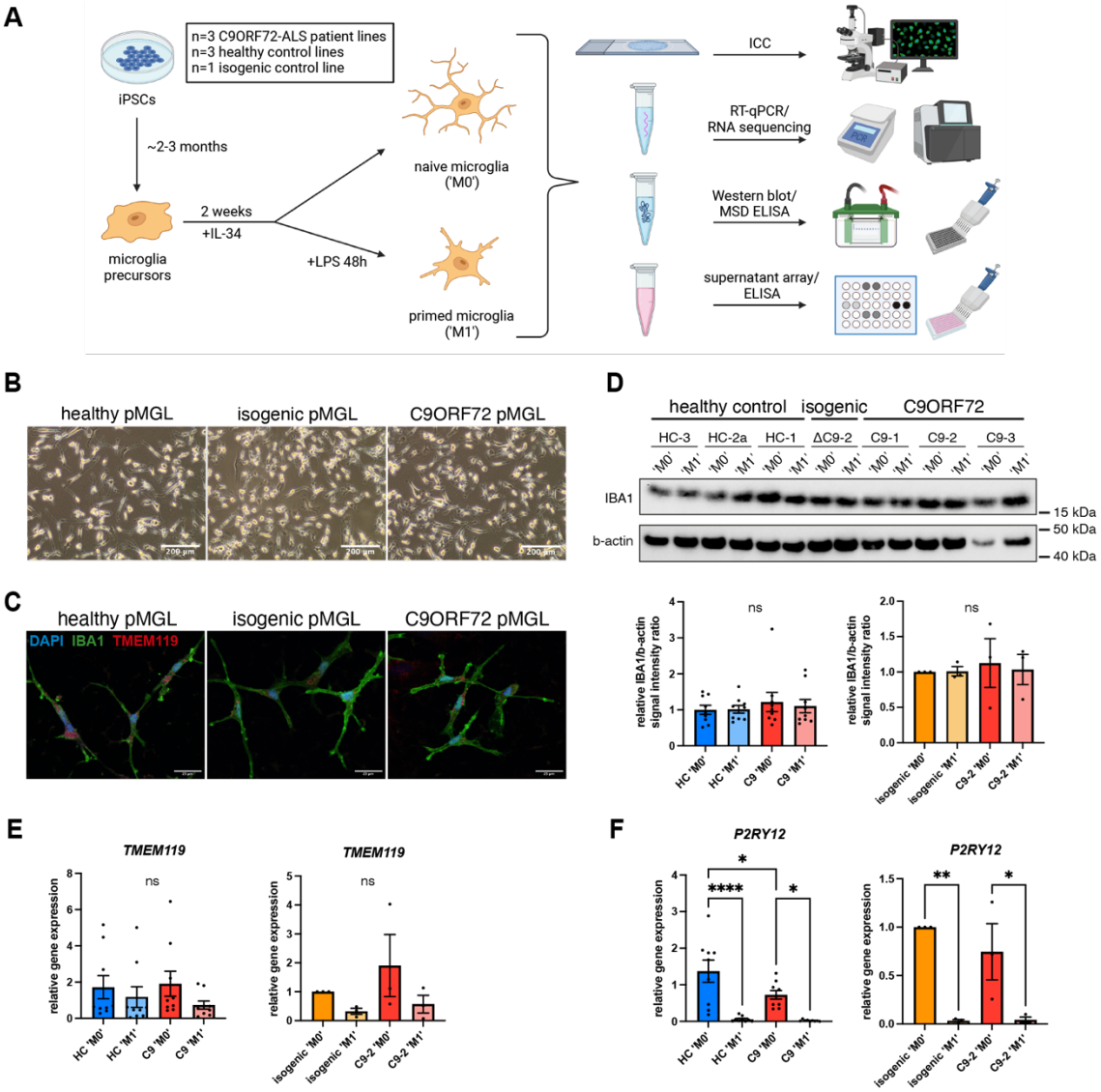


Figure 4.1: iPSC microglia from C9ORF72-ALS patients show expected microglial morphology, express key microglial markers, and respond to pro-inflammatory stimulation with LPS. A) Schematic overview showing the experimental setup and analyses performed on C9ORF72 (C9) microglia in monoculture (pMGL) in this study. **B)** Live cell images of pMGL differentiated from healthy control, isogenic, and C9 iPSC lines showing typical microglial morphology. Scale bars: 200 µm. **C)** Exemplar immunofluorescent images of healthy control, isogenic, and C9 pMGL showing branched microglial morphology and expression of the microglial markers IBA1 and TMEM119. Scale bars: 25 µm. **D)** Top: Exemplar Western blot against the microglial marker IBA1 in 'M0'/ 'M1' (100 ng/mL LPS, 48 h) healthy, isogenic, and C9 pMGL. Bottom: Quantification shows equal IBA1 expression in the C9-healthy pMGL (n=3 lines per condition, n=3 differentiations each) and isogenic-C9-2 pMGL comparisons (n=1 line per condition, n=3 differentiations each) normalised to the housekeeping gene b-actin. **E, F)** RT-qPCR for *TMEM119* and *P2RY12* expression in 'M0' and 'M1' pMGL normalised to the housekeeping gene *TBP* shows reduced *P2RY12* expression in C9 pMGL versus controls, reaching statistical significance for the C9-healthy pMGL comparison, while *TMEM119* expression is not significantly different (n=3 lines per condition in the C9-healthy pMGL comparison; n=1 line per condition in isogenic-C9-2 pMGL comparison; n=3 differentiations per line). Single data points and means ± SEM. One-way ANOVA with Tukey's post-hoc test (**D-F**). The Western blots and quantification in **D** were performed by Sumedha Nalluru, an MSc Neuroscience student I supervised in the lab.

4.3 C9ORF72-ALS iPSC microglia show C9ORF72 haploinsufficiency and express dipeptide repeat proteins

Hereafter, I analysed C9ORF72 microglia for the presence of key pathological features associated with the HRE in *C9ORF72*, namely the loss-of-function mechanism C9ORF72 haploinsufficiency and the expression of DPRs as gain-of-function products. Results from previous studies regarding the expression of C9ORF72 in different tissues and cell types have been questioned due to the non-specificity of the antibodies employed. I therefore used extensively validated antibodies for Western blotting against C9ORF72 (Laflamme et al., 2019). Comparing the expression of C9ORF72 in healthy iPSC microglia and MNs, I detected significantly higher C9ORF72 expression in microglia (Figure 4.2A). This finding confirms previous observations of high C9ORF72 expression in microglia in mice (O'Rourke et al., 2016; Yvanka de Soysa et al., 2022), reinforcing a crucial role for C9ORF72 in microglial function and suggesting that microglial C9ORF72 loss-of-function is likely to have pronounced effects.

I then assessed the expression of *C9ORF72* and its variants 1 and 2/3 by RT-qPCR. *C9ORF72* expression was significantly increased in LPS-primed microglia (Figure 4.2B-D), likely due to the involvement of C9ORF72 in the endo-/lysosomal pathway that is activated by LPS stimulation. Compared with healthy controls, C9ORF72 microglia showed a numeric decrease in *C9ORF72* expression which did not reach statistical significance (Figure 4.2B-D). Western blotting confirmed significant upregulation of C9ORF72 expression in LPS-treated microglia (Figure

4.2E). Furthermore, C9ORF72 microglia showed significantly reduced C9ORF72 expression compared with healthy control microglia, demonstrating C9ORF72 haploinsufficiency (Figure 4.2E). The isogenic-C9-2 comparison showed no difference in C9ORF72 levels (Figure 4.2E), indicating the absence of C9ORF72 haploinsufficiency in this comparison, in line with previous results from our group on MNs generated from the same isogenic-C9-2 line pair (Ababneh et al., 2020).

I then proceeded to examine C9ORF72 microglia for the presence of gain-of-function products of the HRE in *C9ORF72.* In collaboration with the Isaacs Lab (University College London, UK), I used their previously validated MSD ELISA platform (Simone et al., 2018) for the quantification of the DPRs Poly(GA) and Poly(GP). In C9ORF72 iPSC MNs generated from C9ORF72-ALS patients, both DPRs were readily detectable, while they were absent in both healthy and isogenic controls (Figure 4.2F, G). C9ORF72 microglia also expressed Poly(GA) and Poly(GP), notably, at lower levels than in the MNs generated from the same lines (Figure 4.2F, G). However, the high variability of the samples did not allow for a meaningful statistical comparison. Finally, considering the significant increase in C9ORF72 expression at gene and protein level in response to LPS treatment, I assessed if pro-inflammatory stimulation affected DPR expression in C9ORF72 microglia. However, 48 h and 6 d of LPS priming led to little change in Poly(GA) expression in C9ORF72 microglia (Figure 4.2H).

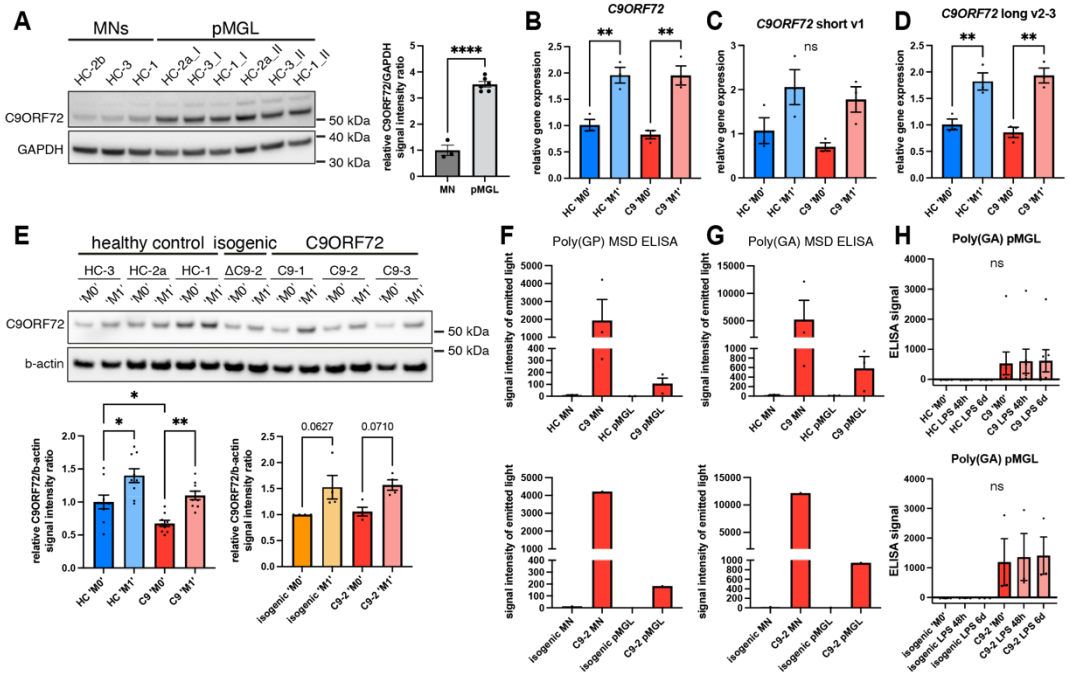


Figure 4.2: iPSC microglia from C9ORF72-ALS patients show C9ORF72 haploinsufficiency and express the DPRs Poly(GA) and Poly(GP). A) Left: Western blot against C9ORF72 comparing healthy control motor neurons (MNs) and microglia (pMGL). I/II indicate different differentiations for the same line. Right: Quantification showing significantly increased C9ORF72 expression in pMGL compared with MNs normalised to the housekeeping gene GAPDH. **B-D)** RT-qPCR for the expression of the whole *C9ORF72* gene and variant 1 (v1, encoding the short isoform) and variants 2/3 (v2-3, encoding the long isoform) in 'M0' and 'M1' (100 ng/mL LPS, 48 h) pMGL showing significantly increased expression after stimulation normalised to the housekeeping gene *TBP* but no differences between genotypes (n=3 lines per condition, n=1 differentiation). **E)** Top: Exemplar Western blot against C9ORF72 in 'M0' and 'M1' healthy, isogenic, and C9 pMGL. Bottom: Quantification shows increased C9ORF72 expression after LPS treatment normalised to the housekeeping gene b-actin. C9ORF72 haploinsufficiency is found in C9 pMGL compared with healthy controls (n=3 lines per condition, n=3 differentiations each) but not in the isogenic-C9-2 comparison (n=1 line per condition, n=3 differentiations each). **F, G)** Analysis of Poly(GP) (**F**) and Poly(GA) (**G**) expression by MSD ELISA in healthy, isogenic, and C9 MNs and pMGL. Both DPRs are detectable in C9 MNs and pMGL but not controls, while pMGL have lower expression (n=1 differentiation for n=3 lines for top graphs, n=1 line for bottom graphs). Single data points and means ± SEM. **H)** Quantification of Poly(GA) expression in pMGL after 48 h and 6 d of LPS treatment (100 ng/mL) by MSD ELISA shows no changes in response to treatment (n=3 lines per condition in the C9-healthy pMGL comparison with n=2-3 differentiations per line; n=1 line per condition in isogenic-C9-2 pMGL comparison; n=3 differentiations per line). Single data points and means ± SEM. Two-tailed unpaired t-test (**A**). One-way ANOVA with Tukey's post-hoc test (**B-E, H**). No statistical tests were performed on **F** and **G** due to the high variability of the samples. The Western blot in **A** was performed by Emily Carroll, another DPhil student in the lab. The Western blots and quantification in **E** were performed by Sumedha Nalluru, an MSc Neuroscience student I supervised in the lab. The MSD ELISAs for **F-H** were performed by Mireia Carcolé (Isaacs Lab, University College London, UK).

Together, these data outline a key role for C9ORF72 in microglia and the presence of C9ORF72 loss-of-function and HRE-associated gain-of-function products in C9ORF72 microglia. C9ORF72 microglia have thus far been primarily

associated with loss-of-function toxicity through C9ORF72 haploinsufficiency (Lall et al., 2021; O'Rourke et al., 2016), which I also detected between C9ORF72 and healthy control microglia. I therefore focused on this comparison by RNA sequencing next to investigate whether C9ORF72 iPSC microglia showed a mutation-associated disease transcriptional signature. The absence of C9ORF72 haploinsufficiency in the isogenic-C9-2 comparison might be specific to this isogenic line or clone; however, it allowed me to investigate in additional experiments whether a disease phenotype would be present in the absence of C9ORF72 haploinsufficiency, which would likely be driven by gain-of-function products.

4.4 C9ORF72-ALS iPSC microglia have a dysregulated transcriptome

Next, I performed RNA sequencing to investigate whether C9ORF72 iPSC microglia showed a mutation-associated disease transcriptional signature. I analysed microglia from all six C9ORF72 and healthy control lines, in their unstimulated state and after priming with LPS for 48 h, to investigate if subtle phenotypes might be uncovered by pro-inflammatory stimulation. Three technical replicates per condition and line were sequenced by the Oxford Genomics Centre at the Wellcome Centre for Human Genetics. I then performed the subsequent bioinformatical analysis of the sequencing data myself.

First, I evaluated the expression of microglial markers in the RNA sequencing data. Confirming the RT-qPCR results, I found clear expression of the microglial

markers *TMEM119* and *P2RY12* as well as *TREM2*, *MERTK*, *C1QA*, *PROS1*, *GAS6*, and *GPR34* (Figure 4.3A). LPS led to a notable reduction for multiple of these marker genes, indicating a response to pro-inflammatory treatment also in the RNA sequencing dataset (Figure 4.3A). For exploratory analysis, I then performed PCA. The PCA plot showed substantial overlap for both genotypes under unstimulated conditions (Figure 4.3B). All LPS-treated samples separated out from the unstimulated samples on PC2 (Figure 4.3B). The top two genes for PC2 loading were the key pro-inflammatory genes *CXCL5* (C-X-C Motif Chemokine Ligand 5) and *IL1B*, reinforcing that PC2 represents the response to treatment. In addition, there was a small shift on PC2 between the LPS-stimulated C9ORF72 and healthy microglia population, indicating that LPS treatment uncovered subtle transcriptomic differences between the genotypes (Figure 4.3B). Both genotypes, with and without stimulation, separated out on PC6 (Figure 4.3C), confirming a moderately dysregulated transcriptome in C9ORF72 microglia compared with healthy controls.

I then performed differential expression analysis and found 121 differentially expressed genes (DEGs) for the 'M0' healthy-C9ORF72 comparison, while LPS treatment increased the number of DEGs to 175 (Figure 4.3D). There was substantial overlap, with 62 DEGs overlapping for the 'M0' and 'M1' comparisons. For instance, these DEGs included *ITGB4* (Integrin Subunit Beta 4), *ITGB6*, *KLK6* (Kallikrein-6), and *CALHM2* (Calcium Homeostasis Modulator Family Member 2) (Figure 4.3E). While several of these showed an overall low expression, *CALHM2* was comparably highly expressed. Intriguingly, increased microglial *Calhm2*

expression has previously been connected with neurodegeneration and neuroinflammation in a mouse model for AD, with its KO reducing a pro-inflammatory microglial phenotype and amyloid-β deposition (Cheng et al., 2021).

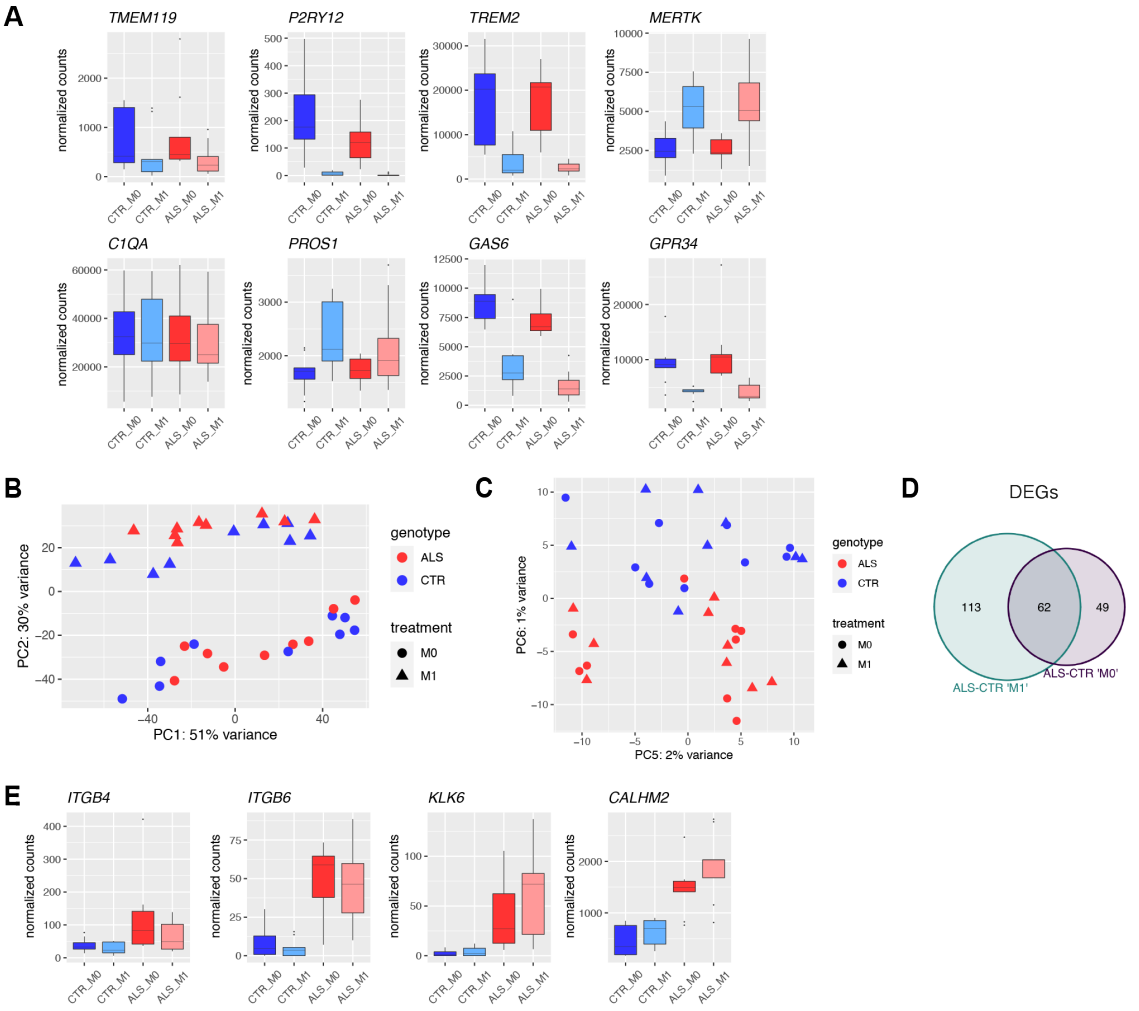


Figure 4.3: RNA sequencing of C9ORF72-ALS iPSC microglia shows transcriptomic differences with controls. A) Normalized counts from RNA sequencing analysis confirming the expression of the microglial markers *TMEM119*, *P2RY12, TREM2, MERTK, C1QA, PROS1, GAS6,* and *GPR34* in unstimulated ('M0') and LPS-treated (100 ng/mL, 48 h, 'M1') healthy and C9ORF72 (C9) microglia (pMGL) (n=3 lines per condition, n=3 differentiations each). **B)** PCA plot based on the top 500 most variable genes with biggest variance in 'M0' and 'M1' healthy and C9 pMGL showing PC1 and PC2 (n=3 lines per condition, n=3 differentiations each) with response to LPS treatment on PC2. **C)** PCA plot for PC5 and PC6 comparing C9 and healthy pMGL (n=3 lines per condition, n=3 differentiations each) showing separation between both genotypes on PC6. **D)** Venn diagram showing differentially expressed genes (DEGs) and overlap for 'M0' and 'M1' comparisons. **E)** Normalized counts from RNA sequencing analysis showing DEGs with significantly increased expression in both 'M0' and 'M1' C9 pMGL versus healthy controls (n=3 lines per condition, n=3 differentiations each). Single data points or dot plots.

I then explored the dysregulation of pathways, focsussing on enrichment of GO terms with GSEA on a ranked list of the log_2fc in gene expression for the whole transcriptome. Notably, under unstimulated conditions, one immune response term but primarily development and chromatid-associated terms were enriched in unstimulated C9ORF72 microglia by GSEA (Figure 4.4A). Evaluating the top 10 GO 'M0' cellular components, there was enrichment of two ECM-associated terms (Figure 4.4B), while no enrichment of GO molecular function terms was found in 'M0' C9ORF72 microglia. However, after LPS treatment, C9ORF72 microglia demonstrated positive enrichment of several terms associated with immune cell activation (Figure 4.4C) and cytokines/chemokines (Figure 4.4D) by GSEA. In addition, I found negative enrichment for ECM, lysosomes, and several membrane-associated cellular component terms in 'M1' C9ORF72 microglia (Figure 4.4E).

In summary, these data reveal the dysregulation of several pathways in C9ORF72 compared with control microglia. C9ORF72 microglia showed particular enrichment of pathways associated with immune cell activation and cytokine release, lysosomes, and the ECM (Figure 4.4F).

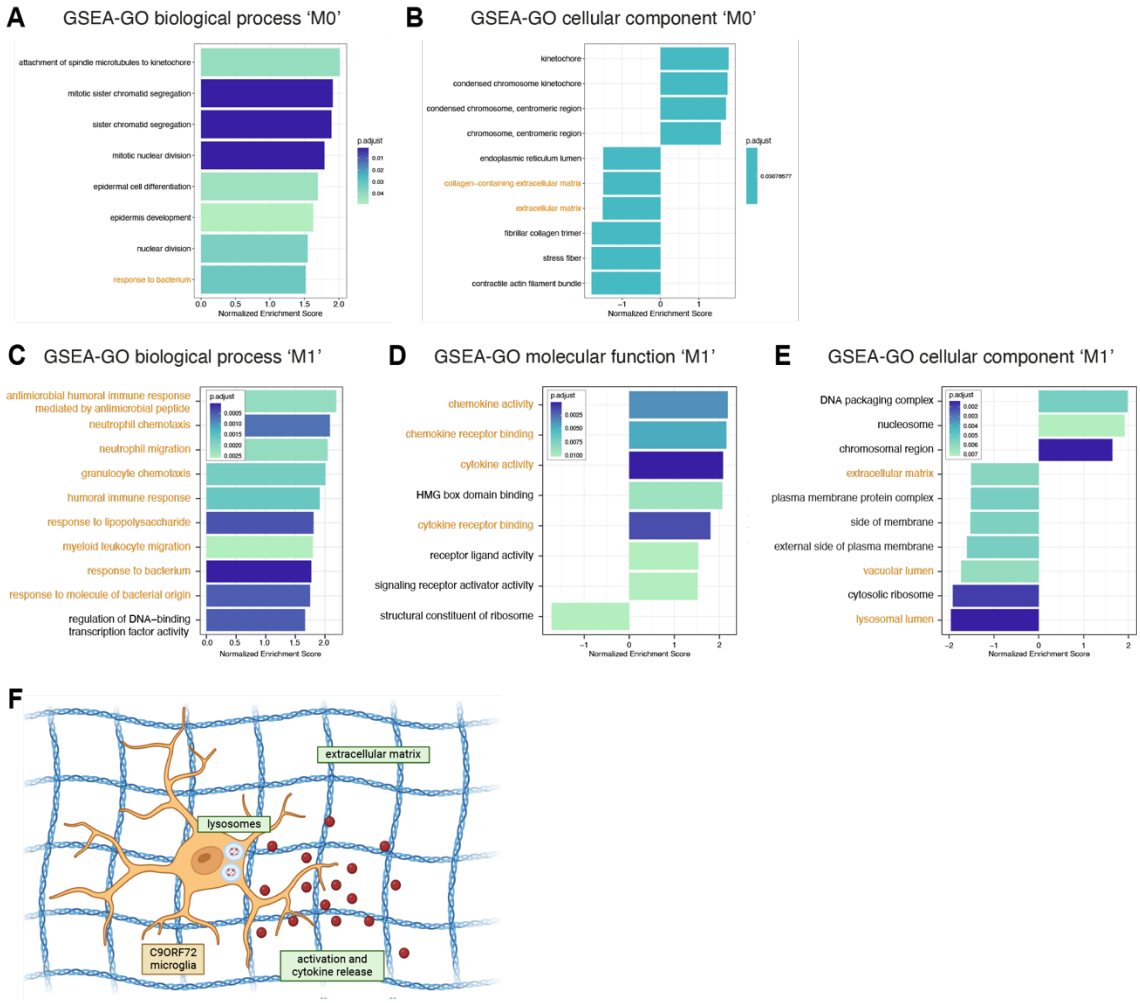


Figure 4.4: RNA sequencing of C9ORF72-ALS iPSC microglia identifies dysregulation of pathways associated with immune cell activation, cytokines, lysosomes, and the extracellular matrix. A, B) Bar plots showing top 10 significantly different GO biological process (**A**) and cellular component (**B**) terms for 'M0' C9ORF72 (C9) versus healthy microglia (pMGL) comparison. x-axis shows Normalized Enrichment Score (NES) based on GSEA using the whole transcriptome ranked by log2fc. The Benjamini-Hochberg corrected p-values for pathway enrichment for each term is indicated by the colour of the bars. Particularly interesting terms are highlighted in orange. **C-E)** Bar plots showing top 10 significantly different GO biological process (**C**), molecular function (**D**), and cellular component (**E**) terms for 'M1' (100 ng/mL LPS, 48 h) C9 versus healthy pMGL comparisons. x-axis shows NES based on GSEA using the whole transcriptome ranked by log_2fc. The Benjamini-Hochberg corrected p-values for pathway enrichment for each term is indicated by the colour of the bars. Particularly interesting terms are highlighted in orange. **F)** Summary schematic illustrating the pathways with most prominent enrichment in C9 pMGL in the RNA seq analysis.

4.5 C9ORF72-ALS iPSC microglia show a phagocytosis deficit and lysosomal impairment

Considering that C9ORF72 localizes to phago-/lysosomes in macrophages (Laflamme et al., 2019) and the negative enrichment of lysosomes in C9ORF72 microglia in the RNA-sequencing, I proceeded to assess the phago-lysosomal pathway. First, I characterised the phagocytic capacity of C9ORF72 microglia using pH-sensitive yeast particles. 150 min after the addition of the particles, I observed a strong increase in the number and area of fluorescent particles per cell (Figure 4.5A). Treatment with Cytochalasin D and Bafilomycin A1, to block phagocytic uptake and lysosomal degradation, respectively, abolished the appearance of fluorescent spots within the cells, confirming their uptake through phagocytosis and lysosome-mediated degradation (Figure 4.5B).

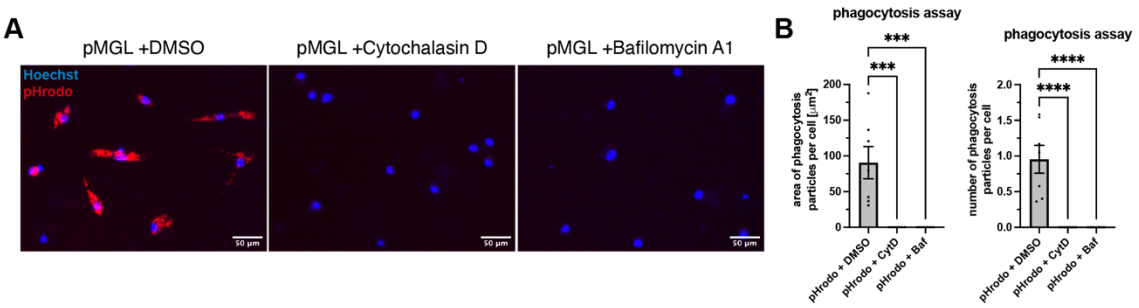


Figure 4.5: Setup of an assay to analyse phagocytosis in C9ORF72-ALS microglia. A) Exemplar images of healthy microglia (pMGL) 150 min after the addition of pHrodo particles, treated with DMSO as vehicle control, Cytochalasin D (CytD), a phagocytosis inhibitor, or Bafilomycin A1 (Baf), an inhibitor of lysosomal degradation. Scale bars: 50 µm. **B)** Quantification of the area and number of phagocytosed particles within pMGL confirming phagocytic uptake and lysosomal degradation of pHrodo particles (datapoints are n=1 view field for n=7 lines, n=1 differentiations). Single data points and means ± SEM. One-way ANOVA with Tukey's post-hoc test (**B**).

I then added pHrodo particles to C9ORF72 and control microglia and compared the phagocytic uptake after 150 min. C9ORF72 microglia showed a significantly reduced area of phagocytosed particles and a numeric reduction in the phagocytosis particles per cell compared with healthy controls (Figure 4.6A-C), indicating

a phagocytosis deficit. The comparison between the isogenic control and C9-2 did not show statistically significant differences (Figure 4.6A-C). To investigate if this phagocytic deficit was associated with dysregulated expression of phagocytosis receptors, I evaluated the levels of the two key phagocytosis genes *TREM2* and *TYROBP* (TYRO protein tyrosine kinase-binding protein) in the RNA sequencing dataset (Figure 4.3A, Figure 4.6D). There was no difference in their expression between genotypes, indicating that the observed phagocytic deficit is likely to be independent of phagocytic receptors.

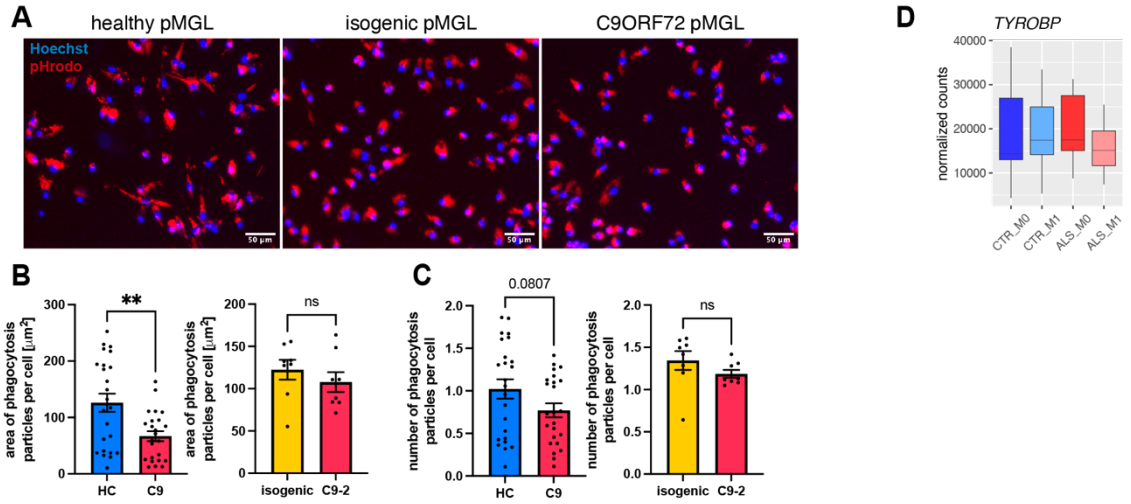


Figure 4.6: C9ORF72-ALS iPSC microglia show a phagocytosis deficit. A) Exemplar images of healthy, isogenic, and C9ORF72 (C9) pMGL 150 min after the addition of pHrodo phagocytosis particles. Scale bars: 50 µm. **B, C)** Quantification of the area (**B**) and number (**C**) of phagocytosed particles in pMGL shows a phagocytosis deficit in C9 compared with healthy but not isogenic pMGL (datapoints are n=4 view fields for n=3 lines (C9-healthy comparison) and n=1 line (C9-isogenic comparison), n=2 differentiations). **D)** Normalized counts from RNA sequencing analysis showing no differences in expression of the phagocytosis receptor *TYROBP* between genotypes (n=3 lines per condition, n=3 differentiations each). Single data points and means ± SEM or box plots. Two-tailed unpaired t-test (**B, C**).

I therefore investigated if the dysfunctional phagocytosis activity might be associated with lysosomal impairment. Western blot quantification of the lysosomal marker LAMP1 showed no differences between C9ORF72 microglia and controls (Figure 4.7A). However, the analysis of lysosomal morphology via immunofluorescent staining for LAMP1 showed an aberrant staining pattern in C9ORF72

microglia compared with the homogenous distribution of LAMP1-positive lysosomes in healthy controls (Figure 4.7B). To assess this quantitatively, I analysed the area and number of LAMP1-positive particles. I found a significantly reduced area of LAMP1-positive lysosomes in C9ORF72 microglia compared with healthy but not isogenic controls (Figure 4.7C). The number of LAMP1-positive particles was moderately reduced, but this trend did not reach statistical significance (Figure 4.7D).

In summary, these data outline a phagocytosis deficit and aberrant lysosomal morphology in C9ORF72 microglia compared with healthy but not isogenic microglia, suggesting this phenotype is likely driven by C9ORF72 haploinsufficiency.

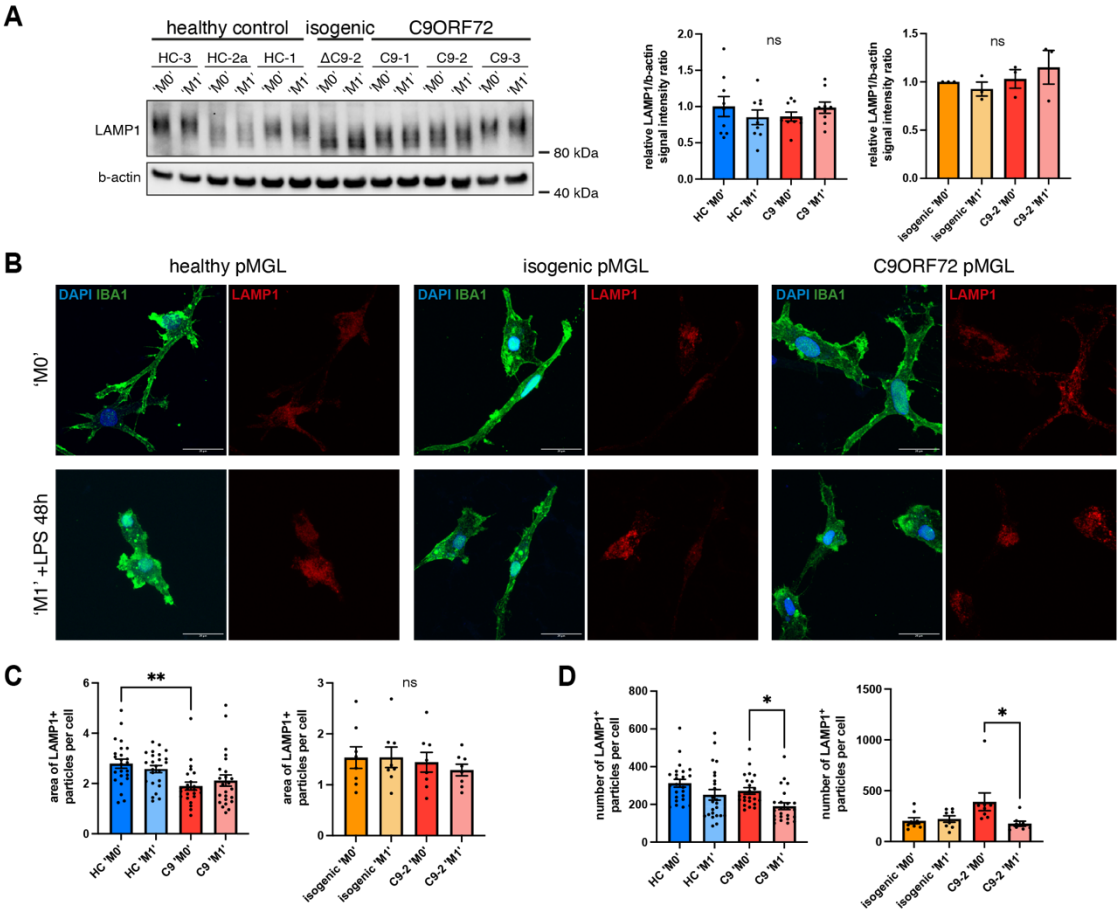


Figure 4.7: C9ORF72-ALS iPSC microglia show aberrant lysosomal morphology. A) Left: Exemplar Western blot against the lysosomal marker LAMP1 in unstimulated ('M0') and LPS-treated (100 ng/mL, 48 h, 'M1') healthy, isogenic, and C9ORF72 (C9) pMGL. Right: Quantification shows equal LAMP1 expression in the C9-healthy pMGL (n=3 lines per condition, n=3 differentiations each) and isogenic-C9-2 pMGL comparisons (n=1 line per condition, n=3 differentiations each) normalised to the housekeeping gene b-actin. **B)** Exemplar images of 'M0' and 'M1' healthy, isogenic, and C9 IBA1-positive pMGL stained for the lysosomal marker LAMP1. Scale bars: 20 µm. **C, D)** Quantification of the area (**C**) and number (**D**) of LAMP1-positive lysosomes showing lysosomal impairment in C9 pMGL compared with healthy pMGL (datapoints are n=4 view fields for n=3 lines (C9-healthy comparison) and n=1 line (C9-isogenic comparison), n=2 differentiations). Single data points and means ± SEM. One-way ANOVA with Tukey's post-hoc test (**A, C, D**). Some of the Western blots and quantifications in **A** were performed by Sumedha Nalluru, an MSc Neuroscience student I supervised in the lab.

4.6 C9ORF72-ALS iPSC microglia have a pro-inflammatory cytokine/chemokine profile and upregulate NFκB

The strong enrichment of immune cell activation and cytokine/chemokine-associated pathways in the RNA-sequencing dataset prompted me to evaluate the cytokine profile in C9ORF72 microglia. First, I analysed the expression of the key

pro-inflammatory cytokines *IL1A*, *IL1B*, *IL6*, and *IL10*. All of these cytokines increased in the RNA-sequencing dataset in LPS-primed C9ORF72 microglia compared with healthy controls (Figure 4.8A) reaching statistical significance for *IL1A* (adjusted p=0.03). Additionally, I analysed the expression of the key pro-inflammatory cytokine IL1B by Western blot, which increased after *C9orf72* KO in previous studies (Lall et al., 2021; O'Rourke et al., 2016). In agreement, in LPS-primed C9ORF72 microglia, the expression of IL1B was significantly increased compared with healthy controls (Figure 4.8B). In contrast, in the isogenic-C9-2 comparison, IL1B expression was equal (Figure 4.8B).

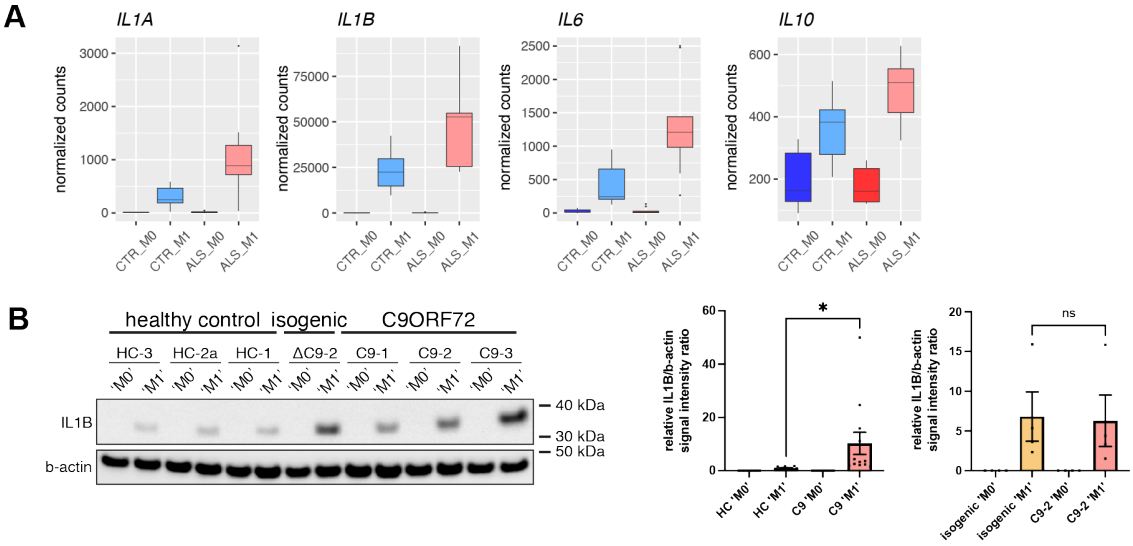


Figure 4.8: C9ORF72-ALS iPSC microglia upregulate the pro-inflammatory cytokines *IL1A*, *IL1B*, *IL6*, and *IL10*. A) Normalized counts from RNA seq analysis for *IL1A*, *IL1B*, *IL6*, and *IL10* in unstimulated ('M0') and LPS-treated (100 ng/mL, 48 h, 'M1') healthy, isogenic, and C9ORF72 (C9) microglia (pMGL). All cytokines increased in LPS-treated C9 pMGL compared with healthy controls, reaching statistical significance for *IL1A* (adjusted p=0.03) (n=3 lines per condition, n=3 differentiations each). **B)** Left: Exemplar Western blot against IL1B in 'M0'/'M1' healthy, isogenic, and C9 pMGL. Right: Quantification shows significantly increased IL1B expression in the C9-healthy (n=3 lines per condition, n=4 differentiations each) but not the isogenic-C9-2 pMGL comparison (n=1 line per condition, n=4 differentiations each) normalised to the housekeeping gene b-actin. Single data points and means ± SEM or boxplots. One-way ANOVA with Tukey's post-hoc test (**B**). The Western blots and quantifications in **B** were performed by Sumedha Nalluru, an MSc Neuroscience student I supervised in the lab.

The expression of inflammatory cytokines/chemokines including IL1B is regulated, amongst others, by two master regulators, the NFκB and NLRP3 inflammasome pathways (Rhee et al., 2007; Swanson et al., 2019). Using the RNA sequencing datasets to explore both pathways, I found that the levels of *NFKB1*, *NFKB2, and NLRP3* were not substantially different between C9ORF72 and healthy control microglia (Figure 4.9A). Western blotting confirmed equal expression of NFκB in C9ORF72 and control microglia (Figure 4.9B). In contrast, the phosphorylated thus active form of NFκB (p-NFκB) (Christian et al., 2016) was significantly upregulated in C9ORF72 microglia compared with healthy controls, also when normalizing to the total NFκB expression (Figure 4.9B). The comparison with isogenic control microglia showed no significant difference in p-NFκB expression (Figure 4.9B). NLRP3 expression was numerically increased in LPS-treated C9ORF72 microglia compared with healthy and isogenic controls (Figure 4.9C), but this difference did not reach statistical significance.

These data show that C9ORF72 microglia compared with healthy controls have a pro-inflammatory profile, with increased activation of the NFκB-IL1B pathway. Considering the absence of corresponding effects in the isogenic-C9-2 comparison, this phenotype is likely driven by C9ORF72 haploinsufficiency. I therefore additionally proceeded to harness the isogenic-C9-2 line pair to identify dysregulated cytokines/chemokines which, in the absence of C9ORF72 haploinsufficiency, would likely be due to gain-of-function toxicity.

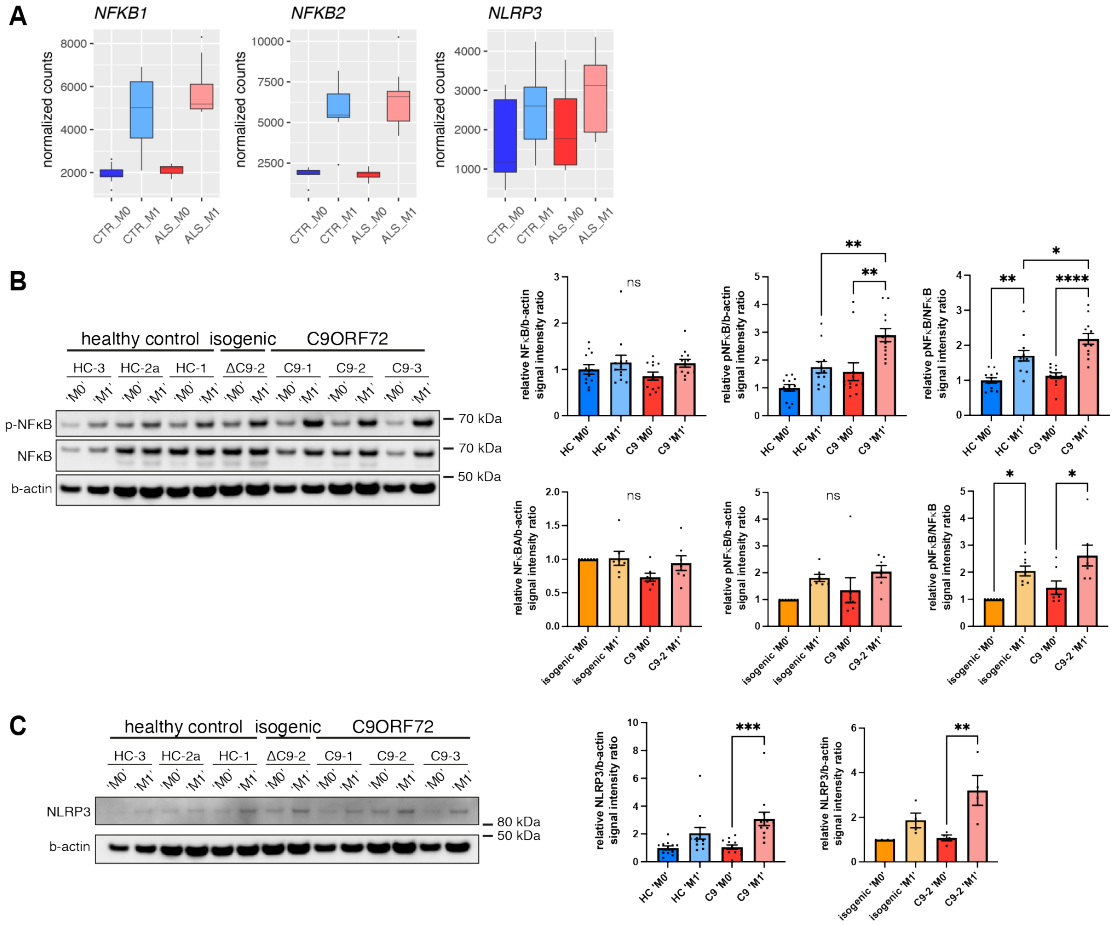


Figure 4.9: C9ORF72-ALS iPSC microglia upregulate the NFκB pathway and show a numeric increase in NLRP3. A) Normalized counts from RNA seq analysis for *NFKB1*, *NFKB2*, and *NLRP3* in unstimulated ('M0') and LPS-treated (100 ng/mL, 48 h, 'M1') healthy and C9ORF72 (C9) pMGL. *NFKB1*, *NFKB2*, and *NLRP3* expression is not substantially different (n=3 lines per condition, n=3 differentiations each). **B)** Left: Exemplar Western blot against total and phospho-NFκB in 'M0' and 'M1' healthy, isogenic, and C9 pMGL. Right: Quantification shows no differences in NFκB but significantly increased expression of pNFκB in the C9-healthy pMGL comparison normalised to b-actin and total NFκB (n=3 lines per condition, n=4 differentiations each). The isogenic-C9-2 pMGL comparison shows no difference (n=1 line per condition, n=7 differentiations each). **C)** Left: Exemplar Western blot against NLRP3 in 'M0' and 'M1' healthy, isogenic, and C9 pMGL. Right: Quantification shows a trend to increased NLRP3 expression in C9 pMGL in both comparisons but does not reach statistical significance. Normalised to the housekeeping gene b-actin (n=3 lines per condition for C9-healthy comparison, n=1 line for the isogenic-C9-2 comparison, n=3-4 differentiations each). Single data points and means ± SEM or box plots. One-way ANOVA with Tukey's post-hoc test (**B, C**). Some of the Western blots and quantification in **B** and **C** were performed by Sumedha Nalluru, an MSc Neuroscience student I supervised in the lab.

4.7 C9ORF72-ALS iPSC microglia consistently upregulate expression and release of MMP9

To assess the supernatant cytokine/chemokine profile in the isogenic-C9ORF72 pair in a comprehensive and unbiased manner, I used a membrane-based array,

allowing for the relative quantification of 105 cytokines/chemokines (for details, see Table 2.8) in culture supernatants. Using pooled supernatants from unstimulated and LPS-stimulated microglial cultures from the isogenic-C9ORF72 pair, I identified three targets with differential expression in the culture supernatant. The release of matrix metalloproteinase-9 (MMP9) and growth/differentiation factor 15 (GDF-15) increased in supernatants from LPS-primed C9ORF72 microglia, while CXCL10 expression was reduced (Figure 4.10A). I then used the RNA sequencing dataset to identify overlap with the expression of these targets in the C9ORF72-healthy comparison. In line with the supernatant array, *MMP9* was also increased for the C9ORF72-healthy comparison by RNA sequencing (Figure 4.10B). *GDF-15* and *CXCL10* expression, however, was not changed between C9ORF72 and healthy controls in the RNA sequencing dataset (Figure 4.10B). Next, I performed RT-qPCR and ELISA validation for CXCL10, which was also previously shown to be dysregulated in *C9orf72* KO microglia (Lall et al., 2021). RT-qPCR for *CXCL10* showed a non-significant reduction in LPS-primed C9ORF72 microglia compared with the isogenic control but showed no difference in comparison with healthy microglia, in line with the RNA sequencing data (Figure 4.10B, C). Similarly, CXCL10 release into the supernatant, measured by ELISA, was significantly reduced in supernatants from C9ORF72 microglia compared with the isogenic control but showed no difference compared with healthy microglia (Figure 4.10D). Therefore, only MMP9 expression showed the same trend in expression for the C9-2-isogenic and C9ORF72-healthy comparison, and its upregulation also corresponded well to the enrichment of ECM-associated terms in the RNA-sequencing analysis (Figure 4.4B, E, F). Furthermore, MMP9

has previously been connected with neurodegeneration in murine SOD1 and TDP-43 ALS models (Kaplan et al., 2014; Spiller et al., 2019), rendering it likely that changes in its expression in C9ORF72 microglia would be of biological relevance. I therefore focused on exploring MMP9 and performed a comprehensive assessment of the release and expression of MMP9 at gene and protein level. I confirmed significantly increased release and activity of MMP9 in culture supernatants from C9ORF72 microglia versus both healthy and isogenic controls by ELISA and activity assay (Figure 4.10E, F). Of note, MMP9 was not detectable by ELISA in culture supernatants from motor neurons generated from the same C9ORF72 iPSC lines (data not shown). RT-qPCR and Western blot, allowing the pro-form and active form of MMP9 due to different molecular weights to be distinguished, confirmed significantly increased pro- and active MMP9 expression at gene and protein level in C9ORF72 microglia compared with healthy controls (Figure 4.10G, H). Similarly, the C9ORF72-isogenic comparison showed increased expression at gene and protein level, which reached statistical significance for the active form of MMP9 (Figure 4.10G, H). These data suggest that MMP9 expression in C9ORF72 microglia is consistently upregulated at mRNA and protein level resulting in increased secretion.

Taken together, these data identify increased expression and release of MMP9 in C9ORF72 microglia. Since MMP9 was also dysregulated in the comparison of C9ORF72 and isogenic control microglia, and therefore in the absence of C9ORF72 haploinsufficiency, it is likely that MMP9 upregulation is a consequence of gain-of-function products of the C9ORF72 HRE such as DPRs.

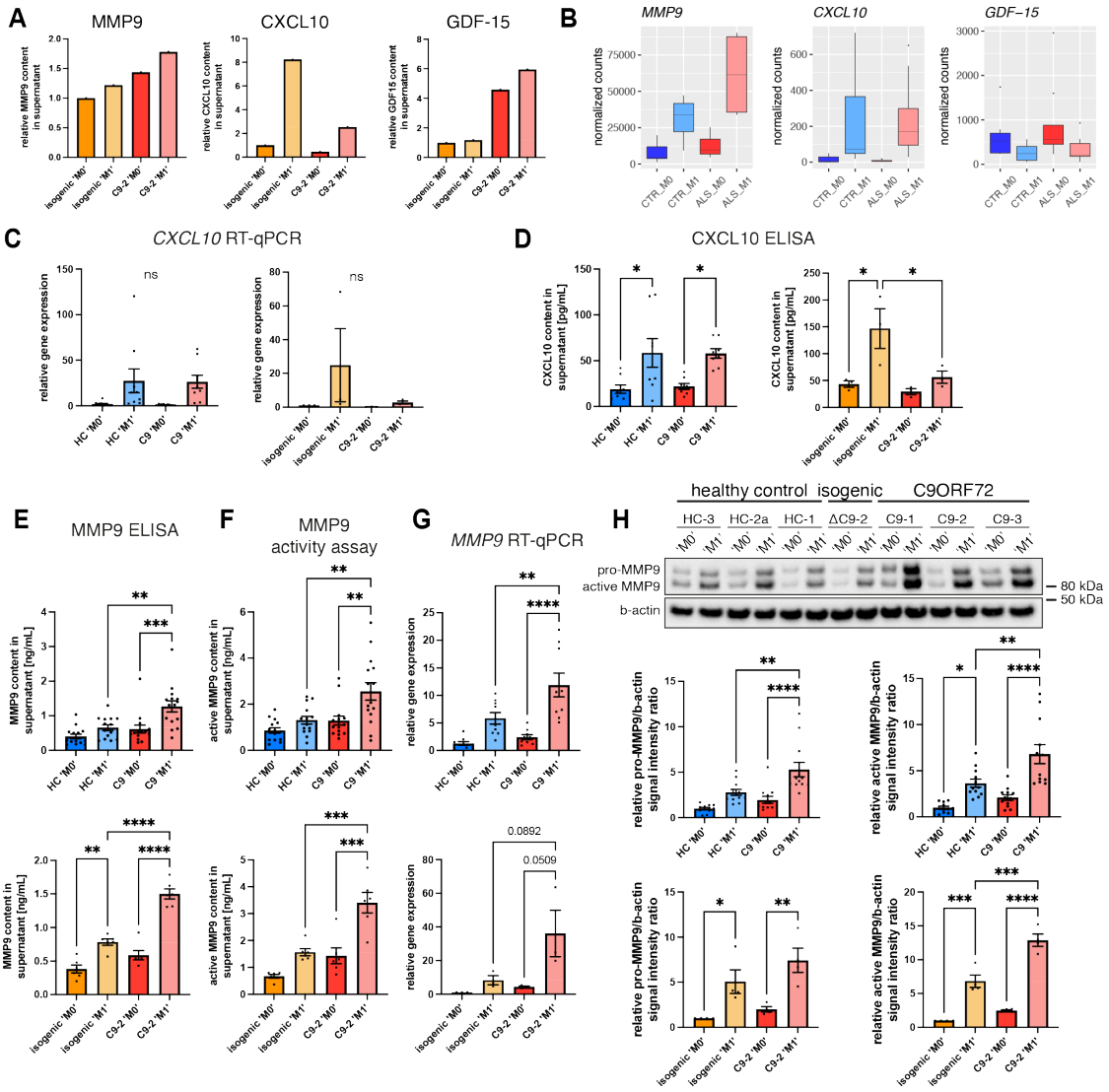


Figure 4.10: C9ORF72-ALS iPSC microglia consistently upregulated release and expression of MMP9. A) Relative fold change in supernatant content for MMP9, CXCL10, and GDF-15 using the Proteome Profiler Human XL Cytokine Array Kit (showing only the key differentially expressed targets) on pooled supernatant samples from unstimulated ('M0') and LPS-treated (100 ng/mL, 48 h, 'M1') C9-2 and isogenic microglia (pMGL) (pooled samples from n=1 lines per condition with n=3 differentiations each). **B)** Normalized counts from RNA seq analysis for *MMP9*, *CXCL10*, and *GDF-15* in 'M0' and 'M1' healthy and C9 pMGL. Only *MMP9* expression overlaps with the cytokine array, being increased in the C9-healthy comparison (n=3 lines per condition, n=3 differentiations each). **C)** RT-qPCR for *CXCL10* normalised to *TBP* as housekeeping gene confirms the RNA sequencing and supernatant array results (n=3 lines per condition for C9-healthy pMGL and n=1 line per condition for isogenic-C9-2 pMGL comparison, n=3 differentiations each). **D)** ELISA for CXCL10 release into the culture supernatant confirms the RNA sequencing and supernatant array results (n=3 lines per condition for C9-healthy pMGL and n=1 line per condition for isogenic-C9-2 pMGL comparison, n=3 differentiations each). **E)** ELISA quantification of MMP9 in supernatants from 'M0'/'M1' healthy, isogenic, and C9 pMGL shows significantly increased MMP9 release in the C9-healthy (n=3 lines per condition, n=5 differentiations each) and isogenic-C9-2 pMGL comparisons (n=1 line per condition, n=6 differentiations each). **F)** Activity assay for active MMP9 in supernatants from 'M0'/'M1' healthy, isogenic, and C9 pMGL shows significantly increased MMP9 activity in the C9-healthy (n=3 lines per condition, n=5 differentiations each) and isogenic-C9-2 pMGL comparison (n=1 line per condition, n=6 differentiations each). **G)** RT-qPCR for *MMP9* expression in 'M0'/'M1' healthy, isogenic, and C9 pMGL normalised to the housekeeping gene *TBP* showing significantly increased MMP9 expression in the C9-healthy (n=3 lines per condition, n=3 differentiations each) and numeric increase in isogenic-

C9-2 pMGL comparison (n=1 line per condition, n=3 differentiations each). **H)** Top: Exemplar Western blot against the pro-form and active form of MMP9 in 'M0'/'M1' healthy, isogenic, and C9 pMGL. Bottom: Quantification shows increased expression of pro-MMP9 in the C9-healthy pMGL comparison and a numeric increase in the isogenic-C9-2 pMGL comparison. Active MMP9 is significantly increased in both comparisons. Both normalised to the housekeeping gene b-actin (n=3 lines per condition for C9-healthy comparison, n=1 line for the isogenic-C9-2 comparison, n=4 differentiations each). Single data points and means ± SEM. No statistical tests were run on **A** due to the small sample size. One-way ANOVA with Tukey's post-hoc test (**C-H**). The assays in **D-F** were performed by Benazir Amein, a research assistant in the lab. Some of the Western blots and quantification in **H** were performed by Sumedha Nalluru, an MSc Neuroscience student I supervised in the lab.

4.8 Discussion and conclusions

In this chapter, I have demonstrated the successful differentiation of human iPSC microglia from C9ORF72-ALS patients and have conducted a phenotypic analysis. C9ORF72 haploinsufficiency and DPR formation, two key pathological features associated with the *C9ORF72* HRE mutation, were present in C9ORF72 microglia. RNA sequencing of C9ORF72 microglia demonstrated enrichment of pathways associated with immune cell activation, cytokine activity, lysosomes, and the ECM, most prominently after priming with LPS. Follow-up experiments outlined a deficit in phagocytosis and aberrant lysosome morphology in C9ORF72 microglia. Mechanistically, I found a pro-inflammatory cytokine/chemokine profile in C9ORF72 microglia, with increased activation of the NFκB-IL1B pathway, and surprisingly identified consistent upregulation and release of MMP9 in C9ORF72 microglia.

I aimed to answer several key questions about the consequences of the HRE mutation in *C9ORF72* on microglia in this chapter. Previous studies (Lall et al., 2021; McCauley et al., 2020; O'Rourke et al., 2016) have demonstrated an important role for C9ORF72 in macrophages in mice, with *C9orf72* KO inducing a

pro-inflammatory profile. However, whether authentic human iPSC microglia from C9ROF72-ALS patients replicate these findings remained an open question in the field, which I endeavoured to address here. During the preparation of this chapter, two pre-prints (Banerjee et al., 2022; Lorenzini et al., 2022) were published on BioRxiv, which also analysed iPSC microglia from C9ORF72-ALS patients. As there is considerable overlap with my findings, I will discuss the data from these preprints along with my results.

I generated human iPSC microglia from three different C9ORF72-ALS patients and three different healthy individuals, and additionally used our recently generated isogenic line as another control for microglia differentiation (Ababneh et al., 2020). First, I demonstrated that C9ORF72 expression is significantly higher in iPSC microglia than in MNs. This observation confirms previous data from mice (O'Rourke et al., 2016) and was also independently shown in human iPSC microglia by (Banerjee et al., 2022), indicating that C9ORF72 is likely to be of crucial importance in microglia. I then focused on loss-of-function and gain-of-function consequences of the C9ORF72 HRE on microglia. Research into the HRE mutation in *C9ORF72* has been very neurocentric; to my knowledge, RNA foci have been demonstrated in post mortem microglia from C9ORF72-ALS patients (Lagier-Tourenne et al., 2013; Mizielinska et al., 2013), but whether C9ORF72 haploinsufficiency or DPR expression is present specifically in microglia in post mortem tissue has not yet been studied (Rostalski et al., 2019). I investigated C9ORF72 expression and demonstrated C9ORF72 haploinsufficiency in C9ORF72 microglia compared with healthy microglia. The comparison between

the C9-2 line and its isogenic control did not show any differences in C9ORF72 expression, indicating the absence of C9ORF72 haploinsufficiency in this comparison. Both preprints on C9ORF72 iPSC microglia (Banerjee et al., 2022; Lorenzini et al., 2022) found haploinsufficiency, compared with both healthy and isogenic controls, suggesting that the absence of C9ORF72 haploinsufficiency in our C9-2-isogenic comparison is likely to be a line-specific observation. Furthermore, I demonstrated the expression of the DPRs Poly(GA) and Poly(GP) in C9ORF72 microglia, confirming that gain-of-function products of the *C9ORF72* HRE are present in C9ORF72 microglia. Whereas (Banerjee et al., 2022) focused on C9ORF72 haploinsufficiency and did not analyse DPR expression, (Lorenzini et al., 2022) also detected Poly(GP) in C9ORF72 microglia. I further showed that Poly(GA) and (GP) expression is notably higher in C9OF72 MNs than in C9ORF72 microglia, suggesting that microglia might have an intrinsic but currently unknown mechanism that allows them to better deal with DPR accumulation, a phenomenon that should be further explored in future studies. This is of particular interest, as LPS stimulation significantly increased C9ORF72 expression in microglia at gene and protein level, which one might expect to correlate with increased formation of DPRs. However, LPS stimulation did not lead to notably increased DPR levels, even after 6 days of continuous LPS treatment. While this observation could be due to a lack of sensitivity of the MSD ELISA, it raises further interest in how C9ORF72 microglia deal with DPR formation and accumulation. Notably, RNA foci have been found in C9ORF72 microglia in post mortem tissue (Mizielinska et al., 2013) and were also detected by (Lorenzini et al., 2022) in C9ORF72 iPSC microglia. A thorough characterization of RNA foci in iPSC

microglia using RNA-FISH was beyond the scope of this thesis, but should be performed in future studies. It would be of particular interest to perform a comparative analysis of C9ORF72 microglia and MNs and to investigate if LPS-priming affects RNA foci in C9ORF72 microglia.

I then performed RNA sequencing to determine whether C9ORF72 microglia display a cell-autonomous transcriptional dysregulation. As C9ORF72 haploinsufficiency has been proposed as the primary mechanism of microglial dysfunction in C9ORF72-ALS, which was present in the C9ORF72-healthy comparison, I focused on this analysis for the RNA sequencing. I used three independent microglial differentiations for all three C9ORF72-ALS lines and the corresponding healthy controls and included both unstimulated and LPS-primed microglia to assess if pro-inflammatory stimulation might uncover subtle transcriptomic differences. Unstimulated C9ORF72 and control microglia showed some differences in their transcriptome, but LPS priming revealed more transcriptomic differences between C9ORF72 microglia and controls. This observation is unsurprising given the numerous genes that are altered or induced in microglia in response to LPS, for example, *Il1b* (Sousa et al., 2018). Focusing on the dysregulation of pathways in C9ORF72 microglia, there was little enrichment of microglia-relevant pathways under unstimulated conditions, suggesting substantial transcriptomic similarity. This observation is in keeping with the RNA sequencing data from (Lorenzini et al., 2022), which showed no substantial difference between unstimulated C9ORF72 and control microglia. LPS priming, however, uncovered positive enrichment of pathways associated with immune cell activation and cytokines in

C9ORF72 microglia in my analyses. Furthermore, I found negative enrichment of lysosome and ECM-associated terms. (Lorenzini et al., 2022) also analysed LPS-primed C9ORF72 microglia but found no substantial transcriptomic differences compared with controls. I used the same LPS concentration for our stimulation paradigm but chose a more chronic approach for stimulation (48 hours) compared with (Lorenzini et al., 2022) (6 hours), which could explain the divergent findings.

Considering the well-documented association of C9ORF72 with endosomes and lysosomes (Beckers et al., 2021; Laflamme et al., 2019), the enrichment of terms connected with lysosomes in the RNA sequencing was not surprising. In functional follow-up experiments, I analysed the phagocytosis-lysosome axis and uncovered a phagocytic deficit in C9ORF72 microglia, which is in line with the findings from (Banerjee et al., 2022) and (Lorenzini et al., 2022). Phagocytic receptor expression was unchanged in the RNA sequencing analysis, but I detected aberrant lysosomal morphology, in line with previous observations in C9ORF72-ALS patient derived neurons (Shi et al., 2018), and lysosomal alterations found in macrophages and microglia from *C9orf72* KO mice (Lall et al., 2021; O'Rourke et al., 2016). These results suggest that the phagocytic deficit might be due to impaired degradation of phagocytosed particles, which corresponds well to the autophagy impairment in C9ORF72 microglia described by (Banerjee et al., 2022). However, I did not perform functional experiments to assess lysosomal function in C9ORF72 microglia, which would be required to confirm this hypothesis. Notably, I did not observe significant differences in phagocytic activity or lysosomal morphology in the C9-isogenic comparison, correlating with the lack of

C9ORF72 haploinsufficiency in this line pair. This suggests that the phago-lysosomal dysfunction is driven by C9ORF72 haploinsufficiency, which is in keeping with the phagocytic dysfunction described by (Banerjee et al., 2022) in iPSC microglia derived from a *C9ORF72* KO line.

Overall, the analysis of pathway enrichment in the RNA sequencing analysis was more informative than the analysis of individual DEGs, with the notable exception of *CALHM2*, which was consistently and significantly upregulated in C9ORF72 microglia. CALHM2 is implicated in calcium signalling, controls calcium homeostasis (Choi et al., 2019b) and, intriguingly, *CALHM2* was amongst the genes associated with ALS in a recent exome sequencing (Nicolas et al., 2018). Increased *CALHM2* expression has previously been found in hippocampal tissue of AD patients and the 5×FAD transgenic mouse model for AD (Cheng et al., 2021). Furthermore, Calhm2 KO ameliorated a pro-inflammatory microglial phenotype, decreased acute LPS-induced neuroinflammation, and reduced amyloid-β deposition in 5×FAD transgenic mice (Cheng et al., 2021). Interestingly, perturbations of microglial calcium signalling were observed in iPSC microglia carrying the ALS-linked FUS^{525L} mutation (Kerk et al., 2022). In future work, it will therefore be of great interest to confirm *CALHM2* upregulation in C9ORF72 microglia at gene and protein level and investigate its role in calcium signalling and the microglial phenotypes discovered in this chapter by CALHM2 KO or knock-down.

Guided by pathway enrichment in our RNA-sequencing analysis and phenotypes described in macrophages/microglia from *C9orf72* KO mice (Lall et al., 2021;

O'Rourke et al., 2016), I focused in more detail on the cytokine profile of C9ORF72 microglia in this chapter. While unstimulated C9ORF72 microglia did not substantially differ from controls, inflammatory cytokines and pathways were upregulated in C9ORF72 microglia after pro-inflammatory priming with LPS. Specifically, the NFκB-IL1B axis was increased in C9ORF72 microglia compared with healthy controls, overlapping substantially with the data independently generated by (Banerjee et al., 2022). However, comparing the isogenic control with its C9ORF72 donor line, I found no differences in the expression of NFκB or IL1B, suggesting this pro-inflammatory phenotype is likely to be driven by C9ORF72 haploinsufficiency. This observation confirms data using macrophages/microglia from *C9orf72* KO mice (Lall et al., 2021; O'Rourke et al., 2016) and iPSC microglia derived from a *C9ORF72* KO line (Banerjee et al., 2022). Interestingly, a dysregulation of cytokine/chemokine-associated pathways was also found in iPSC microglia carrying the ALS-linked FUS^{525L} mutation (Kerk et al., 2022), suggesting this phenotype might be a common feature of different forms of ALS.

Most interestingly and surprisingly, I identified that MMP9 expression and release was significantly upregulated in LPS-primed C9ORF72 microglia, which corresponds well to the enrichment of ECM-associated terms in the RNA sequencing analysis. MMP9 is an endopeptidase that can cleave several constituents of the ECM as well as cell surface receptors, leading to circuit and synaptic reorganization (Reinhard et al., 2015; Vafadari et al., 2016). Owing to its key role in brain physiology, MMP9 dysregulation has been widely implicated in multiple neurodegenerative disorders (Vafadari et al., 2016). Intriguingly, a neurotoxic role for

MMP9 has been demonstrated in previous studies using SOD1 and TDP-43 animal models for ALS (Kaplan et al., 2014; Spiller et al., 2019). However, to my knowledge, this thesis provides the first evidence for MMP9 upregulation specifically in C9ORF72 microglia. Importantly, MMP9 was significantly increased in C9ORF72 microglia compared with both healthy and isogenic controls, indicating that its upregulation is not likely to be a consequence of C9ORF72 haploinsufficiency. This finding is of particular interest, considering that (Banerjee et al., 2022) independently identified MMP9 as an interactor of the C9ORF72 protein by analysing the C9ORF72 interactome in iPSC microglia. In combination, this suggests that MMP9 upregulation could be a direct consequence of HRE-induced alterations in the C9ORF72 protein or gain-of-function products such as DPRs or RNA foci.

The fact that haploinsufficiency was present in microglia in the C9ORF72-healthy control comparison but absent when comparing the isogenic control with its C9ORF72 donor line unexpectedly opened up the opportunity to disentangle the contribution of C9ORF72 haploinsufficiency to the observed phenotypes. The majority of phenotypes were present in the C9ORF72-healthy control comparison, suggesting that C9ORF72 haploinsufficiency is a major driver of disease phenotypes, which is in agreement with previous papers using *C9orf72* KO macrophages/microglia (Lall et al., 2021; McCauley et al., 2020; O'Rourke et al., 2016) and the other C9ORF72 iPSC microglia studies from (Lorenzini et al., 2022) and (Banerjee et al., 2022). However, MMP9 upregulation, for instance, was also present in C9ORF72 microglia in the absence of C9ORF72

haploinsufficiency, suggesting it is, at least partly, driven by gain-of-function toxicity. The contribution of DPRs to the observed phenotypes therefore remains to be determined. Selective expression of DPRs in microglia will be able to address this question in future studies. I did not evaluate RNA foci expression in this chapter, thus their contribution to microglial phenotypes also remains an open question.

Some limitations of the experimental design in this chapter relate to the microglial culture and stimulation paradigm employed. Treatment with 100 ng/mL LPS for 48 hours is a comparably strong and acute stimulation paradigm, which is very useful to simulate a pro-inflammatory environment *in vitro*, but it will be important to assess if it appropriately replicates the environment *in vivo*. It would be useful to perform a more chronic stimulation approach with lower dosages and, additionally, use other stimulants such as TNF-α or TDP-43 protein aggregates. Furthermore, even though iPSC microglia closely resemble *bona fide* human microglial cells, microglia are dependent on the interaction with neurons and other non-neuronal cells, and it will be important to model this crosstalk. It is likely that *in vivo*, pro-inflammatory agents are released by other cell types, for instance astrocytes or infiltrating inflammatory cells, such as T-cells. Similarly, in the context of ALS, degenerating neurons might provide additional cues that influence the microglial phenotype. Therefore, it will be essential to assess this crosstalk between neuronal and other non-neuronal cells and microglia, for instance, using multi-cellular iPSC cultures or microglia transplantation approaches. These would

allow for an assessment of the microglial phenotype in a more complex CNS environment.

In summary, this chapter has unravelled cellular dysfunction and a pro-inflammatory phenotype of C9ORF72 iPSC microglia. These findings therefore set the scene for the investigation of non-cell-autonomous microglial effects on MNs in the next chapter.

5 Investigating effects of C9ORF72-ALS iPSC microglia on motor neurons in co-culture

5.1 Introduction and aims

Having demonstrated cellular dysfunction of C9ORF72 iPSC microglia in chapter 4, I next aimed to evaluate if they might also exert non-cell-autonomous effects on MNs. Evidence from animal models for ALS suggests that microglia contribute to disease progression rather than initiation, and therefore elicit predominantly secondary neurotoxicity. On the other hand, murine co-cultures of mSOD1 microglia and neurons have demonstrated direct microglial neurotoxicity. In the context of C9ORF72-ALS, a recent paper using murine co-cultures of MNs and microglia demonstrated that *C9orf72* KO microglia induced synaptic loss in MNs (Lall et al., 2021), but no other publication had looked at the interplay between C9ORF72 microglia and MNs prior to my DPhil project. To do so, I made use of the co-culture system of MNs and microglia I established and characterised in chapter 3 of this thesis. I decided to focus on the non-cell-autonomous effects of C9ORF72 microglia on MNs to investigate whether C9ORF72 microglia exerted primary neurotoxicity. Therefore, I chose to combine C9ORF72 and control microglia only with healthy MNs to avoid confounding effects of concomitant expression of the HRE in *C9ORF72* in neurons.

I aimed to start my investigations by analysing unstimulated co-cultures for the presence of microglial toxicity. If these did not show any differences, I would then

additionally stimulate co-cultures with LPS to investigate if pro-inflammatory priming would uncover latent microglial neurotoxicity. Specifically, I aimed to analyse the dysregulated microglial pathways uncovered by the phenotypic analysis of microglial monocultures in chapter 4 in co-culture, particularly the cytokine profile. The second aim was then to investigate microglial neurotoxicity through the analysis of the apoptotic marker CC3 in MNs in co-culture as well as the evaluation of neuronal activity and synaptic protein expression.

5.2 Analysis of unstimulated co-cultures of C9ORF72-ALS iPSC microglia and healthy control motor neurons

Aiming to focus on the non-cell-autonomous role of microglia in co-culture, I limited my analyses to co-cultures with WT MNs. Both cell types were co-cultured for at least 14 days, using the co-culture protocol established in chapter 3, expecting that overt differences would become apparent within this time frame (Figure 5.1A).

5.2.1 Motor neuron and microglia markers are equally expressed, while pro-MMP9 expression is upregulated in unstimulated co-cultures

First, I analysed the expression of the MN marker ChAT and the microglial marker IBA1 in co-culture, confirming high and equal expression of both markers in co-cultures of WT MNs with C9ORF72 and control microglia (Figure 5.1B, C). As control, IBA1 was not detectable by Western blotting in MN monocultures (Figure 5.1B). I then aimed to assess the expression of the inflammatory mediators and pathways uncovered by my analysis of C9ORF72 microglial monocultures. In

keeping with the monoculture experiments, the pro-form of MMP9 was significantly upregulated in co-cultures with C9ORF72 microglia compared with healthy controls, and a similar trend, albeit not significant, was observed in comparison with isogenic microglia (Figure 5.1B, D). The active form of MMP9 was not differentially expressed between co-cultures with C9ORF72 microglia and controls, likely due to the lack of LPS stimulation (Figure 5.1B, D). MN monocultures showed no expression of MMP9, confirming its microglial origin (Figure 5.1B).

In summary, these data confirm the successful differentiation of co-cultures of WT MNs and C9ORF72 and control microglia.

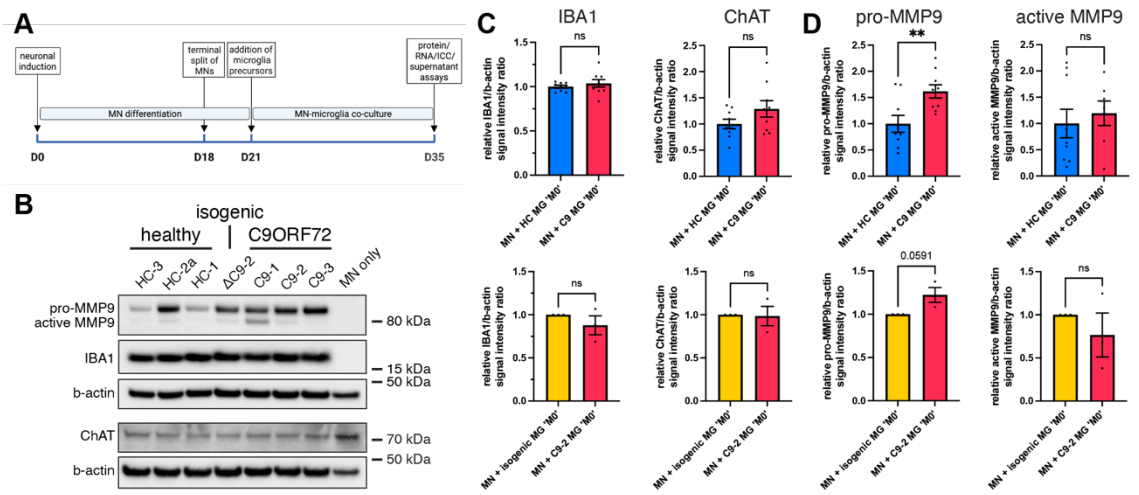


Figure 5.1: Co-cultures of WT motor neurons with C9ORF72 iPSC microglia express MN and microglia markers and upregulate pro-MMP9. A) Schematic overview of experimental setup for MN-microglia co-culture. **B)** Exemplar Western blot against IBA1, ChAT, and MMP9 in co-cultures of healthy control MNs with unstimulated healthy, isogenic, and C9ORF72 (C9) microglia (MG). **C, D)** Quantification normalised to the housekeeping gene b-actin shows equal expression of the microglia marker IBA1 and the MN marker ChAT in co-cultures with unstimulated C9 and control MG. pro-MMP9 is significantly increased in the C9-healthy comparison and shows a numeric increase in the isogenic-C9-2 comparison, while active MMP9 levels are unchanged (n=3 lines for C9 and healthy MG and n=1 line for C9 and isogenic MG, n=3 differentiations each). Single data points and means ± SEM. Two-tailed unpaired t-test (**C, D**). Some of the Western blots and quantifications in **C** and **D** were performed by Sumedha Nalluru, an MSc Neuroscience student I supervised in the lab.

5.2.2 Unstimulated C9ORF72-ALS iPSC microglia do not cause overt neurotoxicity to healthy motor neurons in co-culture

Having set up the disease co-cultures, I sought to investigate if C9ORF72 microglia caused non-cell-autonomous neurotoxicity. To do so, I analysed the expression of the apoptotic marker CC3 in co-cultured MNs as well as the total number of MNs in co-culture. MNs co-cultured with C9ORF72 and healthy and isogenic control microglia showed very low and equal neuronal expression of CC3 (Figure 5.2A, B). Similarly, the numbers of TUJ1-positive neurons were equal in co-culture (Figure 5.2A, B), indicating that unstimulated C9ORF72 microglia did not cause overt neurotoxicity, at least after 14 days of co-culture. Additionally, I quantified neurite density in co-cultures of healthy MNs and C9ORF72 and control microglia. Similarly, there was no difference in neurite density (Figure 5.2C, D).

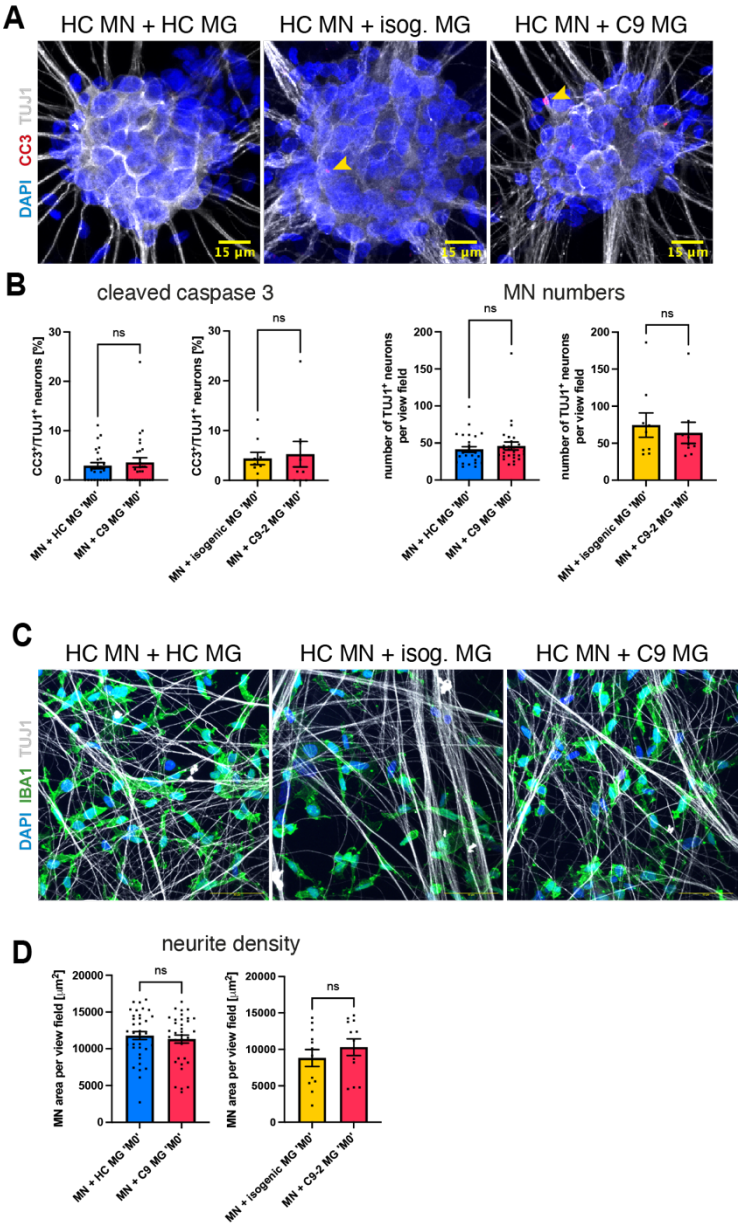


Figure 5.2: Co-cultures of WT motor neurons with C9ORF72 iPSC microglia show no differences in microglia and MN numbers, neuronal expression of cleaved caspase 3, and neurite density. A) Exemplar images of the expression of the apoptosis marker cleaved caspase 3 (CC3) in TUJ1-positive healthy control MNs in co-culture with unstimulated healthy, isogenic, and C9ORF72 (C9) microglia (MG). **B)** Quantification of CC3 expression and MN numbers shows no difference between co-cultures with C9 and control MG (datapoints are n=3 view fields for n=3 lines (C9-healthy comparison) and n=1 line (C9-isogenic comparison), n=3 differentiations each). Scale bars: 15 µm. **C)** Exemplar images of TUJ1-positive neurites in co-culture with unstimulated IBA1-positive healthy, isogenic, and C9 MG. **D)** Quantification of neurite density shows no difference between co-cultures with C9 and control MG (datapoints are n=4 view fields for n=3 lines (C9-healthy comparison) and n=1 line (C9-isogenic comparison), n=3 differentiations). Scale bars: 50 µm. Single data points and means ± SEM. Two-tailed unpaired t-test (**B, D**). The confocal images in **A** were taken and the quantifications in **B** performed by Lucy Farrimond, another DPhil student in the lab.

Given previous reports of *C9orf72* KO microglia promoting synaptic loss (Lall et al., 2021), I also investigated synaptic protein expression and activity in MNs in

co-culture. To do so, I first quantified the number and area of synaptophysin puncta in co-culture, which showed no significant differences between co-cultures with C9ORF72 microglia and controls (Figure 5.3A, B). In addition, I used MEAs to analyse neuron activity in co-culture. The results confirmed the expected neuronal activity in co-culture but showed no difference between C9ORF72 and healthy and isogenic microglia (Figure 5.3C).

In summary, these data demonstrate that unstimulated C9ORF72 microglia do not alter the survival or function of two-week co-cultured MNs.

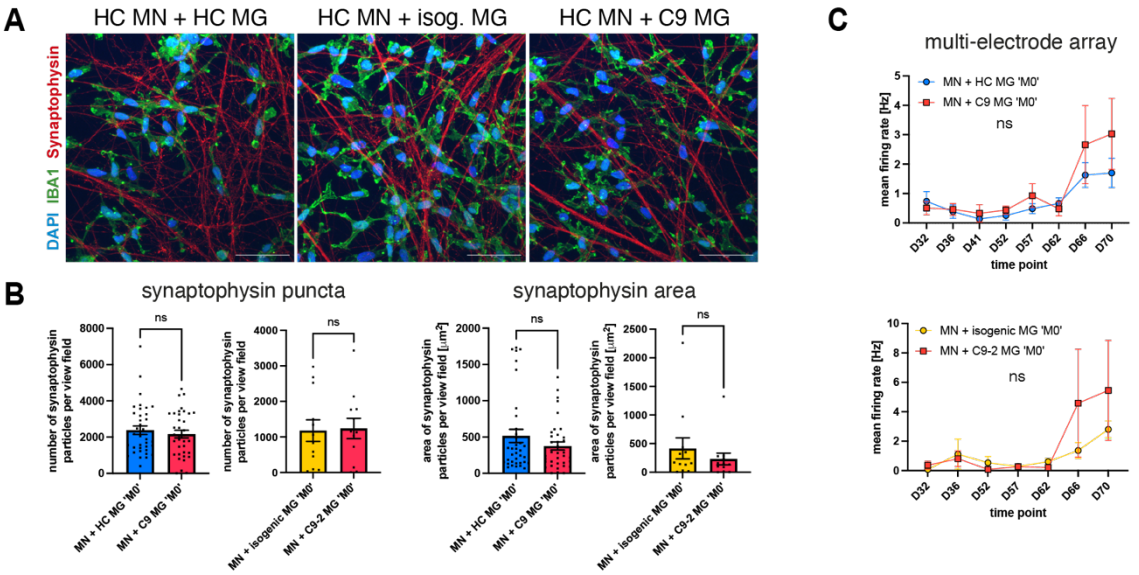


Figure 5.3: Co-cultures of WT motor neurons with C9ORF72 iPSC microglia show no differences in synaptophysin expression and neuronal activity. A) Exemplar images of synaptophysin staining in co-culture with unstimulated IBA1-positive healthy, isogenic, and C9ORF72 (C9) MG. **B)** Quantification of the area and number of synaptophysin particles shows no difference between co-cultures with C9 and control MG (datapoints are n=4 view fields for n=3 lines (C9-healthy comparison) and n=1 line (C9-isogenic comparison), n=3 differentiations each). Scale bars: 50 µm. **C)** Multi-electrode array analysis of healthy MNs in co-culture with C9 and control MG shows no differences in the mean firing rate (datapoints are n=2 wells per differentiation for n=3 lines (C9-healthy comparison) and n=1 line (C9-isogenic comparison), n=3 differentiations each). Single data points and means ± SEM. Two-tailed unpaired t-test (**B**). Two-way ANOVA with Tukey's post-hoc test (**C**).

5.2.3 Unstimulated C9ORF72-ALS iPSC microglia show a dysregulated supernatant profile and upregulate DPP4 release in co-culture with healthy MNs

Having observed no effects of unstimulated C9ORF72 microglia on co-cultured WT MNs, I opted to assess the supernatant profile of the co-cultures. I hypothesised that a dysregulated profile might serve as an early marker for microglial dysregulation which, if present, could translate into overt effects on MNs upon prolonged culture duration or stimulation. To assess the supernatant profile, I used the same membrane-based cytokine/chemokine array I had used to analyse microglial monocultures. Indeed, co-cultures of MNs with C9ORF72 microglia showed a substantially different supernatant profile compared with healthy and isogenic microglia (Figure 5.4A). Furthermore, there was considerable overlap between the C9ORF72-healthy and C9ORF72-isogenic comparisons (Figure 5.4A). Neurotrophic factors, such as BDNF or IGFBP-2 (Insulin-like growth factor (IGF) binding protein 2), and pro-inflammatory molecules, including IL6, TNF-α and CXCL10, were dysregulated in co-cultures with C9ORF72 microglia compared with both controls. Intriguingly, I found the strongest increase in both comparisons for dipeptidyl peptidase 4 (DPP4). DPP4 has previously been implicated in neurodegeneration in AD, with DPP4 inhibition having shown beneficial outcomes (Valverde et al., 2021), and DPP4 shedding has been connected with MMP9 (Rohrborn et al., 2014). To validate this finding, I quantified the DPP4 content in co-culture supernatants using ELISA. In keeping with the cytokine array, there was a strong and significant upregulation of DPP4 in co-cultures with C9ORF72 microglia compared with both healthy and isogenic control microglia

(Figure 5.4B). Supernatants from microglial monocultures showed no significant differences between C9ORF72 microglia and controls (Figure 5.4C), whereas supernatants from MNs derived from the same C9ORF72 iPSC lines showed almost no release of DPP4 (Figure 5.4D). These results suggest that DPP4 is released from microglia in co-culture, while the contact with neurons seems to be required for its upregulation in C9ORF72 microglia.

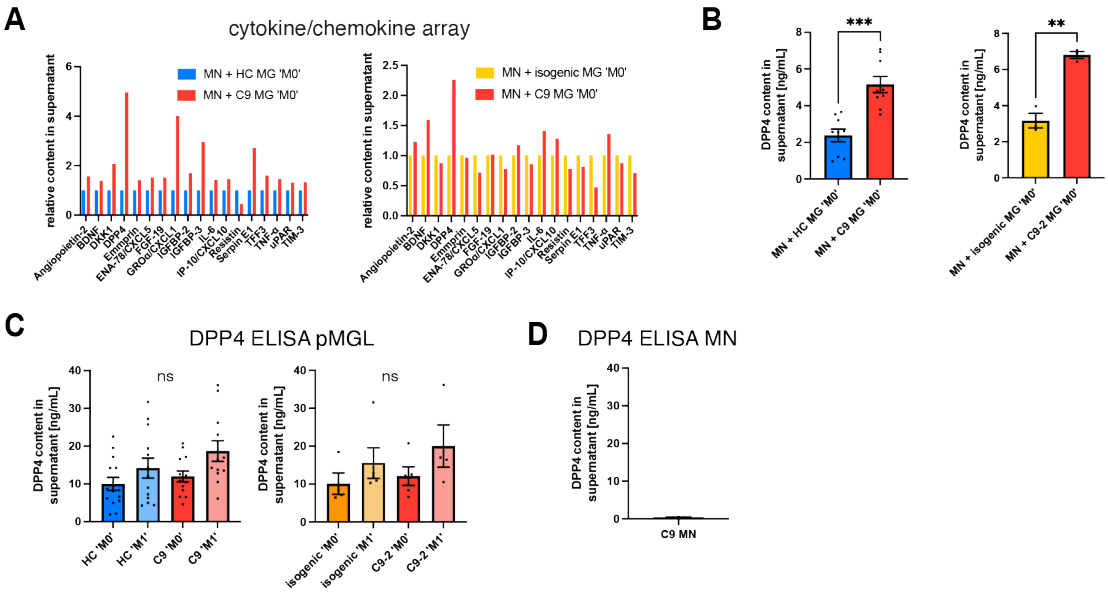


Figure 5.4: Co-cultures of WT motor neurons with C9ORF72 iPSC microglia have a dysregulated cytokine profile and upregulate DPP4 release. A) Relative fold change in co-culture supernatant content for selected targets (only key differentially expressed targets shown) using the Proteome Profiler Human XL Cytokine Array Kit. Supernatant samples from healthy MNs co-cultured with unstimulated C9ORF72 (C9), healthy, and isogenic MG show a dysregulated cytokine profile (pooled samples from n=3 lines (C9-healthy comparison) and n=1 line (C9-isogenic comparison) with n=3 differentiations each). **B)** ELISA quantification of DPP4 content in co-culture supernatants from healthy MNs co-cultured with unstimulated C9, healthy, and isogenic MG shows significantly increased DPP4 levels in both comparisons (n=3 lines for C9-healthy comparison and n=1 line for C9-isogenic comparison, with n=3 differentiations each). **C)** ELISA quantification shows no statistical difference in DPP4 content in culture supernatants from unstimulated ('M0') and LPS-treated (100 ng/mL, 48 h, 'M1') healthy, isogenic, and C9 microglia monocultures (pMGL) (n=3 lines per condition for C9-healthy pMGL and n=1 line per condition for isogenic-C9-2 pMGL comparison, n=4-5 differentiations each). **D)** ELISA quantification shows DPP4 is barely released from C9 MNs in monoculture (n=3 lines, n=1 differentiation each). Single data points and means ± SEM. Two-tailed unpaired t-test (**B**) and one-way ANOVA with Tukey's post-hoc test (**C**). The ELISAs in **B-D** were performed by Benazir Amein, a research assistant in the lab.

Together, these data demonstrate an altered cytokine profile of C9ORF72 microglia in co-culture with MNs in absence of overt neurotoxicity and identify DPP4

release into the supernatant as a putative biomarker for early microglial dysfunction.

5.3 Analysis of LPS-primed co-cultures of C9ORF72-ALS iPSC microglia and healthy control motor neurons

The dysregulated cytokine profile in unstimulated co-cultures and the phenotype of LPS-stimulated C9ORF72 microglial monocultures led me to speculate that pro-inflammatory priming might uncover non-cell-autonomous effects of C9ORF72 microglia on MNs. To investigate this hypothesis, I generated new co-cultures of healthy control MNs and C9ORF72 and control microglia and stimulated them repetitively with LPS (3 doses over 10 days) (Figure 5.5A).

5.3.1 LPS-primed co-cultures express motor neuron and microglia markers and upregulate p-NFκB, pro-MMP9, and active MMP9

The resulting stimulated co-cultures expressed the MN marker ChAT and the microglia marker IBA1 (Figure 5.5B, C). ChAT expression showed a mild but significant reduction in stimulated co-cultures with C9ORF72 microglia compared with healthy control but not isogenic microglia (Figure 5.5B, C). IBA1 expression was equal in all conditions and absent in MN monocultures (Figure 5.5B, C). I then analysed stimulated co-cultures for the expression of the pro-inflammatory mediators I found to be different in C9ORF72 microglial monocultures. Both the pro-form and active form of MMP9 were significantly upregulated in stimulated co-cultures with C9ORF72 microglia compared with both healthy and isogenic microglia (Figure 5.5B, D). MN monocultures showed no expression of MMP9,

confirming its microglial origin (Figure 5.5B). I also analysed the activation of the NFκB pathway (Figure 5.5B, E). Total NFκB expression was similar between the different conditions, but the level of p-NFκB increased in co-cultures with C9ORF72 microglia compared with healthy controls, reaching statistical significance when normalised to the total NFκB level (Figure 5.5B, E). The C9ORF72-isogenic comparison showed no significant differences (Figure 5.5E), recapitulating my observations in C9ORF72 microglial monocultures. As expected, NFκB and, to a lesser extent, p-NFκB, were also detectable in MN monocultures, suggesting neuronal NFκB might contribute to the observed activation of the NFκB pathway.

Taken together, these data confirm the successful generation of LPS-primed C9ORF72 microglia-MN co-cultures with upregulation of the pro-inflammatory mediators p-NFκB and MMP9.

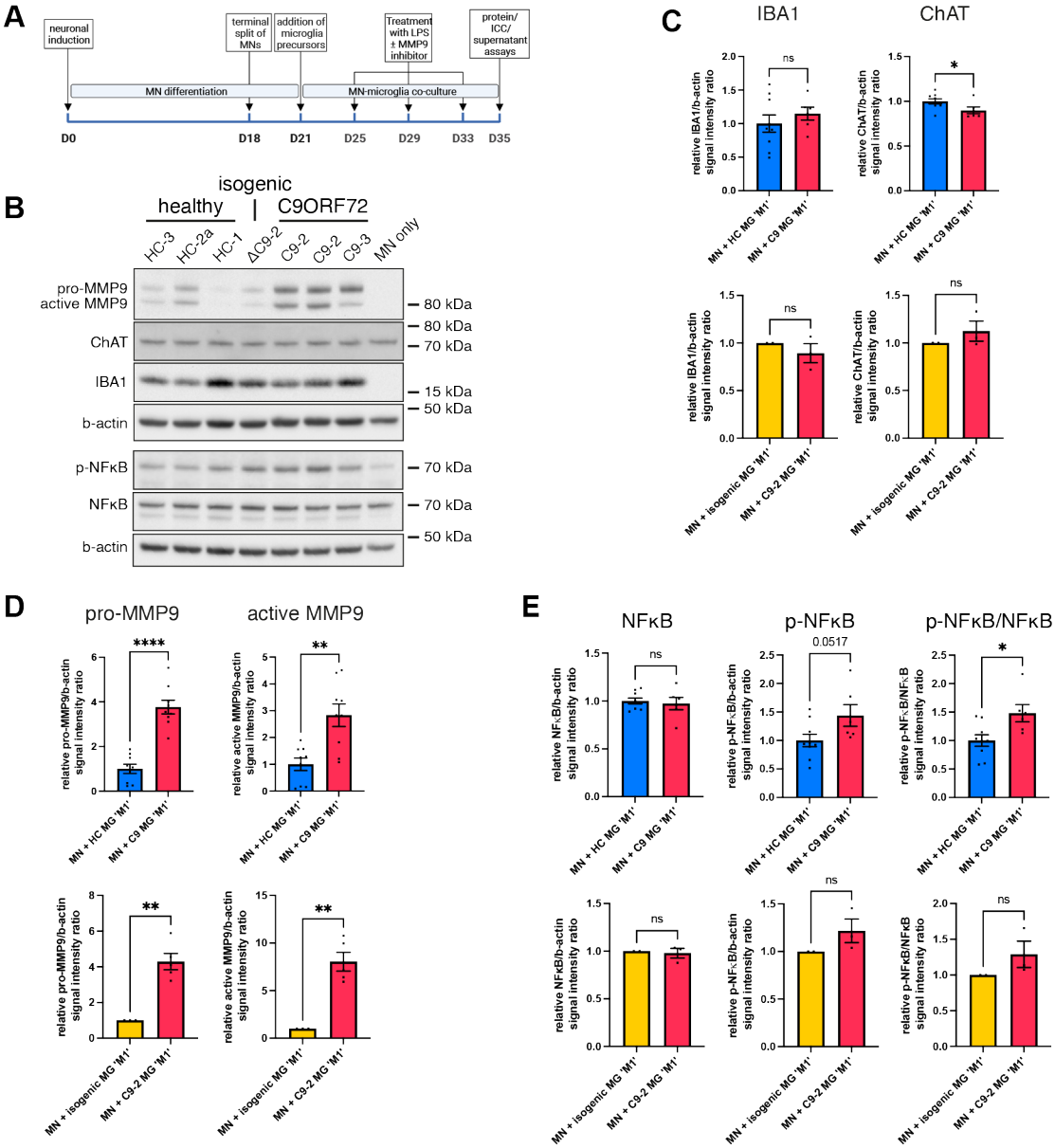


Figure 5.5: LPS-primed co-cultures of WT MNs and C9ORF72 microglia express MN and microglia markers and upregulate pro-MMP9, active MMP9, and p-NFκB. A) Schematic overview of experimental setup for LPS-stimulated MN-microglia co-cultures. **B)** Exemplar Western blot against IBA1, ChAT, MMP9, NFκB, and p-NFκB in co-cultures of healthy control MNs with LPS-primed ('M1') healthy, isogenic, and C9ORF72 (C9) microglia (MG). **C-E)** Quantification normalised to the housekeeping gene b-actin shows equal expression of the microglia marker IBA1 in co-cultures with 'M1' C9 and control MG. The MN marker ChAT shows a mild but significant decrease in co-cultures with C9 MG compared with healthy but not isogenic MG. pro-MMP9 and active MMP9 are significantly increased in co-cultures with C9 MG compared with healthy and isogenic MG. NFκB levels are unchanged, but p-NFκB is significantly upregulated in co-cultures with C9 MG compared with healthy but not isogenic MG (n=2-3 lines for C9 and healthy MG and n=1 line for C9 and isogenic MG, n=1-5 differentiations each). Single data points and means ± SEM. Two-tailed unpaired t-test (**C-E**).

5.3.2 LPS-primed C9ORF72-ALS iPSC microglia induce apoptosis of healthy control motor neurons in co-culture in an MMP9-dependent manner

I then analysed LPS-primed co-cultures for non-cell-autonomous effects of C9ORF72 microglia on neurons. To assess microglial neurotoxicity, I again assessed the percentage of MNs positive for the apoptotic marker CC3 as well as the total number of MNs in co-culture. Compared with unstimulated co-cultures (Figure 5.2A, B), the neuronal expression of CC3 was substantially higher after LPS priming (Figure 5.6A, B). MNs in co-culture with C9ORF72 microglia showed significantly higher neuronal CC3 expression compared with both healthy and isogenic controls (Figure 5.6A, B), indicating that LPS-primed C9ORF72 microglia induced apoptosis in MNs in co-culture. The number of MNs was equal in all conditions (Figure 5.6A, C), suggesting that the activation of neuronal apoptosis did not yet lead to substantial neurodegeneration at this time point.

I then hypothesised that the increased microglial MMP9 expression might contribute to their non-cell-autonomous neurotoxicity. To investigate this hypothesis, I treated LPS-stimulated co-cultures concomitantly with an MMP9 inhibitor that had previously been successfully applied *in vivo* (Kaplan et al., 2014). Indeed, simultaneous administration of LPS and the MMP9 inhibitor reduced CC3 expression in MNs, abolishing the significant difference between co-cultures with healthy and C9ORF72 microglia (Figure 5.6A, B). Furthermore, comparing co-cultures with C9-2 microglia and isogenic control microglia, treatment with the MMP9 inhibitor fully rescued neuronal CC3 expression (Figure 5.6A, B). Of note, treatment

of co-cultured control microglia with the MMP9 inhibitor resulted in no significant differences compared with DMSO-treated controls, supporting a specific effect of MMP9 inhibition on C9ORF72 microglia. These data suggest that the increased expression of MMP9 in C9ORF72 microglia directly contributes to their neurotoxic properties in co-culture.

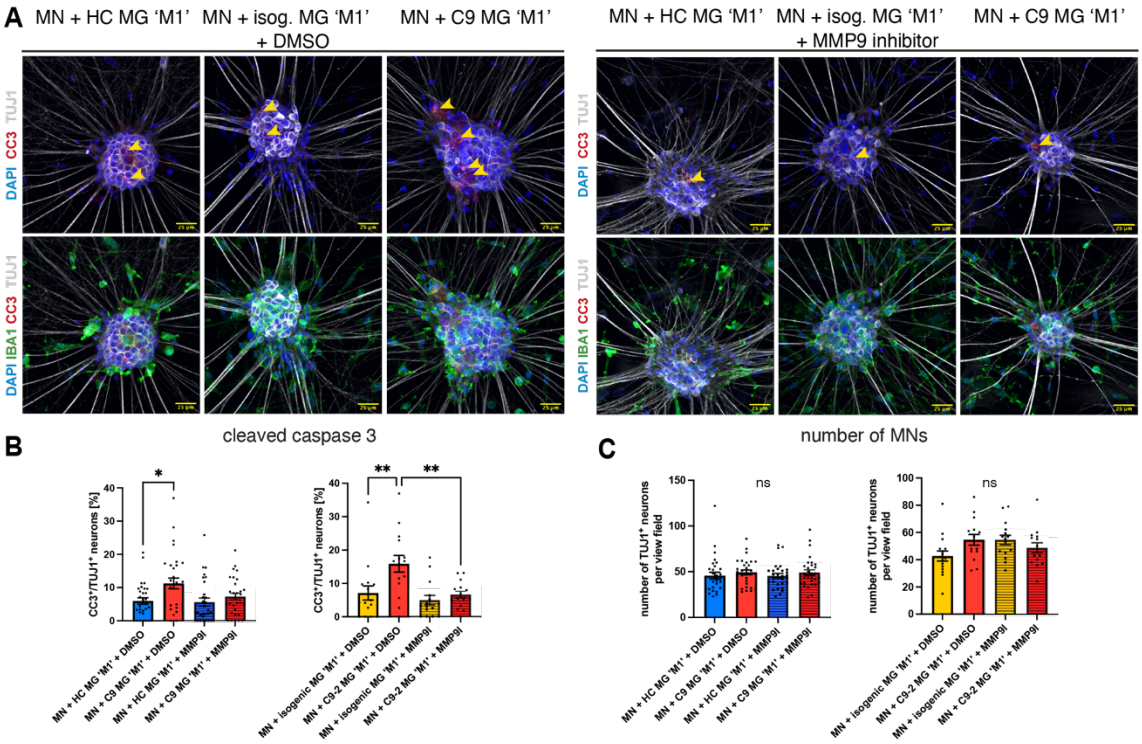


Figure 5.6: LPS-primed C9ORF72 microglia induce apoptosis in co-cultured healthy motor neurons via an MMP9-dependent mechanism. A) Exemplar images of the expression of the apoptosis marker cleaved caspase 3 (CC3) in TUJ1-positive healthy control MNs in co-culture with 'M1' healthy, isogenic, and C9ORF72 (C9) IBA1-positive MG plus DMSO as vehicle control or MMP9 inhibitor 1 (3 μM, MMP9I). **B)** Quantification shows that CC3 expression is significantly increased in co-culture with C9 compared with healthy and isogenic MG. Administration of MMP9I ameliorates microglial neurotoxicity. Datapoints are n=5 view fields for n=3 lines for C9-healthy comparison (n=1-3 differentiations each) and n=1 line for C9-isogenic comparison (n=3 differentiations each). Scale bars: 25 μm. **C)** Quantification shows equal numbers of TUJ1-positive healthy MNs in co-culture with 'M1' IBA1-positive C9ORF72 (C9), healthy, and isogenic MG (datapoints are n=5 view fields for n=3 lines (C9-healthy comparison) and n=1 line (C9-isogenic comparison), n=2-3 differentiations each). Single data points and means ± SEM. One-way ANOVA with Tukey's post-hoc test (**B, C**). The confocal images in **A** were taken and the quantifications in **B** and **C** performed by Lucy Farrimond, another DPhil student in the lab.

5.3.3 LPS-primed co-cultures show no differences in synaptophysin expression, neuronal activity, or neurite density

Next, I assessed whether stimulated co-cultures showed differences in synaptic protein expression, neuronal activity, or connectivity. Analysing the number and area of synaptophysin puncta, I found no differences between co-cultures with C9ORF72 microglia and controls (Figure 5.7A). Similarly, MEA recordings showed no difference in the neuronal mean firing rate (Figure 5.7B). Of note, I had to limit the recordings to 14 days post-stimulation, as the cells became prone to detach from the MEA plate afterwards, rendering the resulting readings unreliable. It is therefore possible that I missed differences in electrical activity that would have become apparent after prolonged co-culture. Finally, I also quantified neurite density and found no differences between co-cultures with C9ORF72 and control microglia (Figure 5.7C).

In summary, these data suggest that LPS-primed C9ORF72 microglia do not cause alterations to the synaptic protein expression, activity, or neurite density of MNs in co-culture.

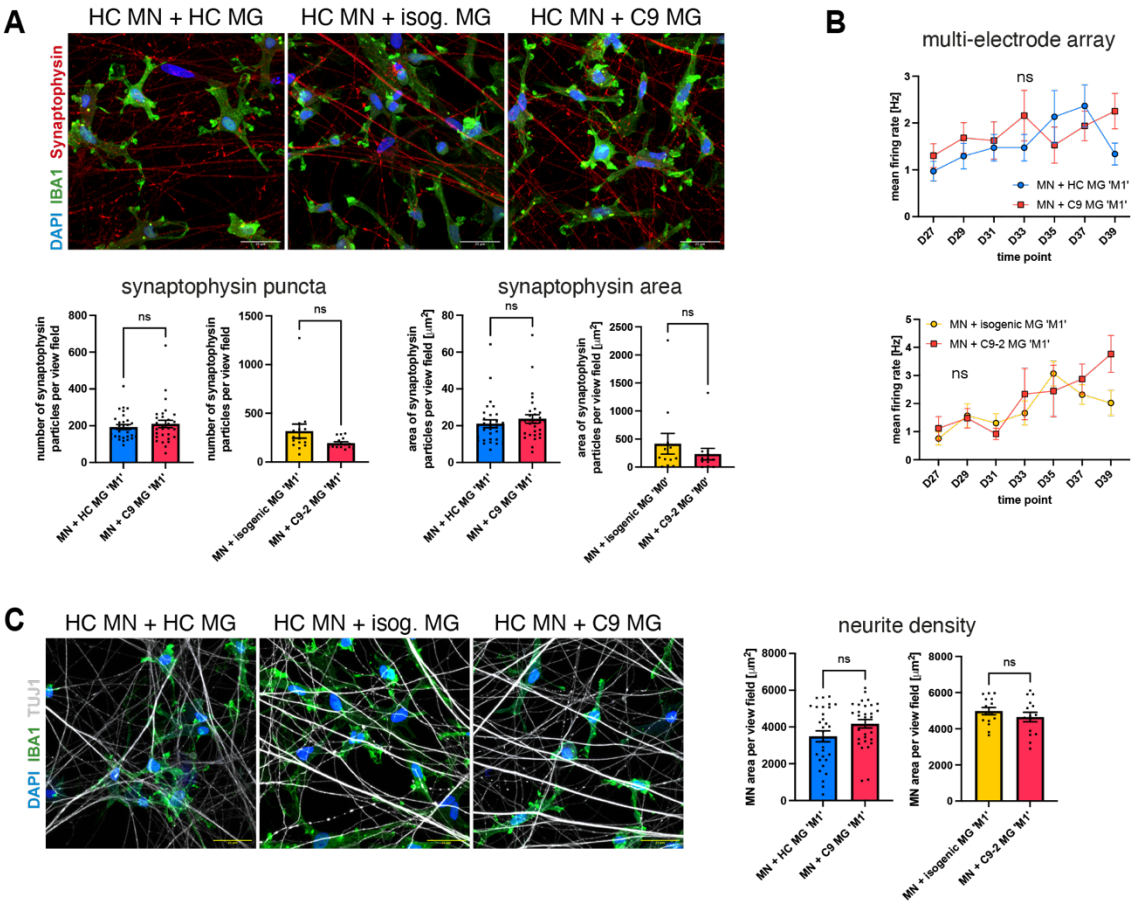


Figure 5.7: LPS-primed C9ORF72 microglia do not alter synaptophysin expression, neuronal activity, or neurite density of co-cultured healthy motor neurons. A) Top: exemplar images of synaptophysin staining in co-culture with IBA1-positive 'M1' healthy, isogenic, and C9ORF72 (C9) MG. Bottom: Quantification of the area and number of synaptophysin particles shows no difference between co-cultures with C9 and control MG (datapoints are n=5 view fields for n=3 lines (C9-healthy comparison) and n=1 line (C9-isogenic comparison), n=2-3 differentiations each). Scale bars: 25 µm. **B)** Multi-electrode array analysis of healthy MNs in co-culture with 'M1' C9, healthy and isogenic MG shows no differences in the mean firing rate (datapoints are n=3 wells per differentiation for n=3 lines (C9-healthy comparison) and n=1 line (C9-isogenic comparison), n=2 differentiations each). **C)** Left: exemplar images of TUJ1-positive neurites in co-culture with 'M1' IBA1-positive healthy, isogenic, and C9 MG. Right: Quantification of neurite density shows no difference between co-cultures with C9 and control MG (datapoints are n=5 view fields for n=3 lines (C9-healthy comparison) and n=1 line (C9-isogenic comparison), n=2-3 differentiations). Scale bars: 25 µm. Single data points and means ± SEM. Two-tailed unpaired t-test (**A, C**), two-way ANOVA with Tukey's post-hoc test (**B**).

5.3.4 LPS-primed co-cultures have a dysregulated cytokine profile and upregulate DPP4 release in an MMP9-dependent manner

Finally, I evaluated the cytokine profile in stimulated co-cultures, again using a membrane-based array. Several cytokines and chemokines showed a different relative expression in co-cultures with C9ORF72 microglia compared with healthy

controls, with upregulation of IL6, MCP-3, MIP-1α/β, MIP-3α and DPP4, and downregulation of BAFF, IL18 Bpa, and TFF3, amongst others (Figure 5.8A). Intriguingly, concomitant administration of the MMP9 inhibitor decreased the release of several cyto-/chemokines, notably MCP-3, MIP-1α/β, MIP-3α, DPP4, and Endoglin. Importantly, MMP9 inhibition reduced the relative expression of Endoglin and DPP4 only in co-cultures with C9ORF72 but not control microglia (Figure 5.8A), suggesting a specific effect on C9ORF72 microglia. ELISA confirmed significant up-regulation of DPP4 in co-culture with C9ORF72 microglia compared with healthy and isogenic controls by ELISA, with MMP9 inhibition significantly reducing DPP4 release into the supernatant (Figure 5.8B). DPP4 release into the culture supernatant therefore directly reflects MMP9 activity.

In summary, these data suggest LPS-primed co-cultures have a dysregulated cytokine profile and increase DPP4 release in an MMP9-dependent manner.

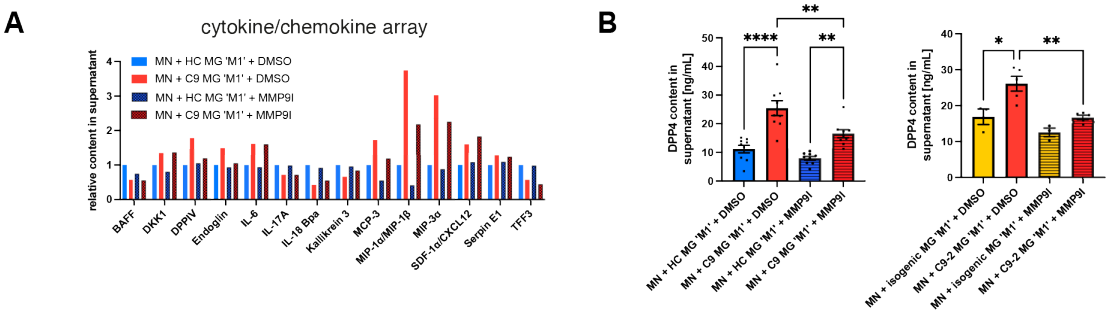


Figure 5.8: LPS-primed co-cultures of C9ORF72 microglia and healthy motor neurons have a dysregulated cytokine profile and upregulate DPP4 release in an MMP9-dependent manner. A) Relative fold change in co-culture supernatant content for selected targets using the Proteome Profiler Human XL Cytokine Array Kit. Supernatant samples from healthy MNs co-cultured with 'M1' C9, healthy, and isogenic MG plus DMSO as vehicle control or MMP9I (3 μM) show a dysregulated cytokine profile (pooled samples from n=3 lines (C9-healthy comparison) and n=1 line (C9-isogenic comparison), n=1-3 differentiations each). **B)** ELISA quantification of DPP4 content in co-culture supernatants shows significantly increased DPP4 levels in co-cultures with C9 MG, which is significantly reduced after MMP9I treatment (n=3 lines for C9-healthy comparison and n=1 line for C9-isogenic comparison, n=1-3 differentiations each). Single data points and means ± SEM. One-way ANOVA with Tukey's post-hoc test (**B**). The ELISAs in **B** were performed by Benazir Amein, a research assistant in the lab.

5.4 Discussion and conclusions

Having characterised a pro-inflammatory phenotype of C9ORF72 microglia in monoculture experiments in chapter 4, I investigated in this chapter whether C9ORF72 microglia elicited non-cell-autonomous effects on spinal MNs in co-culture. For this, I employed the co-culture paradigm of spinal MNs and microglia established and characterised in chapter 3 of this thesis. I found that unstimulated C9ORF72 microglia have a dysregulated supernatant profile in co-culture but do not affect the activity, neurite density, or survival of healthy spinal MNs. However, after LPS priming, C9ORF72 microglia induced apoptosis of WT spinal MNs in co-culture. Concomitant application of an MMP9 inhibitor ameliorated the neurotoxic properties of C9ORF72 microglia. In addition, C9ORF72 microglia upregulated DPP4 release in co-culture, which decreased after MMP9 inhibitor treatment.

To exclude confounding effects of the simultaneous presence of the HRE in *C9ORF72* in MNs and to focus on primary non-cell-autonomous toxic effects of C9ORF72 microglia, I limited my analyses to co-cultures with WT MNs. A comprehensive analysis of neuron numbers, neuronal expression of apoptotic markers, neurite density or neuronal activity showed no evidence for overt non-cell-autonomous toxicity in unstimulated co-cultures. However, upon repetitive priming of co-cultures with LPS, C9ORF72 microglia non-cell-autonomously induced apoptosis in MNs, uncovering direct neurotoxic effects of C9ORF72 microglia. These findings suggest that C9ORF72 microglia are latently neurotoxic but require a pro-inflammatory environment to unfold their damaging properties. It is

possible that C9ORF72 astrocytes, which show multiple facets of dysfunction (Vahsen et al., 2021), or other immune cells provide these pro-inflammatory factors and skew microglia towards toxicity. Triple-culture experiments with iPSC MNs, microglia, and astrocytes or other cell types would be a means to address this outstanding question. On the other hand, a limitation of this study is the comparably short co-culture interval, and it is possible that pro-longed non-stimulated co-cultures might also show non-cell-autonomous microglial toxicity without the requirement for external pro-inflammatory stimuli.

Whereas the preprint on C9ORF72 microglia by (Lorenzini et al., 2022) did not investigate non-cell-autonomous toxicity, (Banerjee et al., 2022) also analysed co-cultures of C9ORF72 ALS patient-derived iPSC MNs and microglia for neurotoxicity. In line with my results, they described, upon addition of α-amino-3-hydroxy-5-methyl-4-isoxazolepropionic acid (AMPA) for 24 h, to model excitotoxicity, a significant reduction in neuron numbers in co-cultures of C9ORF72 MNs and C9ORF72 microglia compared with co-cultures of isogenic MNs and isogenic microglia, indicating microglial toxicity. However, (Banerjee et al., 2022) did not investigate co-cultures of control MNs and C9ORF72 microglia or the combination of C9ORF72 MNs with control microglia. The direct non-cell-autonomous contribution of microglia is therefore difficult to disentangle in their experimental approach, and the toxic microglial effect they describe might be a secondary potentiation of primary neuronal dysfunction that is intrinsic to C9ORF72 neurons. The findings in this chapter are therefore, to my knowledge, the first to describe primary non-cell-autonomous toxicity C9ORF72 microglia.

The analysis of synaptic protein expression and neuron activity in co-cultures in this chapter showed no differences, which is in contrast with previous experiments showing that C9ORF72 KO microglia promote synapse loss *in vivo* and in murine co-cultures (Lall et al., 2021). It is possible that human C9ORF72 microglia behave different than murine microglia due to well-known species-differences. Alternatively, synaptic deficits might become apparent after longer co-culture or pro-longed stimulation, which should be explored in future experiments. On the other hand, this phenotype might only be present after full *C9ORF72* KO but not in authentic human C9ORF72 microglial cells, in which the reduction in C9ORF72 expression is substantially smaller and where gain-of-function products are simultaneously present.

Mechanistically, I found that MMP9 is consistently upregulated in C9ORF72 microglia-MN co-cultures and showed that the neurotoxic effect of C9ORF72 microglia is directly mediated by MMP9, as treatment with an MMP9 inhibitor ameliorated apoptotic marker expression in co-cultured MNs. MMP9 inhibition has previously resulted in beneficial effects in a mutant $SOD1^{G93A}$ model for ALS, also using the same MMP9 inhibitor used here (Kaplan et al., 2014), as well as a TDP-43 based mouse model for sporadic ALS (Spiller et al., 2019). However, reduction or inhibition of MMP9 in these studies was limited to MNs or generically affected all cells in the CNS. To my knowledge, this thesis is the first to provide evidence for MMP9 inhibition as a therapeutic strategy in a human model for C9ORF72-ALS and with a specific focus on microglia. The neuroprotective effect could

either be mediated through direct inhibition of soluble MMP9 in culture, or an indirect influence on MMP9-dependent cellular phenotypes in C9ORF72 microglia. Future studies assessing MMP9 inhibition more widely, in iPSC models and animal models, and using different strategies for MMP9 inhibition, for instance, different inhibitors or viral gene modulation, will be needed to further assess if MMP9 inhibition can be performed more widely in ALS models.

Finally, I also investigated the release of potential biomarkers from C9ORF72 microglia. One key candidate which requires further investigation is MMP9 itself, previously shown to be increased in the serum of ALS patients in an early biomarker study (Beuche et al., 2000). MMP9 was also elevated in the spinal cord and skin of mutant $SOD1^{G93A}$ transgenic mice (Fang et al., 2010). Future studies should therefore analyse MMP9 expression in different biofluids from C9ORF72 patients. In addition, I identified DPP4 release from C9ORF72 microglia as an early event in co-culture with MNs. DPP4 is a peptidase that has previously been implicated in neurodegeneration in AD (Angelopoulou and Piperi, 2018), with DPP4 inhibition having shown beneficial outcomes (Valverde et al., 2021), but it has not yet been connected with ALS. Importantly, DPP4 levels decreased in response to MMP9 inhibitor treatment, indicating its potential to serve as a novel biomarker for microglial dysfunction. DPP4 shedding by MMP9 has previously been demonstrated in adipocytes (Rohrborn et al., 2014) and could represent the underlying mechanism. Hence, DPP4 levels should also be analysed in the biofluids of C9ORF72-ALS patients. While I have shown that DPP4 is connected with MMP9, it currently remains unclear if DPP4 contributes to the neurotoxic

effects of C9ORF72 microglia in co-culture. DPP4 inhibitors are available and have been successfully used in a model for AD (Valverde et al., 2021). It would therefore be interesting to inhibit DPP4 expression and investigate if this also ameliorates the neurotoxic properties of C9ORF72 microglia in co-culture.

A question that currently remains unanswered is the response of C9ORF72 microglia to mutant C9ORF72 associated primary neuronal dysfunction in MNs. Experiments with MNs and microglia expressing mutant or WT C9ORF72 in different permutations will be able to answer this outstanding question but were beyond the scope of this study. As discussed above, (Banerjee et al., 2022) have provided first evidence for a toxic effect of C9ORF72 microglia in co-culture with C9ORF72 MNs in response to AMPA treatment. In future studies, it will be particularly interesting to disentangle the contribution of microglia and MNs to toxicity using different combinations of mutant and control microglia and MNs. These different permutations will help to elucidate and contrast the contribution of primary versus secondary neuronal and microglial dysfunction. Furthermore, it will be of interest to examine the effect of microglia on aggregated TDP-43 or DPRs in C9ORF72 neurons, to see if microglia can provide some neuroprotection against protein aggregates in co-culture, as suggested by an animal model for TDP-43 proteinopathy (Spiller et al., 2018), or whether neuronal aggregates will activate C9ORF72 microglia and potentiate their non-cell-autonomous toxicity.

Another key question that remains to be addressed is the contribution of C9ORF72 loss-of-function and gain-of-function toxicity to the phenotypes of

C9ORF72 microglia. This study as well as previous papers using *C9orf72* KO macrophages/microglia or the two other studies on C9ORF72 iPSC microglia (Banerjee et al., 2022; Lall et al., 2021; Lorenzini et al., 2022; McCauley et al., 2020; O'Rourke et al., 2016) agree that some phenotypes, for instance, lysosomal or autophagy dysfunction or increased pro-inflammatory cytokine expression, are connected with C9ORF72 haploinsufficiency. (Banerjee et al., 2022) also showed that the toxic effect of C9ORF72 microglia in co-culture related to haploinsufficiency-mediated autophagy dysfunction. However, the findings in this study also suggest that DPRs as gain-of-function products might contribute to the cell-autonomous and non-cell-autonomous dysfunction of C9ORF72 microglia, evidenced, for instance, by MMP9 upregulation-mediated neurotoxicity in our C9ORF72-isogenic line pair in the absence of C9ORF72 haploinsufficiency. Selective expression of DPRs in microglia in future studies will help to address this question.

Taken together, this chapter has provided further evidence for the non-cell-autonomous dysfunction of C9ORF72 microglia and has revealed neurotoxicity of C9ORF72 microglia mediated by MMP9 as a new therapeutic target to counteract neuronal apoptosis in C9ORF72-ALS. Furthermore, I have identified MMP9-dependent DPP4 release as a novel putative biomarker for microglial dysfunction in culture, paving the way for future studies that modulate their expression in preclinical models but also assess the levels of MMP9 and DPP4 in the biofluids of C9ORF72-ALS patients.

6 Discussion and conclusions

The overarching aim of my thesis was to improve the understanding of the pathophysiological role of microglia in ALS with a specific focus on ALS caused by HREs in the *C9ORF72* gene. Various models have previously been used to investigate microglia in ALS; there is broad consensus from human post mortem and neuroimaging studies, biomarker investigations, and preclinical models that microglia are activated and strongly associated with the pathophysiological cascade in ALS. Specifically, animal models for different ALS mutations suggest that microglia adopt neurotoxic properties over the ALS disease course, but rather contribute to disease progression than to disease initiation. Less is known, however, about the role of microglia in C9ORF72-ALS, even though the HRE in the *C9ORF72* gene is the commonest genetic variant associated with ALS. The *C9ORF72* HRE is thought to cause loss-of-function and gain-of-function toxicity through C9ORF72 haploinsufficiency and the production of RNA foci and DPRs, respectively. Developing an animal model that captures all of these pathomechanisms has posed a significant challenge, and therefore research into microglia in C9ORF72-ALS has focused on C9ORF72 loss-of-function. Mimicking C9ORF72 haploinsufficiency through *C9orf72* KO in mice resulted in a pro-inflammatory state in macrophages and microglia, but whether this phenotype is replicated in human microglial cells has been an open question, firstly, due to species-specific differences between rodent and human microglia and secondly, due to the lack of modelling gain-of-function toxicity. Furthermore, whether C9ORF72-ALS microglia elicit non-cell-autonomous toxicity on MNs has been unclear. Therefore, in this thesis, I aimed to improve the understanding of the role

of C9ORF72 microglia by using iPSC technology, allowing the generation of microglia from C9ORF72-ALS patients that retain their genetic background. First, I established differentiations of iPSC microglia and then combined them with iPSC spinal MNs in a novel co-culture system, allowing me to harness it for phenotyping experiments with patient-derived cells. Second, I analysed iPSC microglia generated from C9ORF72-ALS patients in monoculture and determined that the presence of the *C9ORF72* HRE resulted in a pro-inflammatory and dysfunctional microglial phenotype. Third, I co-cultured C9ORF72 microglia with MNs using the model established in this thesis and uncovered non-cell-autonomous toxicity of C9ORF72 microglia. Fourth, I discovered that increased expression and release of MMP9 from C9ORF72 microglia is one of the molecular determinants of microglial neurotoxicity. Finally, I outlined MMP9-depedent microglial DPP4 release as a novel putative biomarker for microglial dysfunction in culture.

6.1 The contribution of microglia to C9ORF72-ALS pathophysiology

The data obtained in this thesis show that the *C9ORF72* HRE leads to a pro-inflammatory microglial phenotype resulting in toxic effects on MNs in co-culture after LPS priming. This suggests that C9ORF72 microglia play an active role in MN degeneration in C9ORF72-ALS. The findings from my thesis show substantial overlap with two pre-prints prepared independently and in parallel to our investigations (Banerjee et al., 2022; Lorenzini et al., 2022). Our combined results suggest that C9ORF72-ALS microglia are intrinsically dysregulated through the presence of the *C9ORF72* HRE but that additional external stimuli are required

for them to fully unfold their pro-inflammatory phenotype. This is particularly relevant for the non-cell-autonomous toxicity of C9ORF72 microglia, which only became apparent after LPS stimulation in my investigations and, similarly, only in response to excitotoxic AMPA treatment in the study by (Banerjee et al., 2022). Of note, this observation does not exclude that cellular ageing, as it naturally occurs over many years in ALS patients before the disease becomes clinically apparent in later life, might be sufficient for C9ORF72 microglia to become overtly neurotoxic. More prolonged cultures could help to decipher if C9ORF72 microglia become overtly neurotoxic over time, but it is possible that the differentiated iPSC-derived cell types are generally too immature to capture such a phenotype. A means to overcome this potential obstacle might be the application of a cocktail of chemicals to enhance cellular senescence as recently described by (Hergenreder et al., 2022).

An important open question that remains unanswered at present is the relative contribution of MNs and microglia to MN cell death. I focused in this thesis on the non-cell-autonomous effects of microglia on MNs, by only co-culturing disease and healthy microglia with healthy MNs. Future work will therefore necessitate the culture of both healthy and mutant microglia and healthy and mutant MNs in all four permutations. This approach will help elucidate whether primary MN damage activates microglia in C9ORF72-ALS, if mutant microglia exacerbate C9ORF72 MN death, and whether healthy microglia can ameliorate the dysfunction of C9ORF72 MNs. These experiments will be crucial in order to ultimately determine whether C9ORF72 microglia represent a therapeutic target in ALS.

More widely, it will be important to study iPSC-derived microglia from other genes with common variants associated with ALS, such as *TARDBP* or *SOD1*, but also sporadic patients in order to determine if microglial activation can be targeted in ALS. Interestingly, iPSC-derived microglia carrying the ALS-linked FUS^{525L} mutation also demonstrated dysregulated cytokine signalling by RNA sequencing but did not display functional defects in phagocytosis or cytokine release using a very limited cytokine panel (Kerk et al., 2022). A phenotype that is consistently replicated across different mutations, model systems, and laboratories could then form the basis for more targeted drug screening approaches.

6.2 MMP9 as a therapeutic target in C9ORF72-ALS

Of particular importance is the finding that MMP9 is one of the molecular determinants of C9ORF72 microglial toxicity, which is successfully ameliorated through application of a selective MMP9 inhibitor. MMP9 downregulation or inhibition has previously been beneficial in the mutant $SOD1^{G93A}$ model for ALS, using the same MMP9 inhibitor I used here (Kaplan et al., 2014), and a TDP-43 based mouse model for sporadic ALS (Spiller et al., 2019). On the other hand, ubiquitous *MMP9* KO had a mild but deleterious effect on survival in mutant $SOD1^{G93A}$ mice in a different study (Dewil et al., 2005). However, these publications were focused on the role of MMP9 in MNs or ubiquitously in the CNS, and, to my knowledge, this thesis provides the first evidence for a toxic role of microglial MMP9 in an ALS model and, specifically, in C9ORF72-ALS. Future work will be required to determine if targeting MMP9 might be of wider interest as a therapeutic strategy for ALS by replicating these data with different MMP9-inhibiting

drugs and in a broader range of models for C9ORF72-ALS. However, metalloproteinases are of great physiological importance and not easily therapeutically targeted *in vivo* (Vandenbroucke and Libert, 2014); a thorough investigation of potential side effects of MMP9-modulating therapy will therefore be of crucial importance, particularly considering the absence of beneficial effects in the study by (Dewil et al., 2005), which postulated that the absence of MMP9 in neurons might offset the protective effects of deleting MMP9 from microglia. Associated with this, the MMP9-associated increase in DPP4 requires further experimental investigation. DPP4 is a peptidase that has previously been implicated in neurodegeneration in AD (Angelopoulou and Piperi, 2018) with DPP4 inhibition having shown beneficial outcomes (Valverde et al., 2021). It remains to be determined if DPP4 release is merely a bystander effect of increased microglial MMP9 expression or whether it contributes to the neurotoxic effects of C9ORF72 microglia. Various DPP4 inhibitors are available and, importantly, already in clinical use for patients with type 2 diabetes mellitus (Rohrborn et al., 2015). Future work should therefore include the investigation of whether the application of DPP4 inhibitors can also ameliorate the neurotoxic properties of C9ORF72 microglia in co-culture to assess if DPP4 is mechanistically involved in non-cell-autonomous toxicity.

6.3 Microglial release of MMP9 and DPP4 as biomarker candidates for C9ORF72-ALS

Another key finding of this thesis is the consistently increased release of MMP9 into the supernatant of microglial monocultures. MMP9 has been suggested as a biomarker candidate in a variety of neurological and non-neurological diseases,

for instance, haemorrhagic stroke, PD, and different types of cancer (Huang, 2018; Liu et al., 2022; Lu et al., 2021). Furthermore, MMP9 has previously also been connected to ALS, with increased levels in the serum of ALS patients (Beuche et al., 2000) and in the spinal cord and skin of mutant $SOD1^{G93A}$ transgenic mice (Fang et al., 2010). However, to my knowledge, MMP9 has not yet been analysed in the biofluids of ALS patients with different genetic forms, particularly C9ORF72-ALS. It should be noted, though, that MMP9 levels did not substantially increase in the supernatants of co-cultures with MNs, even in stimulated cultures in which C9ORF72 microglia caused neurotoxicity. It is therefore possible that increased MMP9 expression only translates into an elevated release into the supernatant in microglial monocultures, while it is either not released or more rapidly degraded in co-culture. Nonetheless, a comprehensive investigation of MMP9 levels in the serum, CSF, and other biofluids of ALS patients is warranted, and it should be a priority of future experiments to assess the potential of MMP9 as a biomarker candidate for C9ORF72-ALS.

In addition, DPP4 release from C9ORF72 microglia as an early event in co-culture with MNs raises interest in its potential as a biomarker. DPP4 has been suggested as an inflammatory biomarker for several diseases, for instance, different forms of cancer (Enz et al., 2019), but it has not yet been connected with ALS. Importantly, DPP4 levels were already elevated in non-stimulated co-cultures prior to overt neurotoxicity and then decreased in response to MMP9 inhibitor treatment, indicating its potential to serve as a novel biomarker for microglial

dysfunction. The analysis of DPP4 levels in the biofluids of ALS patients should therefore be another priority of future experiments.

If MMP9 and DPP4 levels are indeed raised in biofluids of ALS patients, the comparison and integration with other promising biomarker candidates for non-neuronal cells, notably CHIT1 and CHI3L1, will be of interest. This could include the analysis of MMP9 and DPP4 pre- and post-symptom onset, to better understand their contribution to disease pathogenesis in patients, although these assessments will be complicated by the fact that other cellular sources in addition to microglia would be likely to contribute to biomarker release *in vivo*.

6.4 *C9ORF72* HRE loss-of-function versus gain-of-function effects on microglia

The combined findings from my investigations and the preprints by (Banerjee et al., 2022; Lorenzini et al., 2022) demonstrate that C9ORF72 loss-of-function and gain-of-function toxicity are present in C9ORF72 microglia, as C9ORF72 haploinsufficiency, DPRs, and RNA foci were detected across the different studies. The data in this thesis suggest that several pro-inflammatory phenotypes, notably, the increased activity of NFκB and elevated expression of pro-inflammatory cytokines such as IL1B, are driven by C9ORF72 haploinsufficiency, which is well aligned with the findings from murine *C9orf72* KO microglia (Lall et al., 2021; O'Rourke et al., 2016) and human iPSC *C9ORF72* KO microglia (Banerjee et al., 2022). I have provided preliminary evidence for the presence of microglial phenotypes in the absence of C9ORF72 haploinsufficiency in this thesis, which could

be due to the presence of gain-of-function products such as DPRs. Future experiments will require the selective expression of DPRs and/or RNA foci in iPSC microglia to determine the relative contribution of gain-of-function products to C9ORF72 microglial dysfunction.

6.5 The utility of human iPSC microglia for modelling ALS

The combined findings from this thesis and previous studies on iPSC microglia show that they are a viable model to study human microglia through the presence of a transcriptome that closely resembles *bona fide* human microglia, the expression of microglial markers, and proper microglial functionality such as phagocytic capacity. Although iPSC microglial cultures are labour-intensive, expensive and require lengthy differentiation protocols, they allow for the investigation of otherwise largely inaccessible cells with an accurate human disease genetic background, which represents a substantial advantage over rodent models. As shown in this thesis, microglial monocultures are of great use for the study of cell-autonomous phenotypes by RNA sequencing, secretome analysis, and functional experiments. Yet, microglia are particularly dependent on crosstalk with other cells and exposure to neurons, which, as shown previously and in this thesis, supports a homeostatic and physiological state. The iPSC field is currently moving towards establishing more complex multicellular models, and this thesis has contributed to this by establishing a novel co-culture of iPSC microglia and spinal MNs. It can be expected that future research endeavours will further optimise multi-cellular systems to stepwise provide even more physiological models. This will, however, require significant amendments and improvements. The addition of more cell

types, for instance, other glial cell types such as astrocytes and oligodendrocytes will be required as well as the combination with other neuronal cell types. Regarding an improved understanding of ALS, neuronal populations that would be of interest for co-culture experiments are other affected cell types, such as Betz cells, for which proper differentiation protocols still need to be developed, or relatively spared cell types, such as sensory neurons. While iPSC-derived neuronal subtype differentiation and specification is now comparably easily achieved through well-defined patterning steps, the field is only beginning to achieve a more defined identity for iPSC glial cells. The definition and comparison of different populations of microglial cells, e.g., cortical versus spinal iPSC microglia, or subpopulations of disease microglia, achievable through single cell approaches, would be an important step forward. Furthermore, human-rodent chimaera experiments where iPSC microglia are transplanted into rodents might be of complementary use, as they will permit assessing the contribution of iPSC microglia to disease pathophysiology in an *in vivo* setup. Finally, it will be important to synchronise efforts and join forces for multiple different laboratories to cross validate experimental data from iPSC models. iPSC research particularly suffers from intra- and inter-lab variability, and it seems likely that one lab in isolation will not be able to resolve these issues, while multi-centre and multinational efforts will have a better chance of success.

6.6 Closing remarks

ALS is a heterogeneous disease with a complex pathophysiology, but the combination of biomarker and imaging investigations in patients, post mortem studies,

animal models, and stem cell research is starting to shed light on the underlying mechanism. Rather than focusing solely on the dysfunction of neurons, a broader approach that also factors in the contribution of non-neuronal cells, notably microglia, will be key to an improved understanding of the disease for drug screening, and ultimately the development of much-needed treatment options.

7 Bibliography

Ababneh, N.A., Scaber, J., Flynn, R., Douglas, A., Barbagallo, P., Candalija, A., Turner, M.R., Sims, D., Dafinca, R., Cowley, S.A.*, et al.* (2020). Correction of amyotrophic lateral sclerosis related phenotypes in induced pluripotent stem cell-derived motor neurons carrying a hexanucleotide expansion mutation in C9orf72 by CRISPR/Cas9 genome editing using homology-directed repair. Hum Mol Genet *29*, 2200-2217.

Abud, E.M., Ramirez, R.N., Martinez, E.S., Healy, L.M., Nguyen, C.H.H., Newman, S.A., Yeromin, A.V., Scarfone, V.M., Marsh, S.E., Fimbres, C.*, et al.* (2017). iPSC-Derived Human Microglia-like Cells to Study Neurological Diseases. Neuron *94*, 278-293 e279.

Al-Chalabi, A., Calvo, A., Chio, A., Colville, S., Ellis, C.M., Hardiman, O., Heverin, M., Howard, R.S., Huisman, M.H.B., Keren, N.*, et al.* (2014). Analysis of amyotrophic lateral sclerosis as a multistep process: a population-based modelling study. The Lancet Neurology *13*, 1108-1113.

Al-Chalabi, A., van den Berg, L.H., and Veldink, J. (2017). Gene discovery in amyotrophic lateral sclerosis: implications for clinical management. Nat Rev Neurol *13*, 96-104.

Alexianu, M.E., Kozovska, M., and Appel, S.H. (2001). Immune reactivity in a mouse model of familial ALS correlates with disease progression. Neurology *57*, 1282-1289.

Alliot, F., Godin, I., and Pessac, B. (1999). Microglia derive from progenitors, originating from the yolk sac, and which proliferate in the brain. Developmental Brain Research *117*, 145-152.

Almeida, S., Krishnan, G., Rushe, M., Gu, Y., Kankel, M.W., and Gao, F.B. (2019). Production of poly(GA) in C9ORF72 patient motor neurons derived from induced pluripotent stem cells. Acta Neuropathol *138*, 1099-1101.

Alonso, A., Logroscino, G., and Hernan, M.A. (2010). Smoking and the risk of amyotrophic lateral sclerosis: a systematic review and meta-analysis. J Neurol Neurosurg Psychiatry *81*, 1249-1252.

Amoroso, M.W., Croft, G.F., Williams, D.J., O'Keeffe, S., Carrasco, M.A., Davis, A.R., Roybon, L., Oakley, D.H., Maniatis, T., Henderson, C.E.*, et al.* (2013). Accelerated high-yield generation of limb-innervating motor neurons from human stem cells. J Neurosci *33*, 574-586.

Andres-Benito, P., Dominguez, R., Colomina, M.J., Llorens, F., Povedano, M., and Ferrer, I. (2018). YKL40 in sporadic amyotrophic lateral sclerosis: cerebrospinal fluid levels as a prognosis marker of disease progression. Aging (Albany NY) *10*, 2367-2382.

Angelopoulou, E., and Piperi, C. (2018). DPP-4 inhibitors: a promising therapeutic approach against Alzheimer's disease. Ann Transl Med *6*, 255.

Armon, C. (2009). Smoking may be considered an established risk factor for sporadic ALS. Neurology *73*, 1693-1698.

Balendra, R., and Isaacs, A.M. (2018). C9orf72-mediated ALS and FTD: multiple pathways to disease. Nat Rev Neurol *14*, 544-558.

Banerjee, P., Mehta, A.R., Nirujogi, R.S., Cooper, J., James, O.G., Nanda, J., Longden, J., Burr, K., Salzinger, A., Paza, E.*, et al.* (2022). Cell-autonomous immune dysfunction driven by disrupted autophagy in C9orf72-ALS iPSC-derived microglia contributes to neurodegeneration. bioRxiv, 2022.2005.2012.491675.

Beck, J., Poulter, M., Hensman, D., Rohrer, J.D., Mahoney, C.J., Adamson, G., Campbell, T., Uphill, J., Borg, A., Fratta, P.*, et al.* (2013). Large C9orf72 hexanucleotide repeat expansions are seen in multiple neurodegenerative syndromes and are more frequent than expected in the UK population. Am J Hum Genet *92*, 345-353.

Beckers, J., Tharkeshwar, A.K., and Van Damme, P. (2021). C9orf72 ALS-FTD: recent evidence for dysregulation of the autophagy-lysosome pathway at multiple levels. Autophagy *17*, 3306-3322.

Beeldman, E., Raaphorst, J., Klein Twennaar, M., Govaarts, R., Pijnenburg, Y.A.L., de Haan, R.J., de Visser, M., and Schmand, B.A. (2018). The cognitive profile of behavioural variant FTD and its similarities with ALS: a systematic review and meta-analysis. J Neurol Neurosurg Psychiatry *89*, 995-1002.

Beers, D.R., and Appel, S.H. (2019). Immune dysregulation in amyotrophic lateral sclerosis: mechanisms and emerging therapies. Lancet Neurol *18*, 211-220.

Beers, D.R., Henkel, J.S., Xiao, Q., Zhao, W., Wang, J., Yen, A.A., Siklos, L., McKercher, S.R., and Appel, S.H. (2006). Wild-type microglia extend survival in PU.1 knockout mice with familial amyotrophic lateral sclerosis. Proc Natl Acad Sci U S A *103*, 16021-16026.

Bennett, M.L., Bennett, F.C., Liddelow, S.A., Ajami, B., Zamanian, J.L., Fernhoff, N.B., Mulinyawe, S.B., Bohlen, C.J., Adil, A., Tucker, A.*, et al.* (2016). New tools for studying microglia in the mouse and human CNS. Proc Natl Acad Sci U S A *113*, E1738-1746.

Beuche, W., Yushchenko, M., Mader, M., Maliszewska, M., Felgenhauer, K., and Weber, F. (2000). Matrix metalloproteinase-9 is elevated in serum of patients with amyotrophic lateral sclerosis. Neuroreport *11*, 3419-3422.

Boillee, S., Yamanaka, K., Lobsiger, C.S., Copeland, N.G., Jenkins, N.A., Kassiotis, G., Kollias, G., and Cleveland, D.W. (2006). Onset and progression in inherited ALS determined by motor neurons and microglia. Science *312*, 1389-1392.

Braems, E., Swinnen, B., and Van Den Bosch, L. (2020). C9orf72 loss-of-function: a trivial, stand-alone or additive mechanism in C9 ALS/FTD? Acta Neuropathol *140*, 625-643.

Brettschneider, J., Libon, D.J., Toledo, J.B., Xie, S.X., McCluskey, L., Elman, L., Geser, F., Lee, V.M., Grossman, M., and Trojanowski, J.Q. (2012a). Microglial activation and TDP-43 pathology correlate with executive dysfunction in amyotrophic lateral sclerosis. Acta Neuropathol *123*, 395-407.

Brettschneider, J., Toledo, J.B., Van Deerlin, V.M., Elman, L., McCluskey, L., Lee, V.M., and Trojanowski, J.Q. (2012b). Microglial activation correlates with disease progression and upper motor neuron clinical symptoms in amyotrophic lateral sclerosis. PLoS One *7*, e39216.

Bruttger, J., Karram, K., Wortge, S., Regen, T., Marini, F., Hoppmann, N., Klein, M., Blank, T., Yona, S., Wolf, Y.*, et al.* (2015). Genetic Cell Ablation Reveals Clusters of Local Self-Renewing Microglia in the Mammalian Central Nervous System. Immunity *43*, 92-106.

Buchrieser, J., James, W., and Moore, M.D. (2017). Human Induced Pluripotent Stem Cell-Derived Macrophages Share Ontogeny with MYB-Independent Tissue-Resident Macrophages. Stem Cell Reports *8*, 334-345.

Burberry, A., Suzuki, N., Wang, J.Y., Moccia, R., Mordes, D.A., Stewart, M.H., Suzuki-Uematsu, S., Ghosh, S., Singh, A., Merkle, F.T.*, et al.* (2016). Loss-of-function mutations in the C9ORF72 mouse ortholog cause fatal autoimmune disease. Sci Transl Med *8*, 347ra393.

Butovsky, O., Jedrychowski, M.P., Moore, C.S., Cialic, R., Lanser, A.J., Gabriely, G., Koeglsperger, T., Dake, B., Wu, P.M., Doykan, C.E.*, et al.* (2014). Identification of a unique TGF-beta-dependent molecular and functional signature in microglia. Nat Neurosci *17*, 131-143.

Butovsky, O., and Weiner, H.L. (2018). Microglial signatures and their role in health and disease. Nat Rev Neurosci *19*, 622-635.

Cedarbaum, J.M., Stambler, N., Malta, E., Fuller, C., Hilt, D., Thurmond, B., Nakanishi, A., and Grp, B.A.S. (1999). The ALSFRS-R: a revised ALS functional rating scale that incorporates assessments of respiratory function. Journal of the Neurological Sciences *169*, 13-21.

Chambers, S.M., Fasano, C.A., Papapetrou, E.P., Tomishima, M., Sadelain, M., and Studer, L. (2009). Highly efficient neural conversion of human ES and iPS cells by dual inhibition of SMAD signaling. Nat Biotechnol *27*, 275-280.

Cheng, J., Dong, Y., Ma, J., Pan, R., Liao, Y., Kong, X., Li, X., Li, S., Chen, P., Wang, L.*, et al.* (2021). Microglial Calhm2 regulates neuroinflammation and contributes to Alzheimer's disease pathology. Sci Adv *7*, eabe3600.

Cherry, J.D., Olschowka, J.A., and O'Banion, M.K. (2014). Neuroinflammation and M2 microglia: the good, the bad, and the inflamed. J Neuroinflammation *11*, 98.

Chio, A., Calvo, A., Moglia, C., Mazzini, L., Mora, G., and group, P.s. (2011). Phenotypic heterogeneity of amyotrophic lateral sclerosis: a population based study. J Neurol Neurosurg Psychiatry *82*, 740-746.

Chio, A., Logroscino, G., Traynor, B.J., Collins, J., Simeone, J.C., Goldstein, L.A., and White, L.A. (2013). Global epidemiology of amyotrophic lateral sclerosis: a systematic review of the published literature. Neuroepidemiology *41*, 118-130.

Chio, A., Mazzini, L., D'Alfonso, S., Corrado, L., Canosa, A., Moglia, C., Manera, U., Bersano, E., Brunetti, M., Barberis, M.*, et al.* (2018). The multistep hypothesis of ALS revisited: The role of genetic mutations. Neurology *91*, e635-e642.

Chiu, I.M., Morimoto, E.T., Goodarzi, H., Liao, J.T., O'Keeffe, S., Phatnani, H.P., Muratet, M., Carroll, M.C., Levy, S., Tavazoie, S.*, et al.* (2013). A neurodegeneration-specific gene-expression signature of acutely isolated microglia from an amyotrophic lateral sclerosis mouse model. Cell Rep *4*, 385-401.

Choi, S.Y., Lopez-Gonzalez, R., Krishnan, G., Phillips, H.L., Li, A.N., Seeley, W.W., Yao, W.D., Almeida, S., and Gao, F.B. (2019a). C9ORF72-ALS/FTD-associated poly(GR) binds Atp5a1 and compromises mitochondrial function in vivo. Nat Neurosci *22*, 851-862.

Choi, W., Clemente, N., Sun, W., Du, J., and Lu, W. (2019b). The structures and gating mechanism of human calcium homeostasis modulator 2. Nature *576*, 163-167.

Christian, F., Smith, E.L., and Carmody, R.J. (2016). The Regulation of NF-kappaB Subunits by Phosphorylation. Cells *5*.

Clarke, B.E., and Patani, R. (2020). The microglial component of amyotrophic lateral sclerosis. Brain *143*, 3526-3539.

Colonna, M., and Butovsky, O. (2017). Microglia Function in the Central Nervous System During Health and Neurodegeneration. Annu Rev Immunol *35*, 441-468.

Corcia, P., Tauber, C., Vercoullie, J., Arlicot, N., Prunier, C., Praline, J., Nicolas, G., Venel, Y., Hommet, C., Baulieu, J.L.*, et al.* (2012). Molecular imaging of microglial activation in amyotrophic lateral sclerosis. PLoS One *7*, e52941.

Dafinca, R., Barbagallo, P., Farrimond, L., Candalija, A., Scaber, J., Ababneh, N.A., Sathyaprakash, C., Vowles, J., Cowley, S.A., and Talbot, K. (2020). Impairment of Mitochondrial Calcium Buffering Links Mutations in C9ORF72 and TARDBP in iPS-Derived Motor Neurons from Patients with ALS/FTD. Stem Cell Reports *14*, 892-908.

Dafinca, R., Scaber, J., Ababneh, N., Lalic, T., Weir, G., Christian, H., Vowles, J., Douglas, A.G., Fletcher-Jones, A., Browne, C.*, et al.* (2016). C9orf72 Hexanucleotide Expansions Are Associated with Altered Endoplasmic Reticulum Calcium Homeostasis and Stress Granule Formation in Induced Pluripotent Stem Cell-Derived Neurons from Patients with Amyotrophic Lateral Sclerosis and Frontotemporal Dementia. Stem Cells *34*, 2063-2078.

DeJesus-Hernandez, M., Mackenzie, I.R., Boeve, B.F., Boxer, A.L., Baker, M., Rutherford, N.J., Nicholson, A.M., Finch, N.A., Flynn, H., Adamson, J.*, et al.* (2011). Expanded GGGGCC hexanucleotide repeat in noncoding region of C9ORF72 causes chromosome 9p-linked FTD and ALS. Neuron *72*, 245-256.

Deora, V., Lee, J.D., Albornoz, E.A., McAlary, L., Jagaraj, C.J., Robertson, A.A.B., Atkin, J.D., Cooper, M.A., Schroder, K., Yerbury, J.J.*, et al.* (2020). The microglial NLRP3 inflammasome is activated by amyotrophic lateral sclerosis proteins. Glia *68*, 407-421.

Dewil, M., Schurmans, C., Starckx, S., Opdenakker, G., Van Den Bosch, L., and Robberecht, W. (2005). Role of matrix metalloproteinase-9 in a mouse model for amyotrophic lateral sclerosis. Neuroreport *16*, 321-324.

Dimos, J.T., Rodolfa, K.T., Niakan, K.K., Weisenthal, L.M., Mitsumoto, H., Chung, W., Croft, G.F., Saphier, G., Leibel, R., Goland, R.*, et al.* (2008). Induced pluripotent stem cells generated from patients with ALS can be differentiated into motor neurons. Science *321*, 1218-1221.

Donnelly, C.J., Zhang, P.-W., Pham, J.T., Haeusler, A.R., Heusler, A.R., Mistry, N.A., Vidensky, S., Daley, E.L., Poth, E.M., Hoover, B.*, et al.* (2013). RNA toxicity from the ALS/FTD C9ORF72 expansion is mitigated by antisense intervention. In Neuron, pp. 415-428.

Douvaras, P., Sun, B., Wang, M., Kruglikov, I., Lallos, G., Zimmer, M., Terrenoire, C., Zhang, B., Gandy, S., Schadt, E.*, et al.* (2017). Directed Differentiation of Human Pluripotent Stem Cells to Microglia. Stem Cell Reports *8*, 1516-1524.

Elamin, M., Bede, P., Byrne, S., Jordan, N., Gallagher, L., Wynne, B., O'Brien, C., Phukan, J., Lynch, C., Pender, N.*, et al.* (2013). Cognitive changes predict functional decline in ALS: a population-based longitudinal study. Neurology *80*, 1590-1597.

Enz, N., Vliegen, G., De Meester, I., and Jungraithmayr, W. (2019). CD26/DPP4 - a potential biomarker and target for cancer therapy. Pharmacol Ther *198*, 135-159.

Ewels, P., Magnusson, M., Lundin, S., and Kaller, M. (2016). MultiQC: summarize analysis results for multiple tools and samples in a single report. Bioinformatics *32*, 3047-3048.

Fang, L., Teuchert, M., Huber-Abel, F., Schattauer, D., Hendrich, C., Dorst, J., Zettlmeissel, H., Wlaschek, M., Scharffetter-Kochanek, K., Kapfer, T.*, et al.* (2010). MMP-2 and MMP-9 are elevated in spinal cord and skin in a mouse model of ALS. J Neurol Sci *294*, 51-56.

Feldman, E.L., Goutman, S.A., Petri, S., Mazzini, L., Savelieff, M.G., Shaw, P.J., and Sobue, G. (2022). Amyotrophic lateral sclerosis. Lancet *400*, 1363-1380.

Finger, S. (2005). Jean-Martin Charcot: Clinical Neurology Comes of Age. In Minds Behind the Brain (Oxford University Press), pp. 177-196.

Franklin, H., Clarke, B.E., and Patani, R. (2021). Astrocytes and microglia in neurodegenerative diseases: Lessons from human in vitro models. Prog Neurobiol *200*, 101973.

Frick, P., Sellier, C., Mackenzie, I.R.A., Cheng, C.Y., Tahraoui-Bories, J., Martinat, C., Pasterkamp, R.J., Prudlo, J., Edbauer, D., Oulad-Abdelghani, M.*, et al.* (2018). Novel antibodies reveal presynaptic localization of C9orf72 protein and reduced protein levels in C9orf72 mutation carriers. Acta Neuropathol Commun *6*, 72.

Galatro, T.F., Holtman, I.R., Lerario, A.M., Vainchtein, I.D., Brouwer, N., Sola, P.R., Veras, M.M., Pereira, T.F., Leite, R.E.P., Moller, T.*, et al.* (2017). Transcriptomic analysis of purified human cortical microglia reveals age-associated changes. Nat Neurosci *20*, 1162-1171.

Gaur, N., Perner, C., Witte, O.W., and Grosskreutz, J. (2020). The Chitinases as Biomarkers for Amyotrophic Lateral Sclerosis: Signals From the CNS and Beyond. Front Neurol *11*, 377.

Gendron, T.F., Chew, J., Stankowski, J.N., Hayes, L.R., Zhang, Y.J., Prudencio, M., Carlomagno, Y., Daughrity, L.M., Jansen-West, K., Perkerson, E.A.*, et al.* (2017). Poly(GP) proteins are a useful pharmacodynamic marker for C9ORF72-associated amyotrophic lateral sclerosis. Sci Transl Med *9*.

Giacomelli, E., Vahsen, B.F., Calder, E.L., Xu, Y., Scaber, J., Gray, E., Dafinca, R., Talbot, K., and Studer, L. (2022). Human stem cell models of neurodegeneration: From basic science of amyotrophic lateral sclerosis to clinical translation. Cell Stem Cell *29*, 11-35.

Gille, B., De Schaepdryver, M., Dedeene, L., Goossens, J., Claeys, K.G., Van Den Bosch, L., Tournoy, J., Van Damme, P., and Poesen, K. (2019). Inflammatory markers in cerebrospinal fluid: independent prognostic biomarkers in amyotrophic lateral sclerosis? J Neurol Neurosurg Psychiatry *90*, 1338-1346.

Ginhoux, F., Greter, M., Leboeuf, M., Nandi, S., See, P., Gokhan, S., Mehler, M.F., Conway, S.J., Ng, L.G., Stanley, E.R.*, et al.* (2010). Fate mapping analysis reveals that adult microglia derive from primitive macrophages. Science *330*, 841-845.

Ginhoux, F., and Prinz, M. (2015). Origin of microglia: current concepts and past controversies. Cold Spring Harb Perspect Biol *7*, a020537.

Gowing, G., Dequen, F., Soucy, G., and Julien, J.P. (2006). Absence of tumor necrosis factor-alpha does not affect motor neuron disease caused by superoxide dismutase 1 mutations. J Neurosci *26*, 11397-11402.

Gray, E., Thompson, A.G., Wuu, J., Pelt, J., Talbot, K., Benatar, M., and Turner, M.R. (2020). CSF chitinases before and after symptom onset in amyotrophic lateral sclerosis. Ann Clin Transl Neurol *7*, 1296-1306.

Guerreiro, R., Wojtas, A., Bras, J., Carrasquillo, M., Rogaeva, E., Majounie, E., Cruchaga, C., Sassi, C., Kauwe, J.S., Younkin, S.*, et al.* (2013). TREM2 variants in Alzheimer's disease. N Engl J Med *368*, 117-127.

Guo, W., Fumagalli, L., Prior, R., and Van Den Bosch, L. (2017). Current Advances and Limitations in Modeling ALS/FTD in a Dish Using Induced Pluripotent Stem Cells. Front Neurosci *11*, 671.

Gurney, M.E., Pu, H., Chiu, A.Y., Dal Canto, M.C., Polchow, C.Y., Alexander, D.D., Caliendo, J., Hentati, A., Kwon, Y.W., Deng, H.X.*, et al.* (1994). Motor neuron degeneration in mice that express a human Cu,Zn superoxide dismutase mutation. Science *264*, 1772-1775.

Haenseler, W., Sansom, S.N., Buchrieser, J., Newey, S.E., Moore, C.S., Nicholls, F.J., Chintawar, S., Schnell, C., Antel, J.P., Allen, N.D.*, et al.* (2017). A Highly Efficient Human Pluripotent Stem Cell Microglia Model Displays a Neuronal-Co-culture-Specific Expression Profile and Inflammatory Response. Stem Cell Reports *8*, 1727-1742.

Hall, E.D., Oostveen, J.A., and Gurney, M.E. (1998). Relationship of microglial and astrocytic activation to disease onset and progression in a transgenic model of familial ALS. Glia *23*, 249-256.

Hardiman, O., Al-Chalabi, A., Chio, A., Corr, E.M., Logroscino, G., Robberecht, W., Shaw, P.J., Simmons, Z., and van den Berg, L.H. (2017). Amyotrophic lateral sclerosis. Nat Rev Dis Primers *3*, 17071.

Harms, M.B., Cady, J., Zaidman, C., Cooper, P., Bali, T., Allred, P., Cruchaga, C., Baughn, M., Libby, R.T., Pestronk, A.*, et al.* (2013). Lack of C9ORF72 coding mutations supports a gain of function for repeat expansions in amyotrophic lateral sclerosis. Neurobiol Aging *34*, 2234 e2213-2239.

Henkel, J.S., Engelhardt, J.I., Siklos, L., Simpson, E.P., Kim, S.H., Pan, T., Goodman, J.C., Siddique, T., Beers, D.R., and Appel, S.H. (2004). Presence of dendritic cells, MCP-1, and activated microglia/macrophages in amyotrophic lateral sclerosis spinal cord tissue. Ann Neurol *55*, 221-235.

Hergenreder, E., Zorina, Y., Zhao, Z., Munguba, H., Calder, E.L., Baggiolini, A., Minotti, A.P., Walsh, R.M., Liston, C., Levitz, J.*, et al.* (2022). Combined small molecule treatment accelerates timing of maturation in human pluripotent stem cell-derived neurons. bioRxiv, 2022.2006.2002.494616.

Hickman, S., Izzy, S., Sen, P., Morsett, L., and El Khoury, J. (2018). Microglia in neurodegeneration. Nat Neurosci *21*, 1359-1369.

Hu, B.Y., and Zhang, S.C. (2009). Differentiation of spinal motor neurons from pluripotent human stem cells. Nat Protoc *4*, 1295-1304.

Hu, X., Leak, R.K., Shi, Y., Suenaga, J., Gao, Y., Zheng, P., and Chen, J. (2015). Microglial and macrophage polarization-new prospects for brain repair. Nat Rev Neurol *11*, 56-64.

Huang, H. (2018). Matrix Metalloproteinase-9 (MMP-9) as a Cancer Biomarker and MMP-9 Biosensors: Recent Advances. Sensors (Basel) *18*.

Ingre, C., Roos, P.M., Piehl, F., Kamel, F., and Fang, F. (2015). Risk factors for amyotrophic lateral sclerosis. Clin Epidemiol *7*, 181-193.

Jaarsma, D., Teuling, E., Haasdijk, E.D., De Zeeuw, C.I., and Hoogenraad, C.C. (2008). Neuron-specific expression of mutant superoxide dismutase is sufficient to induce amyotrophic lateral sclerosis in transgenic mice. J Neurosci *28*, 2075-2088.

Jiang, J., Zhu, Q., Gendron, T.F., Saberi, S., McAlonis-Downes, M., Seelman, A., Stauffer, J.E., Jafar-Nejad, P., Drenner, K., Schulte, D.*, et al.* (2016). Gain of Toxicity from ALS/FTD-Linked Repeat Expansions in C9ORF72 Is Alleviated by Antisense Oligonucleotides Targeting GGGGCC-Containing RNAs. Neuron *90*, 535-550.

Jonsson, T., Stefansson, H., Steinberg, S., Jonsdottir, I., Jonsson, P.V., Snaedal, J., Bjornsson, S., Huttenlocher, J., Levey, A.I., Lah, J.J.*, et al.* (2013). Variant of TREM2 associated with the risk of Alzheimer's disease. N Engl J Med *368*, 107-116.

Kaplan, A., Spiller, K.J., Towne, C., Kanning, K.C., Choe, G.T., Geber, A., Akay, T., Aebischer, P., and Henderson, C.E. (2014). Neuronal matrix metalloproteinase-9 is a determinant of selective neurodegeneration. Neuron *81*, 333-348.

Karlsson, K.R., Cowley, S., Martinez, F.O., Shaw, M., Minger, S.L., and James, W. (2008). Homogeneous monocytes and macrophages from human embryonic stem cells following coculture-free differentiation in M-CSF and IL-3. Exp Hematol *36*, 1167-1175.

Karumbayaram, S., Novitch, B.G., Patterson, M., Umbach, J.A., Richter, L., Lindgren, A., Conway, A.E., Clark, A.T., Goldman, S.A., Plath, K.*, et al.* (2009). Directed differentiation of human-induced pluripotent stem cells generates active motor neurons. Stem Cells *27*, 806-811.

Kerk, S.Y., Bai, Y., Smith, J., Lalgudi, P., Hunt, C., Kuno, J., Nuara, J., Yang, T., Lanza, K., Chan, N.*, et al.* (2022). Homozygous ALS-linked FUS P525L mutations cell- autonomously perturb transcriptome profile and chemoreceptor signaling in human iPSC microglia. Stem Cell Reports *17*, 678-692.

Kierdorf, K., Erny, D., Goldmann, T., Sander, V., Schulz, C., Perdiguero, E.G., Wieghofer, P., Heinrich, A., Riemke, P., Holscher, C.*, et al.* (2013). Microglia emerge from erythromyeloid precursors via Pu.1- and Irf8-dependent pathways. Nat Neurosci *16*, 273-280.

Kiernan, M.C., Vucic, S., Cheah, B.C., Turner, M.R., Eisen, A., Hardiman, O., Burrell, J.R., and Zoing, M.C. (2011). Amyotrophic lateral sclerosis. Lancet *377*, 942-955.

Kiernan, M.C., Vucic, S., Talbot, K., McDermott, C.J., Hardiman, O., Shefner, J.M., Al-Chalabi, A., Huynh, W., Cudkowicz, M., Talman, P.*, et al.* (2021). Improving clinical trial outcomes in amyotrophic lateral sclerosis. Nat Rev Neurol *17*, 104-118.

Kim, D., Paggi, J.M., Park, C., Bennett, C., and Salzberg, S.L. (2019). Graph-based genome alignment and genotyping with HISAT2 and HISAT-genotype. Nat Biotechnol *37*, 907-915.

LaClair, K.D., Zhou, Q., Michaelsen, M., Wefers, B., Brill, M.S., Janjic, A., Rathkolb, B., Farny, D., Cygan, M., de Angelis, M.H.*, et al.* (2020). Congenic expression of poly-GA but not poly-PR in mice triggers selective neuron loss and interferon responses found in C9orf72 ALS. Acta Neuropathol *140*, 121-142.

Laflamme, C., McKeever, P.M., Kumar, R., Schwartz, J., Kolahdouzan, M., Chen, C.X., You, Z., Benaliouad, F., Gileadi, O., McBride, H.M.*, et al.* (2019). Implementation of an antibody characterization procedure and application to the major ALS/FTD disease gene C9ORF72. Elife *8*.

Lagier-Tourenne, C., Baughn, M., Rigo, F., Sun, S., Liu, P., Li, H.R., Jiang, J., Watt, A.T., Chun, S., Katz, M.*, et al.* (2013). Targeted degradation of sense and antisense C9orf72 RNA foci as therapy for ALS and frontotemporal degeneration. Proc Natl Acad Sci U S A *110*, E4530-4539.

Lall, D., and Baloh, R.H. (2017). Microglia and C9orf72 in neuroinflammation and ALS and frontotemporal dementia. J Clin Invest *127*, 3250-3258.

Lall, D., Lorenzini, I., Mota, T.A., Bell, S., Mahan, T.E., Ulrich, J.D., Davtyan, H., Rexach, J.E., Muhammad, A., Shelest, O.*, et al.* (2021). C9orf72 deficiency promotes microglial-mediated synaptic loss in aging and amyloid accumulation. Neuron *109*, 2275-2291 e2278.

Lamble, S., Batty, E., Attar, M., Buck, D., Bowden, R., Lunter, G., Crook, D., El-Fahmawi, B., and Piazza, P. (2013). Improved workflows for high throughput library preparation using the transposome-based Nextera system. BMC Biotechnol *13*, 104.

Leal-Lasarte, M.M., Franco, J.M., Labrador-Garrido, A., Pozo, D., and Roodveldt, C. (2017). Extracellular TDP-43 aggregates target MAPK/MAK/MRK overlapping kinase (MOK) and trigger caspase-3/IL-18 signaling in microglia. FASEB J *31*, 2797-2816.

Levine, T.P., Daniels, R.D., Gatta, A.T., Wong, L.H., and Hayes, M.J. (2013). The product of C9orf72, a gene strongly implicated in neurodegeneration, is structurally related to DENN Rab-GEFs. Bioinformatics *29*, 499-503.

Li, H., Handsaker, B., Wysoker, A., Fennell, T., Ruan, J., Homer, N., Marth, G., Abecasis, G., Durbin, R., and Genome Project Data Processing, S. (2009). The Sequence Alignment/Map format and SAMtools. Bioinformatics *25*, 2078-2079.

Li, Q., and Barres, B.A. (2018). Microglia and macrophages in brain homeostasis and disease. Nat Rev Immunol *18*, 225-242.

Li, Q., Cheng, Z., Zhou, L., Darmanis, S., Neff, N.F., Okamoto, J., Gulati, G., Bennett, M.L., Sun, L.O., Clarke, L.E.*, et al.* (2019). Developmental Heterogeneity of Microglia and Brain Myeloid Cells Revealed by Deep Single-Cell RNA Sequencing. Neuron *101*, 207-223 e210.

Li, W., Sun, W., Zhang, Y., Wei, W., Ambasudhan, R., Xia, P., Talantova, M., Lin, T., Kim, J., Wang, X.*, et al.* (2011). Rapid induction and long-term self-renewal of primitive neural precursors from human embryonic stem cells by small molecule inhibitors. Proc Natl Acad Sci U S A *108*, 8299-8304.

Liao, B., Zhao, W., Beers, D.R., Henkel, J.S., and Appel, S.H. (2012). Transformation from a neuroprotective to a neurotoxic microglial phenotype in a mouse model of ALS. Exp Neurol *237*, 147-152.

Liao, Y., Smyth, G.K., and Shi, W. (2014). featureCounts: an efficient general purpose program for assigning sequence reads to genomic features. Bioinformatics *30*, 923-930.

Lino, M.M., Schneider, C., and Caroni, P. (2002). Accumulation of SOD1 mutants in postnatal motoneurons does not cause motoneuron pathology or motoneuron disease. Journal of Neuroscience *22*, 4825-4832.

Liu, C.Z., Guo, D.S., Ma, J.J., Dong, L.R., Chang, Q.Q., Yang, H.Q., Liang, K.K., Li, X.H., Yang, D.W., Fan, Y.Y.*, et al.* (2022). Correlation of matrix metalloproteinase 3 and matrix metalloproteinase 9 levels with non-motor symptoms in patients with Parkinson's disease. Front Aging Neurosci *14*, 889257.

Longinetti, E., and Fang, F. (2019). Epidemiology of amyotrophic lateral sclerosis: an update of recent literature. Curr Opin Neurol *32*, 771-776.

Lorenzini, I., Alsop, E., Levy, J., Gittings, L.M., Lall, D., Rabichow, B.E., Moore, S., Pevey, R., Bustos, L., Burciu, C.*, et al.* (2022). Activated iPSC-microglia from C9orf72 ALS/FTD patients exhibit endosomal-lysosomal dysfunction. bioRxiv, 2020.2009.2003.277459.

Love, M.I., Huber, W., and Anders, S. (2014). Moderated estimation of fold change and dispersion for RNA-seq data with DESeq2. Genome Biol *15*, 550.

Lu, J., Wang, J., Lin, Z., Shi, G., Wang, R., Zhao, Y., Zhao, Y., and Zhao, J. (2021). MMP-9 as a Biomarker for Predicting Hemorrhagic Strokes in Moyamoya Disease. Front Neurol *12*, 721118.

Mackenzie, I.R., Frick, P., Grasser, F.A., Gendron, T.F., Petrucelli, L., Cashman, N.R., Edbauer, D., Kremmer, E., Prudlo, J., Troost, D.*, et al.* (2015). Quantitative analysis and clinico-pathological correlations of different dipeptide repeat protein pathologies in C9ORF72 mutation carriers. Acta Neuropathol *130*, 845-861.

Majounie, E., Renton, A.E., Mok, K., Dopper, E.G., Waite, A., Rollinson, S., Chio, A., Restagno, G., Nicolaou, N., Simon-Sanchez, J.*, et al.* (2012). Frequency of the C9orf72 hexanucleotide repeat expansion in patients with amyotrophic lateral sclerosis and frontotemporal dementia: a cross-sectional study. Lancet Neurol *11*, 323-330.

Mancuso, R., Van Den Daele, J., Fattorelli, N., Wolfs, L., Balusu, S., Burton, O., Liston, A., Sierksma, A., Fourne, Y., Poovathingal, S.*, et al.* (2019). Stem-cell-derived human microglia transplanted in mouse brain to study human disease. Nat Neurosci *22*, 2111-2116.

Mantovani, A., Sica, A., and Locati, M. (2005). Macrophage polarization comes of age. Immunity *23*, 344-346.

Marin, B., Hamidou, B., Couratier, P., Nicol, M., Delzor, A., Raymondeau, M., Druet-Cabanac, M., Lautrette, G., Boumediene, F., Preux, P.M.*, et al.* (2014). Population-based epidemiology of amyotrophic lateral sclerosis (ALS) in an ageing Europe--the French register of ALS in Limousin (FRALim register). Eur J Neurol *21*, 1292-1300, e1278-1299.

Masuda, T., Sankowski, R., Staszewski, O., and Prinz, M. (2020). Microglia Heterogeneity in the Single-Cell Era. Cell Rep *30*, 1271-1281.

Maury, Y., Come, J., Piskorowski, R.A., Salah-Mohellibi, N., Chevaleyre, V., Peschanski, M., Martinat, C., and Nedelec, S. (2015). Combinatorial analysis of developmental cues efficiently converts human pluripotent stem cells into multiple neuronal subtypes. Nat Biotechnol *33*, 89-96.

McCauley, M.E., O'Rourke, J.G., Yanez, A., Markman, J.L., Ho, R., Wang, X., Chen, S., Lall, D., Jin, M., Muhammad, A.*, et al.* (2020). C9orf72 in myeloid cells suppresses STING-induced inflammation. Nature *585*, 96-101.

McGeer, P.L., Itagaki, S., Boyes, B.E., and McGeer, E.G. (1988a). Reactive microglia are positive for HLA-DR in the substantia nigra of Parkinson's and Alzheimer's disease brains. Neurology *38*, 1285-1291.

McGeer, P.L., Itagaki, S., and McGeer, E.G. (1988b). Expression of the histocompatibility glycoprotein HLA-DR in neurological disease. Acta Neuropathol *76*, 550-557.

McGeer, P.L., Itagaki, S., Tago, H., and McGeer, E.G. (1987). Reactive microglia in patients with senile dementia of the Alzheimer type are positive for the histocompatibility glycoprotein HLA-DR. Neurosci Lett *79*, 195-200.

McGeer, P.L., Kawamata, T., Walker, D.G., Akiyama, H., Tooyama, I., and McGeer, E.G. (1993). Microglia in degenerative neurological disease. Glia *7*, 84-92.

Mehta, P.R., Jones, A.R., Opie-Martin, S., Shatunov, A., Iacoangeli, A., Al Khleifat, A., Smith, B.N., Topp, S., Morrison, K.E., Shaw, P.J.*, et al.* (2019). Younger age of onset in familial amyotrophic lateral sclerosis is a result of pathogenic gene variants, rather than ascertainment bias. J Neurol Neurosurg Psychiatry *90*, 268-271.

Meissner, F., Molawi, K., and Zychlinsky, A. (2010). Mutant superoxide dismutase 1-induced IL-1beta accelerates ALS pathogenesis. Proc Natl Acad Sci U S A *107*, 13046-13050.

Mejzini, R., Flynn, L.L., Pitout, I.L., Fletcher, S., Wilton, S.D., and Akkari, P.A. (2019). ALS Genetics, Mechanisms, and Therapeutics: Where Are We Now? Front Neurosci *13*, 1310.

Melief, J., Koning, N., Schuurman, K.G., Van De Garde, M.D., Smolders, J., Hoek, R.M., Van Eijk, M., Hamann, J., and Huitinga, I. (2012). Phenotyping primary human microglia: tight regulation of LPS responsiveness. Glia *60*, 1506-1517.

Mizielinska, S., Lashley, T., Norona, F.E., Clayton, E.L., Ridler, C.E., Fratta, P., and Isaacs, A.M. (2013). C9orf72 frontotemporal lobar degeneration is characterised by frequent neuronal sense and antisense RNA foci. Acta Neuropathol *126*, 845-857.

Mori, K., Arzberger, T., Grasser, F.A., Gijselinck, I., May, S., Rentzsch, K., Weng, S.M., Schludi, M.H., van der Zee, J., Cruts, M.*, et al.* (2013a). Bidirectional transcripts of the expanded C9orf72 hexanucleotide repeat are translated into aggregating dipeptide repeat proteins. Acta Neuropathol *126*, 881-893.

Mori, K., Weng, S.M., Arzberger, T., May, S., Rentzsch, K., Kremmer, E., Schmid, B., Kretzschmar, H.A., Cruts, M., Van Broeckhoven, C.*, et al.* (2013b). The C9orf72 GGGGCC repeat is translated into aggregating dipeptide-repeat proteins in FTLD/ALS. Science *339*, 1335-1338.

Muffat, J., Li, Y., Yuan, B., Mitalipova, M., Omer, A., Corcoran, S., Bakiasi, G., Tsai, L.H., Aubourg, P., Ransohoff, R.M.*, et al.* (2016). Efficient derivation of microglia-like cells from human pluripotent stem cells. Nat Med *22*, 1358-1367.

Murphy, N.A., Arthur, K.C., Tienari, P.J., Houlden, H., Chio, A., and Traynor, B.J. (2017). Age-related penetrance of the C9orf72 repeat expansion. Sci Rep *7*, 2116.

Neely, M.D., Litt, M.J., Tidball, A.M., Li, G.G., Aboud, A.A., Hopkins, C.R., Chamberlin, R., Hong, C.C., Ess, K.C., and Bowman, A.B. (2012). DMH1, a highly selective small molecule BMP inhibitor promotes neurogenesis of hiPSCs: comparison of PAX6 and SOX1 expression during neural induction. ACS Chem Neurosci *3*, 482-491.

Neumann, M., Sampathu, D.M., Kwong, L.K., Truax, A.C., Micsenyi, M.C., Chou, T.T., Bruce, J., Schuck, T., Grossman, M., Clark, C.M.*, et al.* (2006). Ubiquitinated TDP-43 in frontotemporal lobar degeneration and amyotrophic lateral sclerosis. Science *314*, 130-133.

Nguyen, M.D., Julien, J.P., and Rivest, S. (2001). Induction of proinflammatory molecules in mice with amyotrophic lateral sclerosis: no requirement for proapoptotic interleukin-1beta in neurodegeneration. Ann Neurol *50*, 630-639.

Nicolas, A., Kenna, K.P., Renton, A.E., Ticozzi, N., Faghri, F., Chia, R., Dominov, J.A., Kenna, B.J., Nalls, M.A., Keagle, P.*, et al.* (2018). Genome-wide Analyses Identify KIF5A as a Novel ALS Gene. Neuron *97*, 1268-1283 e1266.

Nimmerjahn, A., Kirchhoff, F., and Helmchen, F. (2005). Resting microglial cells are highly dynamic surveillants of brain parenchyma in vivo. Science *308*, 1314-1318.

Nolan, M., Scott, C., Gamarallage, M.P., Lunn, D., Carpenter, K., McDonough, E., Meyer, D., Kaanumalle, S., Santamaria-Pang, A., Turner, M.R.*, et al.* (2020). Quantitative patterns of motor cortex proteinopathy across ALS genotypes. Acta Neuropathol Commun *8*, 98.

O'Rourke, J.G., Bogdanik, L., Muhammad, A., Gendron, T.F., Kim, K.J., Austin, A., Cady, J., Liu, E.Y., Zarrow, J., Grant, S.*, et al.* (2015). C9orf72 BAC Transgenic Mice Display Typical Pathologic Features of ALS/FTD. Neuron *88*, 892-901.

O'Rourke, J.G., Bogdanik, L., Yanez, A., Lall, D., Wolf, A.J., Muhammad, A.K., Ho, R., Carmona, S., Vit, J.P., Zarrow, J.*, et al.* (2016). C9orf72 is required for proper macrophage and microglial function in mice. Science *351*, 1324-1329.

Pang, W., and Hu, F. (2021). Cellular and physiological functions of C9ORF72 and implications for ALS/FTD. J Neurochem *157*, 334-350.

Paolicelli, R.C., Jawaid, A., Henstridge, C.M., Valeri, A., Merlini, M., Robinson, J.L., Lee, E.B., Rose, J., Appel, S., Lee, V.M.*, et al.* (2017). TDP-43 Depletion in Microglia Promotes Amyloid Clearance but Also Induces Synapse Loss. Neuron *95*, 297-308 e296.

Paolicelli, R.C., Sierra, A., Stevens, B., Tremblay, M.E., Aguzzi, A., Ajami, B., Amit, I., Audinat, E., Bechmann, I., Bennett, M.*, et al.* (2022). Microglia states and nomenclature: A field at its crossroads. Neuron *110*, 3458-3483.

Pelvig, D.P., Pakkenberg, H., Stark, A.K., and Pakkenberg, B. (2008). Neocortical glial cell numbers in human brains. Neurobiol Aging *29*, 1754-1762.

Peters, O.M., Cabrera, G.T., Tran, H., Gendron, T.F., McKeon, J.E., Metterville, J., Weiss, A., Wightman, N., Salameh, J., Kim, J.*, et al.* (2015). Human C9ORF72

Hexanucleotide Expansion Reproduces RNA Foci and Dipeptide Repeat Proteins but Not Neurodegeneration in BAC Transgenic Mice. Neuron *88*, 902-909.

Philips, T., and Robberecht, W. (2011). Neuroinflammation in amyotrophic lateral sclerosis: role of glial activation in motor neuron disease. Lancet Neurol *10*, 253-263.

Philips, T., and Rothstein, J.D. (2015). Rodent Models of Amyotrophic Lateral Sclerosis. Curr Protoc Pharmacol *69*, 5 67 61-65 67 21.

Phukan, J., Elamin, M., Bede, P., Jordan, N., Gallagher, L., Byrne, S., Lynch, C., Pender, N., and Hardiman, O. (2012). The syndrome of cognitive impairment in amyotrophic lateral sclerosis: a population-based study. J Neurol Neurosurg Psychiatry *83*, 102-108.

Pramatarova, A., Laganière, J., Roussel, J., Brisebois, K., and Rouleau, G.A. (2001). Neuron-Specific Expression of Mutant Superoxide Dismutase 1 in Transgenic Mice Does Not Lead to Motor Impairment. The Journal of Neuroscience *21*, 3369-3374.

Ralph, G.S., Radcliffe, P.A., Day, D.M., Carthy, J.M., Leroux, M.A., Lee, D.C., Wong, L.F., Bilsland, L.G., Greensmith, L., Kingsman, S.M.*, et al.* (2005). Silencing mutant SOD1 using RNAi protects against neurodegeneration and extends survival in an ALS model. Nat Med *11*, 429-433.

Ransohoff, R.M. (2016). A polarizing question: do M1 and M2 microglia exist? Nat Neurosci *19*, 987-991.

Reinhard, S.M., Razak, K., and Ethell, I.M. (2015). A delicate balance: role of MMP-9 in brain development and pathophysiology of neurodevelopmental disorders. Front Cell Neurosci *9*, 280.

Renton, A.E., Majounie, E., Waite, A., Simon-Sanchez, J., Rollinson, S., Gibbs, J.R., Schymick, J.C., Laaksovirta, H., van Swieten, J.C., Myllykangas, L.*, et al.* (2011). A hexanucleotide repeat expansion in C9ORF72 is the cause of chromosome 9p21-linked ALS-FTD. Neuron *72*, 257-268.

Rhee, J.W., Lee, K.W., Kim, D., Lee, Y., Jeon, O.H., Kwon, H.J., and Kim, D.S. (2007). NF-kappaB-dependent regulation of matrix metalloproteinase-9 gene expression by lipopolysaccharide in a macrophage cell line RAW 264.7. J Biochem Mol Biol *40*, 88-94.

Rizzu, P., Blauwendraat, C., Heetveld, S., Lynes, E.M., Castillo-Lizardo, M., Dhingra, A., Pyz, E., Hobert, M., Synofzik, M., Simon-Sanchez, J.*, et al.* (2016). C9orf72 is differentially expressed in the central nervous system and myeloid cells and consistently reduced in C9orf72, MAPT and GRN mutation carriers. Acta Neuropathol Commun *4*, 37.

Roche, J.C., Rojas-Garcia, R., Scott, K.M., Scotton, W., Ellis, C.E., Burman, R., Wijesekera, L., Turner, M.R., Leigh, P.N., Shaw, C.E.*, et al.* (2012). A proposed staging system for amyotrophic lateral sclerosis. Brain *135*, 847-852.

Rohrborn, D., Eckel, J., and Sell, H. (2014). Shedding of dipeptidyl peptidase 4 is mediated by metalloproteases and up-regulated by hypoxia in human adipocytes and smooth muscle cells. FEBS Lett *588*, 3870-3877.

Rohrborn, D., Wronkowitz, N., and Eckel, J. (2015). DPP4 in Diabetes. Front Immunol *6*, 386.

Rosen, D.R., Siddique, T., Patterson, D., Figlewicz, D.A., Sapp, P., Hentati, A., Donaldson, D., Goto, J., O'Regan, J.P., Deng, H.X.*, et al.* (1993). Mutations in Cu/Zn superoxide dismutase gene are associated with familial amyotrophic lateral sclerosis. Nature *362*, 59-62.

Rossi, S., Cozzolino, M., and Carri, M.T. (2016). Old versus New Mechanisms in the Pathogenesis of ALS. Brain Pathol *26*, 276-286.

Rostalski, H., Leskela, S., Huber, N., Katisko, K., Cajanus, A., Solje, E., Marttinen, M., Natunen, T., Remes, A.M., Hiltunen, M.*, et al.* (2019). Astrocytes and Microglia as Potential Contributors to the Pathogenesis of C9orf72 Repeat Expansion-Associated FTLD and ALS. Front Neurosci *13*, 486.

Rutherford, N.J., Heckman, M.G., Dejesus-Hernandez, M., Baker, M.C., Soto-Ortolaza, A.I., Rayaprolu, S., Stewart, H., Finger, E., Volkening, K., Seeley, W.W.*, et al.* (2012). Length of normal alleles of C9ORF72 GGGGCC repeat do not influence disease phenotype. Neurobiol Aging *33*, 2950 e2955-2957.

Ryan, M., Heverin, M., McLaughlin, R.L., and Hardiman, O. (2019). Lifetime Risk and Heritability of Amyotrophic Lateral Sclerosis. JAMA Neurol *76*, 1367-1374.

Sareen, D., O'Rourke, J.G., Meera, P., Muhammad, A.K., Grant, S., Simpkinson, M., Bell, S., Carmona, S., Ornelas, L., Sahabian, A.*, et al.* (2013). Targeting RNA foci in iPSC-derived motor neurons from ALS patients with a C9ORF72 repeat expansion. Sci Transl Med *5*, 208ra149.

Schindelin, J., Arganda-Carreras, I., Frise, E., Kaynig, V., Longair, M., Pietzsch, T., Preibisch, S., Rueden, C., Saalfeld, S., Schmid, B.*, et al.* (2012). Fiji: an open-source platform for biological-image analysis. Nat Methods *9*, 676-682.

Schludi, M.H., Becker, L., Garrett, L., Gendron, T.F., Zhou, Q., Schreiber, F., Popper, B., Dimou, L., Strom, T.M., Winkelmann, J.*, et al.* (2017). Spinal poly-GA inclusions in a C9orf72 mouse model trigger motor deficits and inflammation without neuron loss. Acta Neuropathol *134*, 241-254.

Serio, A., and Patani, R. (2018). Concise Review: The Cellular Conspiracy of Amyotrophic Lateral Sclerosis. Stem Cells *36*, 293-303.

Shi, Y., Lin, S., Staats, K.A., Li, Y., Chang, W.H., Hung, S.T., Hendricks, E., Linares, G.R., Wang, Y., Son, E.Y.*, et al.* (2018). Haploinsufficiency leads to neurodegeneration in C9ORF72 ALS/FTD human induced motor neurons. Nat Med *24*, 313-325.

Sierra, A., Paolicelli, R.C., and Kettenmann, H. (2019). Cien Anos de Microglia: Milestones in a Century of Microglial Research. Trends Neurosci *42*, 778-792.

Simone, R., Balendra, R., Moens, T.G., Preza, E., Wilson, K.M., Heslegrave, A., Woodling, N.S., Niccoli, T., Gilbert-Jaramillo, J., Abdelkarim, S.*, et al.* (2018). G-quadruplex-binding small molecules ameliorate C9orf72 FTD/ALS pathology in vitro and in vivo. EMBO Mol Med *10*, 22-31.

Smeyers, J., Banchi, E.G., and Latouche, M. (2021). C9ORF72: What It Is, What It Does, and Why It Matters. Front Cell Neurosci *15*, 661447.

Soubannier, V., Chaineau, M., Gursu, L., Haghi, G., Franco Flores, A.K., Rouleau, G., Durcan, T.M., and Stifani, S. (2022). Rapid Generation of Ventral Spinal Cord-like Astrocytes from Human iPSCs for Modeling Non-Cell Autonomous Mechanisms of Lower Motor Neuron Disease. Cells *11*.

Sousa, C., Golebiewska, A., Poovathingal, S.K., Kaoma, T., Pires-Afonso, Y., Martina, S., Coowar, D., Azuaje, F., Skupin, A., Balling, R.*, et al.* (2018). Single-cell transcriptomics reveals distinct inflammation-induced microglia signatures. EMBO Rep *19*.

Spencer, P.S., Nunn, P.B., Hugon, J., Ludolph, A.C., Ross, S.M., Roy, D.N., and Robertson, R.C. (1987). Guam amyotrophic lateral sclerosis-parkinsonism-dementia linked to a plant excitant neurotoxin. Science *237*, 517-522.

Spiller, K.J., Khan, T., Dominique, M.A., Restrepo, C.R., Cotton-Samuel, D., Levitan, M., Jafar-Nejad, P., Zhang, B., Soriano, A., Rigo, F.*, et al.* (2019). Reduction of matrix metalloproteinase 9 (MMP-9) protects motor neurons from TDP-43-triggered death in rNLS8 mice. Neurobiol Dis *124*, 133-140.

Spiller, K.J., Restrepo, C.R., Khan, T., Dominique, M.A., Fang, T.C., Canter, R.G., Roberts, C.J., Miller, K.R., Ransohoff, R.M., Trojanowski, J.Q.*, et al.* (2018). Microglia-mediated recovery from ALS-relevant motor neuron degeneration in a mouse model of TDP-43 proteinopathy. Nat Neurosci *21*, 329-340.

Sreedharan, J., Blair, I.P., Tripathi, V.B., Hu, X., Vance, C., Rogelj, B., Ackerley, S., Durnall, J.C., Williams, K.L., Buratti, E.*, et al.* (2008). TDP-43 mutations in familial and sporadic amyotrophic lateral sclerosis. Science *319*, 1668-1672.

Steinacker, P., Verde, F., Fang, L., Feneberg, E., Oeckl, P., Roeber, S., Anderl-Straub, S., Danek, A., Diehl-Schmid, J., Fassbender, K.*, et al.* (2018). Chitotriosidase (CHIT1) is increased in microglia and macrophages in spinal cord of amyotrophic lateral sclerosis and cerebrospinal fluid levels correlate with disease severity and progression. J Neurol Neurosurg Psychiatry *89*, 239-247.

Stephens, M. (2017). False discovery rates: a new deal. Biostatistics *18*, 275-294.

Suh, E., Lee, E.B., Neal, D., Wood, E.M., Toledo, J.B., Rennert, L., Irwin, D.J., McMillan, C.T., Krock, B., Elman, L.B.*, et al.* (2015). Semi-automated quantification of C9orf72 expansion size reveals inverse correlation between hexanucleotide repeat number and disease duration in frontotemporal degeneration. Acta Neuropathol *130*, 363-372.

Suk, T.R., and Rousseaux, M.W.C. (2020). The role of TDP-43 mislocalization in amyotrophic lateral sclerosis. Mol Neurodegener *15*, 45.

Sullivan, P.M., Zhou, X., Robins, A.M., Paushter, D.H., Kim, D., Smolka, M.B., and Hu, F. (2016). The ALS/FTLD associated protein C9orf72 associates with SMCR8 and WDR41 to regulate the autophagy-lysosome pathway. Acta Neuropathol Commun *4*, 51.

Swanson, K.V., Deng, M., and Ting, J.P. (2019). The NLRP3 inflammasome: molecular activation and regulation to therapeutics. Nat Rev Immunol *19*, 477-489.

Takahashi, K., and Yamanaka, S. (2006). Induction of pluripotent stem cells from mouse embryonic and adult fibroblast cultures by defined factors. Cell *126*, 663-676.

Talbot, K. (2009). Motor neuron disease: the bare essentials. Pract Neurol *9*, 303-309.

Talbot, K., Feneberg, E., Scaber, J., Thompson, A.G., and Turner, M.R. (2018). Amyotrophic lateral sclerosis: the complex path to precision medicine. J Neurol *265*, 2454-2462.

Tang, Y., and Le, W. (2016). Differential Roles of M1 and M2 Microglia in Neurodegenerative Diseases. Mol Neurobiol *53*, 1181-1194.

Thiry, L., Hamel, R., Pluchino, S., Durcan, T., and Stifani, S. (2020). Characterization of Human iPSC-derived Spinal Motor Neurons by Single-cell RNA Sequencing. Neuroscience *450*, 57-70.

Thompson, A.G., Gray, E., Bampton, A., Raciborska, D., Talbot, K., and Turner, M.R. (2019). CSF chitinase proteins in amyotrophic lateral sclerosis. J Neurol Neurosurg Psychiatry *90*, 1215-1220.

Thompson, A.G., Gray, E., Thezenas, M.L., Charles, P.D., Evetts, S., Hu, M.T., Talbot, K., Fischer, R., Kessler, B.M., and Turner, M.R. (2018). Cerebrospinal fluid macrophage biomarkers in amyotrophic lateral sclerosis. Ann Neurol *83*, 258-268.

Tondo, G., Iaccarino, L., Cerami, C., Vanoli, G.E., Presotto, L., Masiello, V., Coliva, A., Salvi, F., Bartolomei, I., Mosca, L.*, et al.* (2020). (11) C-PK11195 PET-based molecular study of microglia activation in SOD1 amyotrophic lateral sclerosis. Ann Clin Transl Neurol *7*, 1513-1523.

Turner, B.J., and Talbot, K. (2008). Transgenics, toxicity and therapeutics in rodent models of mutant SOD1-mediated familial ALS. Prog Neurobiol *85*, 94-134.

Turner, M.R., Barnwell, J., Al-Chalabi, A., and Eisen, A. (2012). Young-onset amyotrophic lateral sclerosis: historical and other observations. Brain *135*, 2883-2891.

Turner, M.R., Cagnin, A., Turkheimer, F.E., Miller, C.C., Shaw, C.E., Brooks, D.J., Leigh, P.N., and Banati, R.B. (2004). Evidence of widespread cerebral microglial activation in amyotrophic lateral sclerosis: an [11C](R)-PK11195 positron emission tomography study. Neurobiol Dis *15*, 601-609.

Vafadari, B., Salamian, A., and Kaczmarek, L. (2016). MMP-9 in translation: from molecule to brain physiology, pathology, and therapy. J Neurochem *139 Suppl 2*, 91-114.

Vahsen, B.F., Gray, E., Candalija, A., Cramb, K.M.L., Scaber, J., Dafinca, R., Katsikoudi, A., Xu, Y., Farrimond, L., Wade-Martins, R.*, et al.* (2022). Human iPSC co-culture model to investigate the interaction between microglia and motor neurons. Sci Rep *12*, 12606.

Vahsen, B.F., Gray, E., Thompson, A.G., Ansorge, O., Anthony, D.C., Cowley, S.A., Talbot, K., and Turner, M.R. (2021). Non-neuronal cells in amyotrophic lateral sclerosis - from pathogenesis to biomarkers. Nat Rev Neurol *17*, 333-348.

Valverde, A., Dunys, J., Lorivel, T., Debayle, D., Gay, A.S., Caillava, C., Chami, M., and Checler, F. (2021). Dipeptidyl peptidase 4 contributes to Alzheimer's disease-like defects in a mouse model and is increased in sporadic Alzheimer's disease brains. J Biol Chem *297*, 100963.

van Blitterswijk, M., DeJesus-Hernandez, M., Niemantsverdriet, E., Murray, M.E., Heckman, M.G., Diehl, N.N., Brown, P.H., Baker, M.C., Finch, N.A., Bauer, P.O*., et al.* (2013). Association between repeat sizes and clinical and pathological characteristics in carriers of C9ORF72 repeat expansions (Xpansize-72): a cross-sectional cohort study. The Lancet Neurology *12*, 978-988.

van der Zee, J., Gijselinck, I., Dillen, L., Van Langenhove, T., Theuns, J., Engelborghs, S., Philtjens, S., Vandenbulcke, M., Sleegers, K., Sieben, A*., et al.* (2013). A pan-European study of the C9orf72 repeat associated with FTLD: geographic prevalence, genomic instability, and intermediate repeats. Hum Mutat *34*, 363-373.

van Wilgenburg, B., Browne, C., Vowles, J., and Cowley, S.A. (2013). Efficient, long term production of monocyte-derived macrophages from human pluripotent stem cells under partly-defined and fully-defined conditions. PLoS One *8*, e71098.

Vance, C., Rogelj, B., Hortobagyi, T., De Vos, K.J., Nishimura, A.L., Sreedharan, J., Hu, X., Smith, B., Ruddy, D., Wright, P*., et al.* (2009). Mutations in FUS, an RNA processing protein, cause familial amyotrophic lateral sclerosis type 6. Science *323*, 1208-1211.

Vandenbroucke, R.E., and Libert, C. (2014). Is there new hope for therapeutic matrix metalloproteinase inhibition? Nat Rev Drug Discov *13*, 904-927.

Vanhee, S., De Mulder, K., Van Caeneghem, Y., Verstichel, G., Van Roy, N., Menten, B., Velghe, I., Philippe, J., De Bleser, D., Lambrecht, B.N*., et al.* (2015). In vitro human embryonic stem cell hematopoiesis mimics MYB-independent yolk sac hematopoiesis. Haematologica *100*, 157-166.

Varghese, A.M., Sharma, A., Mishra, P., Vijayalakshmi, K., Harsha, H.C., Sathyaprabha, T.N., Bharath, S.M., Nalini, A., Alladi, P.A., and Raju, T.R. (2013). Chitotriosidase - a putative biomarker for sporadic amyotrophic lateral sclerosis. Clin Proteomics *10*, 19.

Vaughan-Jackson, A., Stodolak, S., Ebrahimi, K.H., Browne, C., Reardon, P.K., Pires, E., Gilbert-Jaramillo, J., Cowley, S.A., and James, W.S. (2021). Differentiation of human induced pluripotent stem cells to authentic macrophages using a defined, serum-free, open-source medium. Stem Cell Reports *16*, 1735-1748.

von Bartheld, C.S., Bahney, J., and Herculano-Houzel, S. (2016). The search for true numbers of neurons and glial cells in the human brain: A review of 150 years of cell counting. J Comp Neurol *524*, 3865-3895.

Vu, L., An, J., Kovalik, T., Gendron, T., Petrucelli, L., and Bowser, R. (2020). Cross-sectional and longitudinal measures of chitinase proteins in amyotrophic lateral sclerosis and expression of CHI3L1 in activated astrocytes. J Neurol Neurosurg Psychiatry *91*, 350-358.

Wang, L., Sharma, K., Deng, H.X., Siddique, T., Grisotti, G., Liu, E., and Roos, R.P. (2008). Restricted expression of mutant SOD1 in spinal motor neurons and interneurons induces motor neuron pathology. Neurobiol Dis *29*, 400-408.

Westeneng, H.J., Debray, T.P.A., Visser, A.E., van Eijk, R.P.A., Rooney, J.P.K., Calvo, A., Martin, S., McDermott, C.J., Thompson, A.G., Pinto, S.*, et al.* (2018). Prognosis for patients with amyotrophic lateral sclerosis: development and validation of a personalised prediction model. Lancet Neurol *17*, 423-433.

Weydt, P., Yuen, E.C., Ransom, B.R., and Moller, T. (2004). Increased cytotoxic potential of microglia from ALS-transgenic mice. Glia *48*, 179-182.

Wichterle, H., Lieberam, I., Porter, J.A., and Jessell, T.M. (2002). Directed differentiation of embryonic stem cells into motor neurons. Cell *110*, 385-397.

Woollacott, I.O., and Mead, S. (2014). The C9ORF72 expansion mutation: gene structure, phenotypic and diagnostic issues. Acta Neuropathol *127*, 319-332.

Xiao, Q., Zhao, W., Beers, D.R., Yen, A.A., Xie, W., Henkel, J.S., and Appel, S.H. (2007). Mutant SOD1(G93A) microglia are more neurotoxic relative to wild-type microglia. J Neurochem *102*, 2008-2019.

York, E.M., LeDue, J.M., Bernier, L.P., and MacVicar, B.A. (2018). 3DMorph Automatic Analysis of Microglial Morphology in Three Dimensions from Ex Vivo and In Vivo Imaging. eNeuro *5*, ENEURO.0266-0218.2018.

Yu, G., Wang, L.G., Han, Y., and He, Q.Y. (2012). clusterProfiler: an R package for comparing biological themes among gene clusters. OMICS *16*, 284-287.

Yvanka de Soysa, T., Therrien, M., Walker, A.C., and Stevens, B. (2022). Redefining microglia states: Lessons and limits of human and mouse models to study microglia states in neurodegenerative diseases. Semin Immunol *60*, 101651.

Zhang, Y., Chen, K., Sloan, S.A., Bennett, M.L., Scholze, A.R., O'Keeffe, S., Phatnani, H.P., Guarnieri, P., Caneda, C., Ruderisch, N.*, et al.* (2014). An RNA-sequencing transcriptome and splicing database of glia, neurons, and vascular cells of the cerebral cortex. J Neurosci *34*, 11929-11947.

Zhao, W., Beers, D.R., Bell, S., Wang, J., Wen, S., Baloh, R.H., and Appel, S.H. (2015). TDP-43 activates microglia through NF-kappaB and NLRP3 inflammasome. Exp Neurol *273*, 24-35.

Zhao, W., Beers, D.R., Henkel, J.S., Zhang, W., Urushitani, M., Julien, J.P., and Appel, S.H. (2010). Extracellular mutant SOD1 induces microglial-mediated motoneuron injury. Glia *58*, 231-243.

Zhou, Q., Mareljic, N., Michaelsen, M., Parhizkar, S., Heindl, S., Nuscher, B., Farny, D., Czuppa, M., Schludi, C., Graf, A.*, et al.* (2020). Active poly-GA vaccination prevents microglia activation and motor deficits in a C9orf72 mouse model. EMBO Mol Med *12*, e10919.

Zu, T., Liu, Y., Banez-Coronel, M., Reid, T., Pletnikova, O., Lewis, J., Miller, T.M., Harms, M.B., Falchook, A.E., Subramony, S.H.*, et al.* (2013). RAN proteins and RNA foci from antisense transcripts in C9ORF72 ALS and frontotemporal dementia. Proc Natl Acad Sci U S A *110*, E4968-4977.

Zurcher, N.R., Loggia, M.L., Lawson, R., Chonde, D.B., Izquierdo-Garcia, D., Yasek, J.E., Akeju, O., Catana, C., Rosen, B.R., Cudkowicz, M.E.*, et al.* (2015). Increased in vivo glial activation in patients with amyotrophic lateral sclerosis: assessed with [(11)C]-PBR28. Neuroimage Clin *7*, 409-414.